PERSPECTIVE

Check for updates

Atoms in molecules in real space: a fertile field for chemical bonding

Ángel Martín Pendás, [ID] *[a] Evelio Francisco, [ID] [a] Dimas Suárez, [ID] [a] Aurora Costales, [ID] [a] Natalia Díaz, [ID] [a] Julen Munárriz, [ID] [a] Tomás Rocha-Rinza[b] and José Manuel Guevara-Vela [ID] [c]

In this perspective, we review some recent advances in the concept of atoms-in-molecules from a real space perspective. We first introduce the general formalism of atomic weight factors that allows unifying the treatment of fuzzy and non-fuzzy decompositions under a common algebraic umbrella. We then show how the use of reduced density matrices and their cumulants allows partitioning any quantum mechanical observable into atomic or group contributions. This circumstance provides access to electron counting as well as energy partitioning, on the same footing. We focus on how the fluctuations of atomic populations, as measured by the statistical cumulants of the electron distribution functions, are related to general multi-center bonding descriptors. Then we turn our attention to the interacting quantum atom energy partitioning, which is briefly reviewed since several general accounts on it have already appeared in the literature. More attention is paid to recent applications to large systems. Finally, we consider how a common formalism to extract electron counts and energies can be used to establish an algebraic justification for the extensively used bond order–bond energy relationships. We also briefly review a path to recover one-electron functions from real space partitions. Although most of the applications considered will be restricted to real space atoms taken from the quantum theory of atoms in molecules, arguably the most successful of all the atomic partitions devised so far, all the take-home messages from this perspective are generalizable to any real space decompositions.

1 Introduction

More than 60 years have passed since Charles Coulson famously uttered the phrase "give us insight not numbers" in a gala dinner speech at a conference in Colorado.[1] As overused as this quote may be, it has lost none of its inspirational power, although in a recent influential article in the Journal of the American Chemical Society,[2] Neese and coworkers argued in favor of having the cake and eating it too with their "give us insight and numbers". Careful examination of this and other contributions shows, however, that many of those who advocate for having it all tend to approach the "insight" side from a "numbers" perspective, choosing methods to interpret the chemical content of a computed wavefunction which are neither general nor unique, and that typically depend on much cruder assumptions than those they would admit on their

"numbers". Arguably, the interpretation face of theoretical chemistry still lags behind the astounding computational advances witnessed in recent times, and the surge of artificial intelligence and machine learning techniques[3,4] will certainly not contribute to improving this asymmetry soon.

Building an uncontested framework to extract chemical information from quantum chemical calculations has proven more difficult than improving the accuracy of the calculations themselves. There are several reasons that can be put forward to justify this fact, which more or less converge on the historical dissociation between the pre-quantum language spoken by chemists and the algebraic formalism of quantum mechanics. Adapting our cherished fuzzy chemical concepts—single and multiple bonds, lone pairs and so on—to the rigid quantum mechanical framework is a task that has been approached from the different perspectives devised to find approximate solutions to Schrödinger's equation. However, although for instance valence bond (VB) and molecular orbital (MO) theory will converge to the true wavefunction in well-defined limits,[5] this will not be necessarily the case with their associated chemical interpretations. This situation has been the source of much confusion and never-ending debates.

It is our opinion that any acceptable solution to this problem must come from directly analyzing the wavefunction Ψ of a system.

[a] *Depto. Química Física y Analítica, Universidad de Oviedo, 33006 Oviedo, Spain. E-mail: ampendas@uniovi.es*

[b] *Instituto de Química, Universidad Nacional Autónoma de México, Circuito Exterior, Ciudad Universitaria, Delegación Coyoacán, México City C.P. 04510, Mexico*

[c] *Departamento de Química Física Aplicada, Universidad Autónoma de Madrid, Madrid 28049, Spain*

This journal is © the Owner Societies 2023

Phys. Chem. Chem. Phys., 2023, **25**, 10231–10262 | **10231**

The resulting interpretation should be independent of how Ψ is built, *i.e.* of the nature of its linearly combined components, be them orthogonal Slater determinants or non-orthogonal VB structures, and also of the type of basis sets, if any, used to construct one-electron functions. These constraints almost necessarily lead us to consider orbital invariant objects, such as reduced density matrices (RDMs) or reduced densities (RDs) of various orders written either in real or in momentum space. Since chemists tend to think of molecules as real objects evolving in real space, most, although not all,[6–8] of these approaches rest on real space RDMs. If atom-centered functions are not allowed to be an essential part of the analysis of Ψ, atoms dissolve in the sea of the N-electron wavefunction, and so does chemistry. In this regard, the authorized voice of Rueden-berg and coworkers resonates when pointing out that in order to build a theory of chemical bonding it is an essential requisite to postulate that atoms are somehow preserved in molecules.[9]

The emergence of atoms in molecules is guaranteed by Kato's cusp theorem in the non-relativistic regime that we will be focusing on.[10] The lowest (first) order reduced density, the electron density $\rho(\boldsymbol{r})$, displays logarithmic cusps at nuclear positions with slopes dependent on their nuclear charges. In fact, the existence of cusps is an easy didactical shortcut to the foundational theorems of density functional theory.[11] The density determines the type and position of the nuclei of a molecule, thus its full Hamiltonian. Although these ideas were not the historical origin of the use of ρ in chemical bonding, it serves well our purposes: the simplest of all the RDMs allows us to recognize the atoms comprising a molecule from its shape. Provided that it is an accepted experimental fact (*e.g.* through X-ray edge absorption spectroscopy) that regions close to the nuclei (the atomic cores in chemical parlance) are not affected much by the environment, the examination of ρ should allow associating with a particular atom not only the nuclear positions but also its vicinities. A program to decompose the density in real space into atomic contributions, or equivalently, to decompose the space itself into atomic regions, should thus be accessible. This endeavor was initiated decades ago by Richard F. W. Bader,[12] who proposed to use the topology induced by an scalar field like the electron density to divide the space into non-overlapping regions. The so-called Quantum Theory of Atoms in Molecules (QTAIM) has been very success-ful, paving the way to many other atomic partitions.

We review in this perspective the general framework behind real space reasoning in the theory of the chemical bond. We start by showing how a common formalism, based on atomic weight factors, can be used to embrace most of the real space atomic partitions defined so far, including fuzzy and non-fuzzy (or non-overlapping) decompositions. We then turn our attention to show how reduced density matrices and their cumulant residuals can be used to access the two faces of bonding, related to electron counting and to the decomposition of the molecular energy. Regarding electron counting, we focus on the statistical distribution of the atomic populations, the so-called electron distribution functions, stressing how the fluctuations of these populations, as measured by the cumulant moments of

their distribution function, are related to bonding indices. Then, we turn our attention to consider the energy decomposition emanating from a real space atomic partition, the interacting quantum atom approach (IQA). Provided that this methodology has already been reviewed,[13] we devote here our efforts to show the latest developments in the field. The electron counting and energy partitioning faces are then linked algebraically, showing how an analytic first order expansion relates bond energies to bond orders. Finally, a brief account describing how to recover one-electron functions (orbitals) from real space cumulant densities is also presented.

2 Atoms in real space

In quantum chemical topology (QCT), the focus is put in extracting chemically relevant information from orbital invariant scalar (or vector) fields that are used to provide a partition of the physical space R^3. Although modern QCT practitioners can choose among a large number of these fields, the easiest and best known partitioning consists of dividing R^3 into as many regions or domains as the number of atoms of a molecule, associating each of these domains with one of the atoms of the system. An isolated atom in real space consists of an atomic nucleus and a given number of electrons characterized by an electron density that extends to infinity, this implying that an isolated atom has an infinite volume and that any point in space should be associated with it. This clear image fades out as soon as the system contains two or more nuclei, linked or not by a chemical bond of whatever kind. To which atom does a point in R^3 belongs? Can a point in space belong to two or more atoms at the same time? Are there better or worse ways to partition R^3 into atomic domains? None of these questions has an answer that satisfies everyone. We describe in this work a number of options that have been proposed over the years to carry out this atomic partition of R^3.

An algebraic approach to the atom-in-the-molecule that encompasses a great variety of possible atomic definitions is obtained through the use of weight factors $\omega_B(\boldsymbol{r})$, associated with chemical objects B, that satisfy[14,15]

$$\sum_B \omega_B(\boldsymbol{r}) = 1 \qquad (1)$$

at any point in space $\boldsymbol{r}$. There are infinite many ways to define the ω_B's, and the chemical objects B need not necessarily be identified with atoms although we will do that here. Of course, this does not preclude the possibility of joining together several atoms into a single object (a functional group) in such a way that the number of terms in eqn (1) remains less than the number of atoms in the molecule.

Under this general framework any atomic partition can be ascribed to one out of two broad categories: fuzzy and non-fuzzy. In the former, each ω_B takes a non-zero value at any $\boldsymbol{r}$ that can be taken as the degree of participation of atom B at that point. In a way, a fuzzy partition can be considered as demo-cratic, as each point belongs to some extent to all the atoms of the system, while leaving a lot of freedom in how the different

10232 | *Phys. Chem. Chem. Phys.*, 2023, **25**, 10231–10262

This journal is © the Owner Societies 2023

atomic weights decay (*vide infra*). In a non-fuzzy decomposition, each point r is associated exclusively with one of the atoms, so that if $\omega_A(r) = 1$ then $\omega_B(r) = 0$ for B $\neq$ A. In these cases, the freedom lies in how the atomic boundaries are chosen.

The shape of fuzzy atomic weights or the interatomic boundaries of non-fuzzy partitions must satisfy several logical as well as chemical constraints. In the first case, we expect the weight of atom B to be close to one in the vicinity of its nucleus and decay faster or slower according to its size, electronegativity, and other descriptors. In the second, we expect an atomic region to be compact, simply connected with a size in agreement with chemical intuition. With these premises, we will now review some of the partitions of both types that have been used to date in QCT.

2.1 Non-fuzzy partitions

If follows from the above discussion that atoms in a non-fuzzy partition do not overlap at all, but they are characterized by a set of mutually exclusive domains Ω_A such that $\omega_A(r \in \Omega_A) = 1$, $\omega_A(r \notin \Omega_A) = 0$ and $\Omega_A \cap \Omega_B = \varnothing$. The full set of atoms exhaust the physical space ($\cup_A \Omega_A = R^3$). We will use Ω_A to refer to the 3D atomic domain of atom A whenever confusion between the atom and its basin is possible. Different non-fuzzy partitions differ in the way of choosing the Ω_A.

Probably the oldest non-fuzzy atomic partition reported comes from basic Solid State Physics,[16] where a 3D region around an atom, the Wigner–Seitz cell, is defined from geometry alone by associating a point in space with its closest nucleus. In a more general context these are the so-called Voronoi cells of a system. A straightforward algorithm to build them starts by building planes that bisect the lines connecting a given nucleus A with all its neighboring nuclei. These planes enclose a polyhedron that unambiguously defines Ω_A. In order to account for the different atomic sizes of, say, atoms A and B, the plane that cuts their inter-nuclear axis can be located closer to one of the two nuclei. This can be done by using a multitude of chemical criteria, *e.g.* the ratio of atomic or ionic radii.[17]

The non-fuzzy atomic regions with Voronoi cells, particularly if the latter do not take into account the different sizes of the atoms, are merely geometric constructs not supported by any theory or method. Endowed with a much deeper physical meaning and defined on the basis of fundamental principles of quantum mechanics lies the QTAIM framework,[12,18] originally introduced by Richard F. W. Bader and his collaborators, which is nowadays used by a growing number of theoretical and non-theoretical chemists. Despite detractors, QTAIM atoms are without a doubt the ones that have the greatest number of virtues from a theoretical point of view.[19] The QTAIM also paved the way to the development of general real space partitions induced by the topology of other scalar fields, like the electron localization function (ELF) of Becke and Edgecombe,[20] that has proven its power in chemistry[21] by isolating bonding and non-boding regions in molecules and solids and providing a simple framework to map arrow pushing onto computational chemistry,[22,23] or the electron localizability indicator (ELI) of Kohout,[6–8,24] that provides a partition similar to that of the ELF.

More recently, other atomic-like topological partitions have been also introduced with their own merits. For instance, the basins of the molecular electrostatic potential (MEP)[25] define neutral atoms by construction, as shown by Gadre,[26,27] and have been used in recent times by Espinosa and coworkers[28] to define zones of nucleophilic and electrophilic influence in molecules and to probe bonding and reactivity by Gadre *et al.*[29] Similarly, the Ehrenfest force vector field has been used to define force-like atoms[30] that behave similarly to QTAIM ones. Its computation is prone to errors from the asymptotically wrong behavior of Gaussian functions, a problem that can be solved by using Slater type orbitals, as shown by Dillen.[31] Using approximate expressions, Tsirelson and coworkers have made use of this and other related fields to provide a very detailed picture of interactions in crystals.[32] Other fields, like the Laplacian of ρ ($\nabla^2\rho(r)$),[33–35] have also been examined, although their basins have not been found as relevant for chemical purposes. Although all of these partitions provide complementary tools in the theory of chemical bonding, we feel that most of them are in a sense heirs to the QTAIM. Actually, MEP or Ehrenfest atoms, for instance, are typically used together with QTAIM ones.

In the QTAIM, the Ω_A regions (customary called atomic basins) are induced by the topology of the molecular electron density $\rho(r)$. The critical points (CPs) of $\rho(r)$ satisfy $\nabla\rho(r_c) = \mathbf{0}$, where $\mathbf{0}$ is the zero vector, and can be degenerate, $\lambda < 3$, or non-degenerate, $\lambda = 3$, where λ is the number of non-null eigenvalues of the Hessian matrix at the point r_c, defined as $H_{ij}(r_c) = (\partial^2\rho(r)/\partial x_i\partial x_j)_{r=r_c}$, with $(x_1,x_2,x_3 \equiv x,y,z)$. The non-degenerate CPs are classified into four categories according to the number of positive (p) and negative (n) eigenvalues of H: when $\sigma = p-n = -3,-1,+1,+3$ $\rho(r_c)$ is a maximum, a first-order saddle-point, a second-order saddle-point, and a minimum, respectively. These CPs are labelled as $(\lambda,\sigma) = (3,-3),(3,-1),(3,+1)$, and $(3,+3)$. The atomic basins are bounded by surfaces that satisfy a zero-flux condition $\nabla\rho(r)\cdot n(r) = 0$, where n is an outer vector normal to the surface, which guarantees that the kinetic energy operator is uniquely defined for a large family of plausible kinetic energy densities within the atomic basin.[19] This result is possibly the main advantage of QTAIM atoms over other possible atomic definitions. Note that the density at nuclear cusps is non-differentiable, although topologically equivalent to a maximum. When using Gaussian basis sets, the nuclear (3,−3) CPs do coincide to a large precision with the actual position of the nuclei, except in the case of very light atoms (say H), where one can find a spurious significant difference between the nuclear position and the maximum of ρ. Most times the number of maxima coincides with the number of nuclei of the system, with a maximum per atom. However, under some conditions, it is possible to find non-nuclear maxima (NNM) in the electron density field. In some cases, these are also spurious maxima, with ρ values very close to zero, that often disappear when the basis set is changed or the quality of the calculation is improved. However, in other cases NNMs do possess real entity and physical meaning, having been successfully related to localized or solvated electrons in electrides.[36,37] Very simple metals like lithium were shown to undergo a metal

This journal is © the Owner Societies 2023

Phys. Chem. Chem. Phys., 2023, **25**, 10231–10262 | **10233**

to insulator transition at high pressure[38] where the metallic electrons localize at interstitial lattice sites, developing clear NNMs. The combined use of several QCT descriptors has also been used to distinguish electrides from similar species, confirming the existence of electride-like gas-phase molecules.[39] When NNMs appear or disappear depending on the molecular geometry and we would like to stick to a common number of maxima at all the geometries, different *tricks* can be used to distribute the space associated with the NNM among all the other atomic basins that do have an associated atomic nucleus. Be that as it may, the existence of NNMs of the electron density can sometimes be aesthetically unsatisfactory. Noorizadeh has proposed using the kinetic energy density, which shows no NNMs, as a substitute of $\rho(r)$ to determine pseudo-QTAIM atomic basins.[40] This author claims that atoms defined in this way satisfy the virial theorem.

The $(3,-1)$ first-order saddle points of ρ are particularly relevant in the QTAIM. They are known as bond critical points (BCPs) and are placed along (or close to) the inter-nuclear line of some pairs of atoms. At equilibrium geometries, these points do correspond to traditional chemical bonds in the vast majority of cases. We will say no more here on this subject. Hundreds of articles have been written about BCPs, their meaning, their relevance to chemical bonding theory,[41,42] and to the computational implementation that aims to locate them quickly and without error. We mention here the algorithm of Yu and Trinkle,[43] a game changer for grid-based data that allows for a very efficient determination of the topology of the electron density in crystals.

The QTAIM has been generalized to systems with several types of quantum particles by Shahbazian and Goli, who have called their method the multi-component QTAIM (MC-QTAIM).[44] The MC-QTAIM has been applied to exotic bonds involving positrons and other elementary particles,[45,46] among several other promising applications.[47]

2.2 Fuzzy partitions

Contrary to the previous case, the weights $\omega_B(r)$ satisfying eqn (1) can all of them be simultaneously non-zero in fuzzy partitions. In this way, every point r is shared to different extents by all the atoms in the system. One of the possible choices of the ω_B's was proposed by Axel Becke,[48] just to facilitate the 3D integration of the one-electron functions that appear in Density Functional Theory (DFT). Indeed, any integral $I = \int F(r)dr$ is exactly given by a sum of atomic contributions $I = \sum_B I_B = \sum_B \int F_B(r)dr$ as long as $F_B(r) = \omega_B(r)F(r)$, and the $\omega_B(r)$ weights satisfy eqn (1). If $F(r) = \rho(r)$ this procedure divides the total electron density into atomic densities.

In his original proposal, Becke defined the $\omega_B(r)$'s by dividing the space into fuzzy Voronoi polyedra that take into account the different atomic sizes through tabulated atomic radii. If, for the time being, we assume that all atoms are equal in size, the classical Voronoi cell of an atom A can be defined as follows. For the pair of atoms A and B, the elliptical coordinate $\mu_{AB} = (r_A - r_B)/R_{AB}$ is defined, where r_A and r_B are the distances from

nuclei A or B to a given point in space, and R_{AB} is the distance between both nuclei. Any point r in the plane that bisects this line has $\mu_{AB} = 0$. If the step function $s(\mu_{AB})$ is defined as $s(\mu_{AB}) = 1$ when $-1 \leq \mu_{AB} \leq 0$ and $s(\mu_{AB}) = 0$ when $0 < \mu_{AB} \leq +1$, the Voronoi cell of atom A is given by a weight $P_A(r) = \Pi_{B \neq A} s(\mu_{AB})$, *i.e.* a point in R^3 with $P_A = 1$ belongs to atom A, otherwise it belongs to a different atom. The above definition provides a non-fuzzy partition of R^3. However, a redefiniton of μ_{AB} in such a way that $s(\mu_{AB})$ does not change abruptly from 1 to 0 in going from A to B allows for a fuzzy generalization of the partition. Becke's choice is $s(\mu) = \frac{1}{2}[1 - p_k(\mu)]$ with $p_k(\mu) = p(p_{k-1}(\mu))$ and $p_1(\mu) = (3/2)\mu - (1/2)\mu^3$. A small value of k, say $k = 1$, gives a slow decrease of $s(\mu)$ as we move away from the nucleus A, and $k \to \infty$ provides again the original exhaustive partition. In general, the choice $k = 3$ is close to optimal and quite appropriate. The equal-atomic-size Becke's partition of R^3 ends by defining $\omega_A(r) = P_A(r) \Big/ \sum_B P_B(r)$ through stockholder sharing, which automatically satisfies eqn (1). To account for the different atomic sizes, Becke replaces μ_{AB} by a new coordinate $\nu_{AB} = \mu_{AB} + a_{AB}(1 - \mu_{AB}^2)$ in the definition of p_k, where $|a_{AB}| \leq 1/2$. The plane that bisects the AB internuclear axis in the original recipe is displaced towards center A or towards center B for positive or negatives values of a_{AB}, respectively. Requiring that any point located in that plane (*i.e.* with $\nu_{AB} = 0$) has $r_A/r_B = R_A/R_B$, where R_A and R_B are Bragg–Slater radii of both atoms, leads to $a_{AB} = u_{AB}/(u_{AB}^2 - 1)$, where $u_{AB} = (\chi_{AB} - 1)/(\chi_{AB} + 1)$ and $\chi_{AB} = R_A/R_B$. When a_{AB} falls outside the $|a_{AB}| \leq 1/2$ range, Becke simply assigns the corresponding endpoint value to it.

Becke's partition method has been improved over the years to avoid some of its weak points. For instance, the atomic radii R_A used in the definition of ν_{AB} can be determined *on the fly* and not from a tabulated list of values. When two atoms A and B are bonded according to QTAIM, R_A and R_B can be obtained from the distance of the BCP to both nuclei. If there is no a BCP point between A and B, the original recipe can be used.[14] This choice leads to a modified Becke's method whose behavior is close to that of the exhaustive QTAIM partition. Another improvement is to change the definition of ν_{AB}, by using[49] $\nu_{AB} = (1 + \mu_{AB} - \chi_{AB}(1 - \mu_{AB}))/(1 + \mu_{AB} + \chi_{AB}(1 - \mu_{AB}))$, which automatically takes into account the possible values of a_{AB} greater than 1/2 or smaller than $-1/2$. This situation is not so uncommon and often happens when A and B have very different sizes. The above scheme, implemented by Salvador and Ramos-Córdoba,[49] has been named topological fuzzy Voronoi cell (TFVC) partition by the authors. In an attempt to the TFVC partition to provide atomic electron populations as similar as possible to the QTAIM values, they choose $k = 4$, which does not imply an appreciable loss of precision of the numerical integrations that are necessary. Voronoi atoms have also been used by Fonseca Guerra and coworkers as a way to define the so-called Voronoi deformation density (VDD) charges.[50] Among their many applications, they have been used to unravel a number of reaction mechanisms and bonding types.[51,52]

As a last variant of Becke's partition, it is worth mentioning about the proposal by Köster *et al.*[53] These authors point out

10234 | *Phys. Chem. Chem. Phys.*, 2023, **25**, 10231–10262

This journal is © the Owner Societies 2023

that the computation of the $\omega_B(r)$'s in the original algorithm grows with the third power of the number of atoms, which means that their calculation can be computationally very expensive. To remedy this they employed a modification of the atomic weight functions proposed by R. E. Stratmann et al.[54] that involves replacing the $p_1(\mu)$ expression used by Becke by another functions $q_1(\mu;a)$, defined as $q_1(\mu;a) = -1$, $q_1(\mu;a) = (3/2)(\mu/a) - (1/2)(\mu/a)^3$, and $q_1(\mu;a) = +1$ for $\mu \leq -a$, $-a < \mu < a$ and $\mu \geq a$, respectively. Moreover, they iterate this function three times to arrive finally at the function $s(\mu;a) = \frac{1}{2}[1 - p\{p[q(\mu;a)]\}]$, which is the analogous to Becke's $s(\mu)$ function. Köster et al. choose $a = 0.7$. The different definition of q_1 depending on the value of μ dramatically reduces the CPU time required to construct the integration grids.

We stress that both Becke and Voronoi-like decompositions are geometric constructions lacking physical meaning. Their usefulness lies in their computational efficiency, or, as in TCFV, in its resemblance to other physically rooted decompositions, like that provided by the QTAIM. A radically different way of dividing the real space into fuzzy atoms is the one proposed by Hirshfeld as soon as in 1977.[55] In order to carry out a population analysis in molecules, Hirshfeld introduced the reasonable idea that, at each point in space, the ratio between the density of one of the atoms ($\rho_A(r)$) and the total electron density ($\rho(r)$) should be the same as the ratio between the atomic density of the isolated atom A ($\rho_A^0(r)$) and the so-called promolecular density $\left(\rho^0(r) = \sum_A \rho_A^0(r)\right)$. In other words

$$\frac{\rho_A(r)}{\rho(r)} = \frac{\rho_A^0(r)}{\sum_A \rho_A^0(r)} = \omega_A(r) \Rightarrow \rho_A(r) = \omega_A(r)\rho(r). \quad (2)$$

The $\rho_A^0(r)$'s are usually taken as the spherically averaged atomic densities of neutral atoms.

An outstanding virtue of the atomic densities defined by eqn (2) is that they minimize the Kullback–Leibler entropy deficiency functional,[56] defined by $S = \sum_A \int \rho_A(r) \ln \left(\rho_A(r)/\rho_A^0(r)\right) dr$, so that these $\rho_A(r)$'s best preserve the information contained in the reference $\rho_A^0(r)$'s. This property places Hirshfeld's and related atoms among the very limited category of atoms-in-the-molecule that satisfy the physical properties or mathematical constraints. We refer the reader to the works of R. Nalewajski regarding the information on theoric treatment of chemical bonding.[57] The original Hirshfeld partition exhibits some clear deficiencies. One of them is the strong dependence of the final electron population of the atoms-in-the-molecule (AIM) on the densities of isolated atoms, which is given by $\bar{n}_A = \int \omega_A(r)\rho(r)dr \equiv \int \rho_A(r)dr$. For instance, the $\bar{n}_{Na}$ and $\bar{n}_{Cl}$ values in the NaCl molecule, when the neutral $\rho_{Na^0}^0$ and $\rho_{Cl^0}^0$ densities of the isolated atoms are used to construct $\rho^0(r)$, are very different from those obtained when the ionic references $\rho_{Na^+}^0$ and $\rho_{Cl^-}^0$ are employed. In the first case, the net charges $q_{Na} = Z_{Na} - \bar{n}_{Na}$ and $q_{Cl} = Z_{Cl} - \bar{n}_{Cl}$ are too small, and far from the values obtained when $\rho_{Na^+}^0$ and $\rho_{Cl^-}^0$ are used in the method. It seems that Hirshfeld's original method tends to provide atomic charges close to those of the isolated atomic densities, and hence it does not account properly for ionic interactions.

There are several recent proposals aimed at improving Hirshfeld's original method. For instance, Bultinck et al.,[58] in an attempt to minimize the strong dependence of the values of the $\bar{n}_A$'s on the atomic densities of isolated atoms, proposed the iterative Hirshfeld partition (Hirshfeld-I). As in the original method, the starting point (iteration zero) is computing the $\omega_A(r)$'s given in eqn (2) from some reference atomic densities $\rho_A^{(0)}(r)$'s. Let us call these initial weights $\omega_A^{(0)}(r)$. They are customary taken as the atomic densities of the isolated neutral atoms, although it has been proven that the final results do not depend on this choice. Next, the net charges of the atoms are computed as $q_A = Z_A - \bar{n}_A^{(1)} = Z_A - \int \rho(r)\omega_A^{(0)}(r)dr$. If $q_A \geq 0$, a new reference atomic density for A is obtained as $\rho_A^{(1)}(r) = (1 - \lambda)\rho_A^{[q_A]}(r) + \lambda\rho_A^{[q_A]+1}(r)$, where $\lambda = q_A - [q_A]$ and $[q_A]$ stands for the integer part of q_A. This procedure is nothing but taking the new reference atomic density for atom A as equal to the interpolated value between the isolated densities of ions with net charges $[q_A]$ and $[q_A] + 1$. An analogous recipe is used in case that $q_A < 0$. Then, improved weight functions $\omega_A^{(1)}(r) = \rho_A^{(1)}(r) \Big/ \sum_A \rho_A^{(1)}(r)$ are obtained, and from them new net charges as $q_A = Z_A - \bar{n}_A^{(2)} = Z_A - \int \rho(r)\omega_A^{(1)}(r)dr$, in an iterative process that converges when the q_A's in two successive cycles are less than a threshold value. A fast iterative procedure has been developed,[59] based on Newton's method, which allows the convergence of the process to be achieved in very few cycles (normally, less than 10). An important point of Hirshfeld-I method is that the final atomic densities $\rho_A(r)$ yield total electron populations of the atoms-in-the-molecule similar to those provided by the atomic references used to calculate the $\omega_A(r)$ weights of the last cycle. Better variants that try to improve on still present caveats have also been published, like in the variational Hirshfeld method proposed by Heidar-Zadeh and coworkers.[60] We will not extend here any more discussing the progressive improvements of Hirshfeld's method. For further information, we refer the reader to ref. 60. We notice that close to fifty years after Hirshfeld's original idea, the literature is riddled with a number of modified Hirshfeld rules that make it difficult for a non-expert to choose among them. This should be contrasted with QTAIM atoms, that have remained constant over that period of time.

Another procedure to obtain atomic densities $\rho_A(r)$, very similar in spirit to the one just discussed, although formally different in its implementation is the iterative stockholder partitioning.[61] Contrary to Hirshfeld-like methods, it does not require any calculation of the atomic densities of isolated atoms. It starts assuming $\omega_A(r)$'s equal to 1 for all the atoms. Then, initial atomic densities are obtained by using

$$\rho_A(r) = \left(\omega_A(r) \Big/ \sum_A \omega_A(r)\right) \times \rho(r) \quad (3)$$

This journal is © the Owner Societies 2023

Phys. Chem. Chem. Phys., 2023, **25**, 10231–10262 | **10235**

These atomic densities are then spherically averaged around their respective nuclei and taken as the next generation of atomic weights,

$$\omega_{\mathrm{A}}(\boldsymbol{r}) = \frac{1}{4\pi}\int \sin(\theta_{\mathrm{A}})\mathrm{d}\theta_{\mathrm{A}}\mathrm{d}\phi_{\mathrm{A}}\rho_{\mathrm{A}}(\boldsymbol{r}) \equiv \langle\rho_{\mathrm{A}}(\boldsymbol{r})\rangle_a. \qquad (4)$$

The above integration is performed numerically and $\boldsymbol{r}$ refers to the absolute position of an electron. The integral itself, however, depends only on r_{A}, the distance from nucleus A to the point $\boldsymbol{r}$. Eqn (3) and (4) are applied until convergence.

All the partitions discussed so far, and also several unreported variants of them, require numerical integrations. In the case of Becke-like partitions, the method was designed to recover a global expectation value (typically, the exchange–correlation energy) by adding up all the atomic components. Many algorithms have been published to perform such integrations, but describing them is beyond the scope of this paper. We only want to point out that they can be grouped into two large families: those used for exhaustive partitions of R^3 (typically, although not exclusively, the QTAIM partition) and those specifically focused on space partitions in fuzzy atoms.

To conclude this subsection, we must finally mention some other procedures that, albeit not strictly being atomic partitions of real space, have been widely used over the years, or are relevant to this particular work. Of course, it is mandatory to mention Mulliken's partition, used almost exclusively in the context of population analyses, and conventionally defined by $\rho(\boldsymbol{r}) = \sum_{\mathrm{A}} \rho_{\mathrm{A}}(\boldsymbol{r})$ with $\rho_{\mathrm{A}}(\boldsymbol{r}) = \sum_{i,j} \rho_{ij}^{\mathrm{A}}\phi_i(\boldsymbol{r})\phi_j(\boldsymbol{r})$, where the ϕ's are nucleus-centered primitive functions, ρ_{ij} are density matrix elements, and $\rho_{ij}^{\mathrm{A}} = \rho_{ij}$, $\rho_{ij}^{\mathrm{A}} = 0$ or $\rho_{ij}^{\mathrm{A}} = (1/2)\rho_{ij}$ when both ϕ_i and ϕ_j, none of them, or only one of them (ϕ_i or ϕ_j) are centered at nucleus A, respectively. Formally similar to Mulliken's atoms are the minimal deformation atoms defined by Fernández-Rico et al.,[62] called deformed atoms-in-molecules (DAM) by these authors. They are determined by requiring that each bicentric contributions to $\rho(\boldsymbol{r})$ has a minimal deformation. In the end, this criterion leads also to $\rho(\boldsymbol{r}) = \sum_{\mathrm{A}} \rho_{\mathrm{A}}(\boldsymbol{r})$ and $\rho_{\mathrm{A}}(\boldsymbol{r}) = \sum_{i,j} \rho_{ij}^{\mathrm{A}}\phi_i(\boldsymbol{r})\phi_j(\boldsymbol{r})$, where ρ_{ij}^{A} takes the same values as in Mulliken's atoms, except when only ϕ_i or ϕ_j is centered at A, in which case $\rho_{ij}^{\mathrm{A}} = \rho_{ij}$ if the function centered at A is the one with the largest exponent, and zero otherwise.

A comparison between the ω_{A} weights for the C and O atoms of the CO molecule in some of the partitions discussed so far is found in Fig. 1 (mod-H is a variant of the Hirshfeld partition that has not been discussed here). As we can see, TFVC with $k = 3$ is the only case for which $\omega_{\mathrm{C}} = \omega_{\mathrm{O}} = 0.5$ at the BCP (denoted by a solid vertical line at about $0.66a_0$). At this point the QTAIM weight for the C (O) atom changes abruptly from 1 (0) to 0 (1). Although the figure illustrates the behavior of ω_{C} and ω_{O} only along the internuclear axis, it seems clear how the resemblance between the QTAIM and TFVC partitions increases as k grows.

An important difference between fuzzy and non-fuzzy atoms is illustrated in Fig. 2, where we have lotted the atomic density of the left-H atom of the H2 molecule in four different
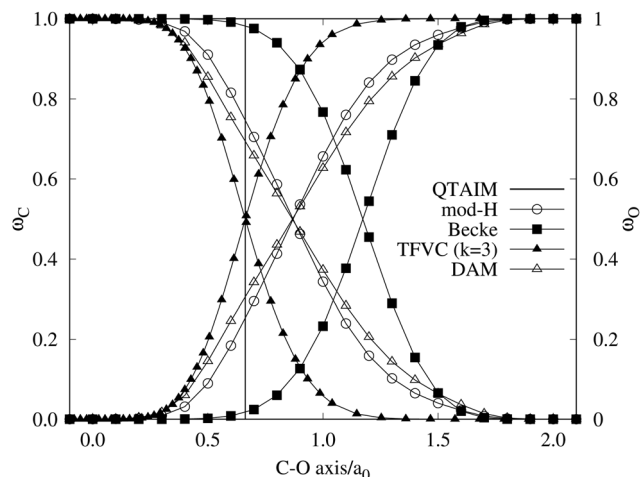

Fig. 1 Hartree-Fock (HF) TZV(2p,3d)++ atomic weight functions $\omega_{\mathrm{A}}(\boldsymbol{r})$ for carbon (A=C) and oxygen (A=O) atoms of the CO molecule along the internuclear axis. C and O nuclei are at the -0.0424 and -2.0424 positions along the C–O axis, respectively. Labels Becke, TFVC ($k = 3$), and DAM stand for the original Becke's partition with Bragg–Slater radii, the modified Becke's partition with topological atoms, defined in the text as topological fuzzy Voronoi cell (TFVC) partition, and the deformed atoms in molecules (DAM) by Fernández-Rico et al., respectively. mod-H refers to a modified Hirshfeld partition not described in the text. Reprinted with permission from J. Chem. Theory Comput., 2006, **2**, 90–102. Copyright 2006 American Chemical Society.

partitions. We can see that the DAM density considerably invades the right part of the figure, that belongs in the QTAIM partition to the right-H atom. To a lesser extent, this situation also happens in the other two fuzzy partitions of the figure (Becke and mod-H). This behavior of overlapping atomic densities is general: fuzzy atoms display appreciable values in areas that, according to the QTAIM exhaustive partition, should be associated with other atomic moieties. Although orbital
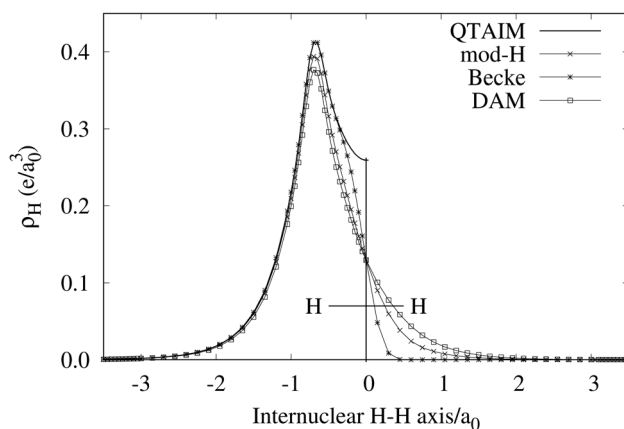

Fig. 2 CAS[2,2]/6-311G(p) atomic density for the left H atom of H2 along the internuclear axis. Left and right H atoms are at -0.7 and $+0.7a_0$, respectively. Labels Becke and DAM have been defined in the text. mod-H refers to a modified Hirshfeld partition not described in the text. CAS[n,m] stands for a complete active space calculation with n electrons in m spin–orbitals. Reprinted with permission from J. Chem. Theory Comput., 2006, **2**, 90–102. Copyright 2006 American Chemical Society.

interpenetration is at the core of chemical thinking, fuzzy atoms seem to be less suitable than non-fuzzy ones as chemical bonding issues are regarded.[14]

3 The two faces of bonding: electron counting and energy decomposition

Once a suitable decomposition of a molecular system into atoms has been chosen, *i.e.*, once a set of atomic weights ω_A has been adopted, all expectation values can be partitioned into domain contributions. In order to simplify as much as possible, we will only consider spin independent operators in what follows. Let us take a general symmetric n-electron operator

$$\hat{O} = \sum_{i_1 < i_2 \ldots < i_n} \hat{o}(\mathbf{r}_{i_1}, \ldots, \mathbf{r}_{i_n}). \tag{5}$$

The structure of this expression includes, for instance, both the kinetic energy, $\hat{T} = \sum_i \nabla_{\mathbf{r}_i}^2$, as well as the interelectron repulsion $\hat{G} = \sum_{i < j} r_{ij}^{-1}$ operators. Defining the nth order reduced density matrix (nRDM) (in McWeeny's normalization convention),[63] as

$$\rho_n(1,\ldots,n;1',\ldots,n') = \binom{N}{n} n! \int \Psi^*(1',\ldots,N')\Psi(1,\ldots,N)d_{n+1}\cdots d_N, \tag{6}$$

where we have abbreviated spin-spatial coordinate $\mathbf{x}_i$ as i, and then the expectation value of operator $\hat{O}$ is given by

$$\langle O \rangle = \frac{1}{n!}\int \hat{o}\, \rho_n(1,\ldots,n;1',\ldots,n')\,d1\cdots dn. \tag{7}$$

As it is customarily done, in this last expression, the operator acts on unprimed coordinates, after which the primed coordinates are equated to the unprimed ones before integration. Partitioning now the position of each electron into atomic regions, *i.e.* introducing a $\sum_A \omega_A(\mathbf{r}_i) = 1$ term for each electron coordinate, we arrive at a general atomic partition of $\langle O \rangle$:

$$\langle O \rangle = \frac{1}{n!}\sum_{A_1}\cdots\sum_{A_n} O_{A_1,\ldots A_n}, \tag{8}$$

where $O_{A_1,\ldots A_n} = \int \omega_{A_1}(1)\cdots\omega_{A_n}(n)\hat{o}\,\rho_n(1,\ldots,n;1',\ldots,n')\,d1\ldots dn$.

In this way, the expectation value of any one-electron operator will become a sum of atomic components, that of a two-electron operator a sum of pairwise additive interatomic terms, *etc.* Typically, but not necessarily, it is the expectation value of the density matrices themselves as well as of the Hamiltonian of the system that are decomposed into atomic contributions. In the first case we come to the electron counting perspective of chemical bonding that divides the number of electrons or electron tuples (pairs, trios, *etc.*) in an atomic-wise manner. Taken to the limit, when each of the N electrons is integrated over some atomic domain, we come to the probability of finding a given partition of the electrons into the m nuclei of the system, what it has been called an electron distribution function (see below).[64] If the one particle density (the diagonal 1RDM) or the electron density (ρ or 1RD) are integrated, we arrive at a population analysis. Similarly, if the pair density (the 2RD) is integrated over two different atomic regions, we get the number of electron pairs between them, N_{AB}, a figure that can be compared to the product of the average electron populations, $N_A \times N_B$.[65] This product would provide the number of pairs if the electron populations of the two centers would be statistically independent. The difference $N_{AB} - N_A N_B$ is thus a measure of the number of pairs shared between the atoms, a quantity that chemists associate with Lewis pairs and with bond orders. Note that this is actually a covariance. Descriptors based on the fluctuation of electron populations lie at the heart of the success of electron counting rules, and can be accessed through the so-called cumulant density matrices (CDMs).

In this regard, Mayer[66] defined a bond order that takes into account the fact that, for atoms which interact with each other, the expectation value $\langle \hat{N}_A \hat{N}_B \rangle$ differs from the product $\langle \hat{N}_A \rangle \times \langle \hat{N}_b \rangle$, where $\hat{N}_A$ and $\hat{N}_B$ are the atomic electron population operators of atoms A and B, respectively. By using a second quantization formalism for non-orthogonal orbitals, he obtained $\delta^{AB} = -2[\langle \hat{N}_A \hat{N}_B \rangle - \langle \hat{N}_A \rangle \times \langle \hat{N}_b \rangle]$. Shortly after, Giambiagi *et al.*[67] rewrote Mayer's expression in the equivalent form $\delta^{AB} = -2 \langle (\hat{N}_A - \langle \hat{N}_A \rangle) \times (\hat{N}_B - \langle \hat{N}_B \rangle) \rangle$, which gives the bond order a clear statistical interpretation, as it measures the correlation between the charge fluctuations on the individual atoms, vanishing when the motions of the electrons in A are independent from the motions of the electrons in B. Some years later, Angyan *et al.*[68] made a comparison between two possible definitions of the bond order: the one derived from the exchange part of the two-particle density matrix and the other expressed as the covariance of the number of electrons between the atomic centers. Both definitions lead to identical formulae, although they predict different δ^{AB}'s for correlated wavefunctions, as a consequence of excluding the correlation component of the two-particle density matrix. Actually, the fluctuation-based definition of the bond order had alreay been proposed in the seventies by Julg and Julg.[69]

If, in contrast, it is the Hamiltonian $\hat{H}$ that is partitioned, we arrive at a decomposition of the total energy in real space. Provided that the standard Coulomb Hamiltonian contains both one-electron (*e.g.* the kinetic energy and electron–nucleus attraction) as well as two-electron operators like the interelectron repulsion, the total energy will be written as a sum of intra- and inter-atomic terms. Separating these two types of contributions is the origin of the interacting quantum atoms (IQA) approach,[14,70] which is probably the only orbital invariant energy decomposition scheme available at this time. As the only non-local operator in $\hat{H}$ is the kinetic energy, the only RDMs needed to perform an IQA decomposition are the non-diagonal 1RDM and the diagonal 2RDM.

We notice that, save the kinetic energy, which is a non-multiplicative operator that modifies non-trivially the 1RDM on which it acts, both the electron–nucleus and electron–electron interactions behave as distance-*scaled* RDMs. Thus, a close relationship between electron-counting descriptors, which depend on domain-averaged RDMs, and some IQA energetic

This journal is © the Owner Societies 2023

Phys. Chem. Chem. Phys., 2023, **25**, 10231–10262 | **10237**

terms exists. This provides a formal justification of the well-known bond-order bond-energy (BEBO) relationships.[71]

3.1 Cumulant densities and density matrices

The nth-order cumulant density matrix (nCDM),[72] ρ_n^c, is obtained after extracting from the nRDM, ρ_n, all those components that can be expressed in terms of RDMs of orders lower than n. If the same procedure is done with the diagonal components or reduced densities (RDs), the so-called cumulant densities (nCDs) are obtained. nCDs and nCDMs contain information about the n-electron correlations in the system. As Paul Ziesche[73] has shown, these objects are actually the generators of the n-particle fluctuations of the electron distribution. In this sense, nCDs are intimately linked to the previously commented electron distribution functions,[64,74,75] see below. Expressions for several cumulants can be found in ref. 76. The first, second and third order ones are, respectively,

$$\rho_1^c(\boldsymbol{r}_1) = \rho_1(\boldsymbol{r}_1), \tag{9}$$

$$\rho_2^c(\boldsymbol{r}_1,\boldsymbol{r}_2) = \rho_1(\boldsymbol{r}_1)\rho_1(\boldsymbol{r}_2) - \rho_2(\boldsymbol{r}_1,\boldsymbol{r}_2), \tag{10}$$

$$\rho_3^c(\boldsymbol{r}_1,\boldsymbol{r}_2,\boldsymbol{r}_3) = \rho_1\rho_2\rho_3 - \frac{1}{2}\hat{S}\rho_1\rho_{23} + \frac{1}{2}\rho_{123}, \tag{11}$$

where $\hat{S}\rho_1\rho_{23} = \rho_1\rho_{23} + \rho_2\rho_{13} + \rho_3\rho_{12}$ are symmetrized products, and ρ_i, ρ_{ij}, and ρ_{ijk} are abbreviations for $\rho_1(\boldsymbol{r}_i)$, $\rho_2(\boldsymbol{r}_i,\boldsymbol{r}_j)$, and $\rho_3(\boldsymbol{r}_i,\boldsymbol{r}_j,\boldsymbol{r}_k)$, respectively. The first order cumulant density is just the electron density, and the second order one coincides with the so-called exchange–correlation density, ρ_2^{xc}, which is immediately related to the McWeeny's exchange–correlation hole:

$$h_{xc}(\boldsymbol{r}_2|\boldsymbol{r}_1) = -\frac{\rho_{xc}(\boldsymbol{r}_1,\boldsymbol{r}_2)}{\rho_1(\boldsymbol{r}_1)} = \frac{\rho_2(\boldsymbol{r}_1,\boldsymbol{r}_2)}{\rho_1(\boldsymbol{r}_1)} - \rho_1(\boldsymbol{r}_2), \tag{12}$$

that measures the difference between the (conditional) probability density of finding an electron at $\boldsymbol{r}_2$ when another is located at $\boldsymbol{r}_1$ and the unconditional one, *i.e.* how the presence of an electron at $\boldsymbol{r}_1$ influences another at $\boldsymbol{r}_2$. Note that the hole integrates to one electron while the exchange–correlation density integrates to the total number of electrons in the system, N.

A relevant feature of nCDs is their extensivity, which allows ρ_{n-1}^c to be obtained from ρ_n^c by integrating out the nth electron:

$$\rho_{n-1}^c(\boldsymbol{r}_1,\ldots,\boldsymbol{r}_{n-1}) = \int \rho_n^c(\boldsymbol{r}_1,\boldsymbol{r}_2,\ldots,\boldsymbol{r}_n)\mathrm{d}\boldsymbol{r}_n. \tag{13}$$

If we recursively apply this relation to electrons n, $n-1,\ldots$, 1 we obtain

$$\int \rho_n^c(\boldsymbol{r}_1,\ldots,\boldsymbol{r}_n)\mathrm{d}\boldsymbol{r}_1\cdots\mathrm{d}\boldsymbol{r}_n = N. \tag{14}$$

Thus, a partition of any nCD into atomic contributions by integrating each of its electron coordinates over a given region provides a decomposition of the N electrons to which the cumulant integrates to, into atomic terms:

$$N = \sum_{A_1}\sum_{A_2}\cdots\sum_{A_n} N_{A_1 A_2\cdots A_n}. \tag{15}$$

The $N_{A_1 A_2\cdots A_n}$ terms in the above expression, with all A_i's different, are n-center generalizations of the N_{AB} two-center

populations, and provide the number of electrons involved in n-center fluctuations/delocalization/bonding. This provides the basis for introducing a hierarchy of electron counting techniques, which lead to the multicenter bonding indices initially introduced by Giambiagi, Bochicchio, Ponec, Bultinck, Matito, Solà and other authors.[77–80] We start by discussing electron counting issues, and move afterwards to energetic ones. The formalism of reduced density matrices of different orders as well as the nCDMs, particularly the second order one, has been widely employed by Alcoba, Bochicchio, Lain, Torre, and others, in the analysis of local spins, the definition of several population analyses and covalent bond-order definitions, atomic valences, or the effectively unpaired electron density,[81–86] using both orbital-based (Mulliken) as well as topological partitions of space.

4 Electron counting

Armed with electrons as well as with energy partitioning, we will now consider how this general framework has been used to build insight into chemical bonding problems. Almost all the results that we will review have been obtained with the exhaustive QTAIM partition, although we stress that, as shown, the underlying methodology can be equally applied to any other partition.

4.1 Electron-number distribution functions

As explained in Section 3, any integral in which a given nRDM or nRD appears as part of the integrand can be appropriately partitioned into atomic (fuzzy or non-fuzzy) contributions. To put it bluntly, an arbitrary function $F(\boldsymbol{r}_1,\ldots,\boldsymbol{r}_N)$, where N is the number of electrons, can be expressed as a sum of m^N contributions, being m the number of atoms of the system:

$$F(\boldsymbol{r}_1,\ldots,\boldsymbol{r}_N) = \sum_{B_1}^m\cdots\sum_{B_N}^m F_{B_1\cdots B_N}(\boldsymbol{r}_1,\ldots,\boldsymbol{r}_N), \tag{16}$$

where

$$F_{B_1\cdots B_N}(\boldsymbol{r}_1,\ldots,\boldsymbol{r}_N) = \omega_{B_1}(\boldsymbol{r}_1)\cdots\omega_{B_N}(\boldsymbol{r}_N)F(\boldsymbol{r}_1,\ldots,\boldsymbol{r}_N). \tag{17}$$

Taking $F(\boldsymbol{r}_1,\ldots,\boldsymbol{r}_N) = 1$, it is evident that, just as eqn (1) performs a partition of R^3 into m domains, eqn (16) defines a partition of the $3N$-dimensional space into m^N regions. Suppose now that we have a normalized N-electron wavefunction Ψ that (for the time being) depends only on the spatial coordinates $\boldsymbol{r}_1,\ldots,\boldsymbol{r}_N$, and take $F(\boldsymbol{r}_1,\ldots,\boldsymbol{r}_N) = \Psi^*(\boldsymbol{r}_1,\ldots,\boldsymbol{r}_N)\Psi(\boldsymbol{r}_1,\ldots,\boldsymbol{r}_N)$, which is nothing but an scaled nRDM, then

$$\sum_{B_1}^m\cdots\sum_{B_N}^m\int\mathrm{d}\boldsymbol{r}_1\cdots\mathrm{d}\boldsymbol{r}_N F_{B_1\cdots B_N}(\boldsymbol{r}_1,\ldots,\boldsymbol{r}_N) = 1. \tag{18}$$

Furthermore, assume that n_1 values of the B_i's are equal to Ω_1, n_2 values are equal to $\Omega_2,\ldots$ and n_m are equal to Ω_m, with $0 \leq n_i \leq N$ and $n_1 + \cdots + n_m = N$. Since $F(\boldsymbol{r}_1,\ldots,\boldsymbol{r}_N)$ is symmetric with respect to the exchange of any two of the coordinates $\boldsymbol{r}_i$ and $\boldsymbol{r}_j$, eqn (18) can then be re-written as

$$\sum_{n_1,n_2,\ldots,n_m} N!\Lambda\int\mathrm{d}\boldsymbol{r}_1\cdots\mathrm{d}\boldsymbol{r}_N F_{B_1\cdots B_N}(\boldsymbol{r}_1,\ldots,\boldsymbol{r}_N) = 1, \tag{19}$$

10238 | *Phys. Chem. Chem. Phys.*, 2023, **25**, 10231–10262

This journal is © the Owner Societies 2023

where $N!\Lambda = N!/[n_1! \times \cdots \times n_m!]$. The number of terms in the summation is equal to $N_{N,m} = (N + m - 1)!/[N!(m - 1)!]$ that counts all the possible ways to choose the $n_1,\ldots,n_m$ set of electron counts such that their sum is equal to N. Similarly, the factor $N!\Lambda$ simply counts the number of different possibilities of choosing the B_i fragments such that n_1 of them coincide with Ω_1, n_2 with Ω_2, and so on. Without any loss of generality it can be assumed that $B_1 = \cdots = B_{n_1} = \Omega_1$, $B_{n_2+1} = \cdots = B_{n_1+n_2} = \Omega_2$, and the last n_m domains are equal to Ω_m.

Eqn (19) is valid for fuzzy or non-fuzzy partitions of R^3. However, in the latter case, where each $\omega_B(r)$ is 0 or 1, it is customary to write it in the form

$$\sum_{n_1, n_2, \ldots, n_m} N!\Lambda \int_D dr_1 \cdots dr_N F(r_1, \ldots, r_N) = 1, \qquad (20)$$

where D is an N-dimensional domain in which the first n_1 electrons are integrated over Ω_1, the second n_2 electrons over $\Omega_2,\ldots$ and the last n_m electrons over Ω_m. Remembering that Ψ is normalized, each term of the above sum is the probability that n_1 electrons are found in Ω_1, n_2 electrons are found in $\Omega_2,\ldots$ and n_m electrons are found in Ω_m

$$p(S) \equiv p(n_1, n_2, \ldots, n_m)$$
$$= N!\Lambda \int_D dr_1 \cdots dr_N F(r_1, \ldots, r_N). \qquad (21)$$

This statement simply arises from Born's interpretation of quantum mechanics. The set $S = (n_1, n_2, \ldots, n_m) \equiv \{n_i\}$ defines a real space resonance structure (RSRS) and, from eqn (20), the sum of all of them, as it should be, is equal to one:

$$\sum_S p(S) = 1. \qquad (22)$$

We have been assuming so far that each Ω_i identifies an *atom-in-the-molecule*. However, the ω_i's of a subset of atoms can be added up to define fragment weight functions. This means that m in all of the above can be identified with the total number of fragments in which we have grouped the atoms of the molecule. For instance, in methane (CH_4), we can define fragment 1 as the carbon atom and fragment 2 as the sum of the four hydrogen atoms. This gives $m = 2$; *i.e.* $R^3 = \Omega_1 + \Omega_2$, with $\Omega_1 \equiv \Omega = \Omega_C$ and $\Omega_1 \equiv \Omega' = \Omega_{H_1} + \Omega_{H_2} + \Omega_{H_3} + \Omega_{H_4}$. In this and all two-fragment partitions of R^3, one has $S = (n_1, n_2)$ and, since $n_1 + n_2 = N$, each RSRS is defined by just providing the number of electrons of one of the fragments; say $n_1 \equiv n$. Then, eqn (21) can be written as

$$p^\Omega(n) = \frac{N!}{n!(N-n)!} \int_\Omega dr_1 \cdots dr_n \int_{\Omega'} dr_{n+1} \cdots dr_N F(r_1, \ldots, r_N). \qquad (23)$$

Although eqn (21) is not properly a probability when the space is divided into fuzzy atoms, eqn (20) still holds in this case and, therefore, we will consider the former as a probability in what follows.

The wavefunction Ψ depends on the full set of electron coordinates $x_1, \ldots, x_N$, where $x_i = r_1 \times \sigma_i$ is the product of a spatial coordinate (r_i) and a spin variable (σ_i). Although the spin variables σ_i have not been included so far in our discussion, the generalization of eqn (21) to take them into account is easy:

$$p(S) = N!\Lambda \sum_{\sigma_1, \ldots, \sigma_N} \int_D dx_1 \cdots dx_N |\Psi(x_1, \ldots, x_N)|^2, \qquad (24)$$

where we have replaced F by $|\Psi|^2$.

As written, eqn (24) does not state what the spin for each of the n_1 electrons in Ω_1, n_2 electrons in Ω_2, *etc.* is. If the N electrons are split in two subsets of N^α α and N^β β electrons, with $N^\alpha + N^\beta = N$, a RSRS is defined now as $S = (S^\alpha; S^\beta) \equiv \{n_1^\alpha, \ldots, n_m^\alpha; n_1^\beta, \ldots, n_m^\beta\}$, $p(S) \equiv p(S^\alpha; S^\beta)$, and the probability that n_1^α α electrons lie in Ω_1, n_2^α α in Ω_2, *etc.*, and n_m^β β electrons lie in Ω_m, can be obtained by considering $2m$ domains, the first m with α spin and the last m with β spin. The result is

$$p(S) = N!\Lambda_\alpha \Lambda_\beta \int_D dx_1 \cdots dx_N |\Psi(x_1, \ldots, x_N)|^2, \qquad (25)$$

where $\Lambda_\sigma = [n_1^\sigma \times \cdots \times n_m^\sigma]^{-1}$ and $\sigma = (\alpha, \beta)$. Now, D is a N-dimensional domain such that the first n_1^α α electrons are integrated over Ω_1, the following n_2^α α electrons over $\Omega_1,\ldots$ and the last n_m^β β electrons over Ω_m. The set of all probabilities, $\{p(S)\}$, is called the electron number distribution function (EDF) of the system for the given partition. When the number of electrons of each spin in each domain is specified one speaks of a spin-resolved EDF. Otherwise, we have a spin-unresolved EDF. There are $N_{N,m} = (N + m - 1)!/[N!(m - 1)!]$ and $N_{N,m} = N_{N\alpha,m} \times N_{N\beta,m} = (N^\alpha + m - 1)!/[N^\alpha!(m - 1)!] \times (N^\beta + m - 1)!/[N^\beta!(m - 1)!]$ probabilities in the spin-unresolved and spin-resolved EDFs, respectively. From their definition, it is notorious that the spin-resolved EDFs give a more detailed information than the spin-unresolved ones, and also that the latter can be obtained by adding the spin-resolved probabilities with a given value of $n_1^\alpha + n_1^\beta$, $n_2^\alpha + n_2^\beta, \ldots$, and $n_m^\alpha + n_m^\beta$.

Fast algorithms to compute the EDF in both cases, especially when the space is partitioned into not too many regions (say $m \leq 6$) and the number of electrons is not too large ($N \leq 30$), have been developed over the years. We refer the reader to the original references to learn more about them.[64,75,87,88] For single-determinant wavefunctions (SDWs) there is no *a priori* difficulty (even for large N's) to calculate all the $p(S)$'s when the space is divided exclusively into two regions $\Omega + \Omega' = R^3$, as an explicit recursive formula was developed by Cancès *et al.*[87] For $m > 2$, there is no explicit formula to compute the EDF. However, in many circumstances, several approximations endowed with a clear physical meaning can be used. Among these, we highlight the so-called core approximation. In the present context, it can be stated as follows: if from the set of molecular orbitals (used almost universally in the construction of Ψ) a number of them are almost entirely localized on one of the fragments, we can simultaneously increase by two (one α plus one β) the number of electrons of that fragment per localized orbital and exclude them from the calculation. In this way, we can reduce the effective value of N considerably and restrict the EDF calculation to the set of *valence* electrons.

It is customary in real space chemical bonding analyses to measure the degree of localization of a (normalized) molecular orbital (MO) $\phi_i(r)$ in a region Ω by the quantity $\langle \phi_i(r) | \phi_i(r) \rangle_\Omega$,

This journal is © the Owner Societies 2023

Phys. Chem. Chem. Phys., 2023, **25**, 10231–10262 | **10239**

i.e. the overlap of this MO with itself in that region. This is the diagonal element of the atomic overlap matrix (AOM), defined by

$$S_{ji}^{*\Omega} = S_{ij}^{\Omega} = \langle \phi_i(\boldsymbol{x}) | \phi_i(\boldsymbol{x}) \rangle_{\Omega} \equiv \delta_{\sigma_i, \sigma_j} \int \omega_{\Omega}(\boldsymbol{r}) \phi_i^*(\boldsymbol{r}) \phi_j(\boldsymbol{r}) \mathrm{d}\boldsymbol{r}. \quad (26)$$

This AOM definition holds for fuzzy and non-fuzzy partitions of space. The AOM integrals in all the domains $\Omega_1, \ldots, \Omega_m$ are the basic building blocks that one needs to compute the EDF in all cases (single- or multi-determinant wavefunctions (MDW), two ($m = 2$) or more ($m > 2$) fragments, ...).

Extremely important for the analysis of chemical bonding by statistical analysis of EDFs is the fact that SDWs give rise to spin-resolved EDFs with α and β subsets of electrons that behave as statistically independent entities. This means that $p(S^{\alpha}; S^{\beta})$ is given by the direct product of the α and β EDFs

$$p(S^{\alpha}; S^{\beta}) = p_{\alpha}(S^{\alpha}) \otimes p_{\beta}(S^{\beta}). \quad (27)$$

This is no longer true for MDWs. However, even in this case, there is a certain degree of α–β statistical independence which greatly facilitates the calculation of the spin-resolved EDF. When Ψ is a MDW we can write it, in general, as

$$\Psi = \sum_r c_r \psi_r, \quad (28)$$

where c_r are (variational or fixed-by-symmetry) coefficients and ψ_r is a Slater determinant built with N-spin orbitals $\phi_1^r, \ldots, \phi_N^r$. When Ψ in eqn (25) is replaced by the above expression, the spin-resolved EDF results[89]

$$p(S) = \sum_{r,s} c_r^* c_s p^{rs}(S^{\alpha}; S^{\beta}), \quad (29)$$

where

$$p^{rs}(S^{\alpha}; S^{\beta}) = N! \Lambda_{\alpha} \Lambda_{\beta} \int_D \mathrm{d}\boldsymbol{x}_1 \ldots \mathrm{d}\boldsymbol{x}_N \psi_r^* \psi_s, \quad (30)$$

and it turns out that it can be written as the direct product of the corresponding components for both spins, $p^{rs}(S^{\alpha}; S^{\beta}) = p_{\alpha}^{rs}(S^{\alpha}) \otimes p_{\beta}^{rs}(S^{\beta})$. Actually, the computational time required to perform this direct product is an important fraction of that needed to obtain the full EDF, especially when the total number of α and β probabilities is very high. In addition to the core approximation that we have already discussed, much computer time can also be saved by neglecting in eqn (28) those determinants with coefficients c_r smaller (in absolute value) than a certain threshold value ε_r, or those rs terms in the sum 29 for which $|c_r^* c_s| < \varepsilon_{rs}$, where ε_{rs} is another (small) threshold value.

Probabilities for single domains obtained through the Cancès fast algorithm[87] have been widely used both using QTAIM and ELF basins.[90] They have also been employed to define a new type of spatial partitioning in which general regions that maximize the probability of finding a given number of electrons are obtained through shape optimization techniques. These have been called maximum probability domains (MPDs),[91] and have been examined in molecules[92,93] in the mean-field regime, and also in solids.[94] MPDs have great potential in the translation of chemical concepts, like the

electron pair of Lewis, to the orbital invariant realm, but are notoriously difficult to compute and to generalize to the correlated regime.[95] Some efforts to elucidate their properties and usefulness in the case of strong correlation have been made through the use of model Hamiltonians like that of Hubbard.[96,97]

4.1.1 Chemical bonding from the statistical analysis of EDFs. Once the EDF of a molecule is available, it is possible to use it to obtain all kinds of statistical information about it. As an example, if all the m-fragment probabilities $p(n_1, n_2, \ldots, n_m)$ are known, the marginal probabilities of having n_1 electrons in Ω_1, n_2 electrons in $\Omega_2, \ldots$, and n_{m-1} electrons in Ω_{m-1} irrespective of the value of n_m are provided by

$$p(n_1, \ldots, n_{m-1}) = \sum_{n_m} p(n_1, n_2, \ldots, n_m). \quad (31)$$

The one-fragment EDF can be obtained as

$$p(n_1) = \sum_{n_2, \ldots, n_m} p(n_1, n_2, \ldots, n_m), \quad \text{or} \quad (32)$$

$$p(n_1) = \sum_{n_2} p(n_1, n_2). \quad (33)$$

We can obviously join several fragments into a single one, and add the probabilities in a different way. For instance, if the EDF for a partition $R^3 = \Omega_1 + \Omega_2 + \Omega_3$ (*i.e.* $m = 3$) is known, and we join Ω_1 and Ω_2 into a new fragment $\Omega' = \Omega_1 \cup \Omega_2$, the $p(n', n_3)$'s are given by

$$p\left(n_1', n_3\right) = \sum_{\substack{n_1, n_2 \\ n_1 + n_2 = n_{1'}}} p(n_1, n_2, n_3). \quad (34)$$

In short, all the probabilities for a given partition are immediately accessible if those for a partition with a larger number of fragments are known.

Now, let us show how EDFs can provide valuable chemical bonding information. If we start from the one-center condensed probabilities, the $p^{\Omega}(n)$ values for a given fragment Ω allow immediate recovery of its average electron population as $\langle n_{\Omega} \rangle = \sum_{n=0}^{N} n \times p^{\Omega}(n)$, whose meaning is obvious: we simply multiply each possible value of the number of electrons in $\Omega(n)$ by its probability of occurrence ($p^{\Omega}(n)$) and carry out the sum for all ns. This value coincides with that obtained by integrating in R^3 the density of the fragment,

$$\langle n_{\Omega} \rangle = \sum_{n=0}^{N} n \times p^{\Omega}(n) = \int \rho_{\Omega}(\boldsymbol{r}) \mathrm{d}\boldsymbol{r}, \quad (35)$$

where $\rho_{\Omega}(\boldsymbol{r}) = \sum_{A \in \Omega} \rho_A(\boldsymbol{r}) = \rho(\boldsymbol{r}) \sum_{A \in \Omega} \omega_A(\boldsymbol{r})$. The sum over A extends to all the atoms that belong to Ω. In non-fuzzy partitions (in the QTAIM, for instance), the integral in eqn (35) amounts to integrating the full density $\rho(\boldsymbol{r})$ over the Ω region:

$$\int \rho_{\Omega}(\boldsymbol{r}) \mathrm{d}\boldsymbol{r} \equiv \int_{\Omega} \rho(\boldsymbol{r}) \mathrm{d}\boldsymbol{r}. \quad (36)$$

At this point we can immediately notice how the EDF expands

our knowledge about the electron distribution. A standard population analysis will simply provide us with an average number of electrons for an atom. With the use of EDFs one clearly learns that the electron population fluctuates and that the average is made up of several electron counts with different probabilities of occurrence. Once this is understood, the relevance of knowing the width of this atomic electron count distribution becomes clear. If the width is very small, the atom will display a very sharp distribution of its number of electrons. We say that its electrons are localized. If, in contrast, the width (variance) is large, these electrons must be necessarily delocalized. Where? The covariance of a two-atom joint distribution will inform us about this. Actually, the cumulants of the EDF are immediately connected with those of the nRDMs.[73,98]

For instance, just as $\langle n_\Omega \rangle$ can be obtained from the EDF or from $\rho(\boldsymbol{r})$ (eqn (35) and (36)), the average $\langle n_A n_B \rangle$, where A and B are any two atoms of the system, can be computed in two different ways:

$$\langle n_A n_B = N_{AB} \rangle = \sum_S n_A n_B p(n_A, n_B) = \int \rho_2^{AB}(\boldsymbol{r}_1, \boldsymbol{r}_2)\mathrm{d}\boldsymbol{r}_1\mathrm{d}\boldsymbol{r}_2, \quad (37)$$

where $\rho_2^{AB}(\boldsymbol{r}_1,\boldsymbol{r}_2) = \omega_A(\boldsymbol{r}_1)\omega_B(\boldsymbol{r}_2)\rho_2(\boldsymbol{r}_1,\boldsymbol{r}_2)$. The covariance $\langle n_A n_B \rangle - \langle n_A \rangle \langle n_B \rangle = \langle (n_A - N_A)(n_B - N_B) \rangle$ (with $N_A \equiv \langle n_A \rangle$ and $N_B \equiv \langle n_B \rangle$) is a measure of the statistical independence between the two atoms. Note that this is the difference $N_{AB} - N_A N_B$ commented above. In the QTAIM, a scaled value of this fluctuation is called the delocalization index (DI) δ^{AB}[99,100]

$$\delta^{AB} = -2\mathrm{cov}(n_A, n_B) = -2\langle (n_A - N_A)(n_B - N_B) \rangle, \quad \text{or} \quad (38)$$

$$= +2\int_A \mathrm{d}\boldsymbol{r}_1 \int_B \mathrm{d}\boldsymbol{r}_2\, \rho_{xc}(\boldsymbol{r}_1, \boldsymbol{r}_2). \quad (39)$$

Thus, the second order cumulant of the probability distribution function is directly related to the atomic-condensed integral of the second order cumulant density. Similar, albeit more cumbersome, relationships exist between the nth order cumulant of the EDFs and integrals of the nCDs, which are used to define multicenter bond orders.[78] We note in passing that electron population fluctuations in spatial domains have been used many times in the literature to quantify electron localization and delocalization.[101,102] It is the fine-grained nature of the EDFs that provides a new look at their intimate nature.

When the electron populations of A and B are independent of each other, one has $p(n_A, n_B) = p(n_A) \times p(n_B)$, and then $\mathrm{cov}(n_A, n_B) = 0$, and $\delta^{AB} = 0$. δ^{AB} is customarily associated with the bond order between A and B, since it is easy to show that when the AOMs are condensed *a là* Mulliken, it coincides with the Wiberg–Mayer[103,104] bond order. It is also closely related to the covalent interaction energy between both atoms. In a two-center molecule AB, the DI is positive definite, since an increase in the number of electrons in A (n_A) is accompanied by a decrease in n_B, and *vice versa*. In molecules with more than two atoms, this is not necessarily the case. There are situations (especially, but not only, in excited electronic states), which can be described as exotic, in which an increase in the population of one atom (say A) leads to an increase in the population of another (say B). This gives rise to positive covariances between

both atoms and, consequently, to negative DIs.[105] As a collorary, the bond order thus measures the statistical dependence of electron populations in two atoms. Similarly, a multicenter bond thus only exist if there is mutual interdependence among the electron populations of more than two atoms.

As pointed out $\delta^{AB} \geq 0$ in diatomic molecules. However, the limit case $\delta^{AB} = 0$ can only occur when there is a single $p(n_A, n_B) \neq 0$ in the molecular EDF. This behaviour can be found, for instance, in the dissociation limit ($R_{AB} \to \infty$) of the ground state of dihydrogen, where the only resonance structure with non-zero probability is that with one electron in each atom. However, one can also show that at the Hartree–Fock (HF) level, δ^{AB} does not vanish at dissociation. At this level of theory, the wavefunction of $H_2 = H_A - H_B$ at any inter-nuclear distante R_{AB} is given by the $\Psi = |\sigma_g \bar{\sigma}_g|$ and the α and β electrons are statistically independent. The probability that the α electron be found in atoms A and B is the same, by symmetry, and equal to $p_\alpha(1, 0) = p_\alpha(0, 1) = \frac{1}{2}$, and the same happens with the β electron, $p_\beta(1, 0) = p_\beta(0, 1) = \frac{1}{2}$. According to eqn (27), the spin-resolved EDF consists of four equal probabilities; namely $p(1, 0; 0, 1) = p(0, 1; 1, 0) = p(1, 0; 1, 0) = p(0, 1; 0, 1) = \frac{1}{4}$. The sum of the first two is the spinless probability of finding one electron in A and the other in B ($p(1,1)$), regardless of their spin, and the third and fourth are the probabilities of finding both electrons in A ($p(2,0)$) and B ($p(0,2)$), respectively. Eqn (35) correctly predicts that each atom has on average one electron, $\langle n_A \rangle = \langle n_B \rangle = 1$. However, eqn (38) gives $\delta^{AB} = 1$ at any R_{AB}, which is clearly wrong and highlights the well-known dissociation problem of the Hartree–Fock model when the two resulting fragments are open shells. A minimum of two determinants are necessary to correctly dissociate dihydrogen. A complete active space calculation with two electrons in two spin–orbitals (CAS[2,2]), with wavefunction $\Psi = c_1|\sigma_g \bar{\sigma}_g| + c_2|\sigma_u \bar{\sigma}_u|$, where c_1 and c_2 are variational coefficients, remedies the problem and results in δ^{AB} values very close to those of a full configuration interaction (full-CI) calculation.[98]

At the equilibrium geometry, the mixing between the $|\sigma_g \bar{\sigma}_g|$ and $|\sigma_u \bar{\sigma}_u|$ configurations in the CAS[2,2] wavefunction of dihydrogen increases $p(1,1)$ from 0.5 in the single-determinant (SD) calculation to about 0.58, and decreases $p(2,0) = p(0,2)$ to 0.21. This behaviour can be easily rationalized (see below), and is quite general. In homonuclear diatomic molecules, electron correlation tends to narrow the distribution of probabilities around its neutral atom ($N_A = N_B = N/2$) value, and this results in a decrease of δ^{AB}. Actually, in the particular case of dihydrogen, it is trivial to prove from eqn (38) and the equality $p(2,0) = p(0,2)$ that $\delta^{AB} = 4p(2,0) = 4p(0,2)$, so that the DI obviously decreases with increasing $p(1,1)$ since $p(1,1) = 1 - p(2,0) - p(0,2)$. This result can be corroborated in Table 1, which contains the EDF in dihydrogen as obtained with different methods. Notice how badly the Mulliken probabilities behave.

Another example of the decrease in δ^{AB} as the width of the distribution decreases can be seen in Fig. 3, where we have

This journal is © the Owner Societies 2023

Phys. Chem. Chem. Phys., 2023, **25**, 10231–10262 | **10241**

Table 1 CAS[2,2] EDF for H_2 using different space partitions. Reprinted with permission from Springer Nature Customer Service Centre Gmb: Springer Nature, Theoretical Chemistry Accounts, generalized electron number distribution functions: real space *versus* orbital space descriptions, E. Francisco *et al.*, 2010

EDF	$p(2,0) = p(0,2)$	$p(1,1)$	δ^{AB}
QTAIM	0.2083	0.5833	0.8332
Becke	0.2126	0.5749	0.8502
Hirshfeld	0.2299	0.5402	0.9196
Mulliken	0.1365	0.7270	0.5460
Löwdin	0.2255	0.5490	0.9019
DAM	0.1561	0.6877	0.6245

Table 2 Hartree−Fock and correlated CAS[10,8] $p(7,7)$ values and delocalization indices, δ^{AB}, for the N_2 molecule. Reprinted with permission from Springer Nature Customer Service Centre Gmb: Springer Nature, Theoretical Chemistry Accounts, generalized electron number distribution functions: real space *versus* orbital space descriptions, E. Francisco *et al.*, 2010

	HF		CAS[10,8]	
	$p(7,7)$	δ^{AB}	$p(7,7)$	δ^{AB}
QTAIM	0.3109	3.0408	0.3937	2.0113
Becke	0.3083	3.1073	0.3738	2.2298
Hirshfeld	0.2987	3.3664	0.3415	2.6879
Mulliken	0.3160	2.9110	0.4651	1.4618
Löwdin	0.2915	3.5613	0.3389	2.7703
DAM	0.3211	2.7834	0.5225	0.9998

plotted the HF and CAS[10,8] $p(n_A,n_B)$ values for several fuzzy partitions of space, as well as in the QTAIM partition, all for the N_2 molecule. Only non-negligible probabilities ($n_A \geq 4$ or $n_B \leq 10$) are included in the figure. We observe that the HF $p(n_A,n_B)$'s are very similar in all the partitions, but differ considerably more in the correlated calculations (except $p(6,8)$, which is very similar in all the cases). If, in a simple way, we estimate the width of the distribution by the value of $p(7,7)$, we would conclude that, according to our previous arguments, the correlated δ^{AB}'s should decrease in the order Löwdin > Hirshfeld > Becke > QTAIM > Mulliken > DAM. As we can see in Table 2 this is what actually happens. The smaller differences between the HF δ^{AB}'s is a consequence of the great similarity between the HF distributions in the different partitions that we have already commented on.

4.2 Modeling EDFs

EDFs allow for an interesting classification of chemical bonds. Let us consider here only the two center case. The EDF for any

Fig. 3 Hartree-Fock and correlated EDF for N_2 according to different space partitions. Reprinted with permission from Springer Nature Customer Service Centre Gmb: Springer Nature, Theoretical Chemistry Accounts, Generalized electron number distribution functions: real space *versus* orbital space descriptions, E. Francisco *et al.*, 2010.

two-electron system divided into two fragments A and B is fully characterized by $p(2,0)$, $p(1,1)$, and $p(0,2)$, which can be collected in the vector

$$\boldsymbol{p}_2 = [p(2,0),p(1,1),p(0,2)]. \tag{40}$$

Since $p(2,0) + p(1,1) + p(0,2) = 1$, only two components of $\boldsymbol{p}_2$ are independent. As seen in the dihydrogen case, $p(2,0) = p(0,2)$, with $p(2,0) = \frac{1}{4}$ or $p(2,0) < \frac{1}{4}$ for single- and multi-determinant descriptions, respectively. These results can be immediately extended to the SD case when both fragments are dissimilar. Let π and $1 - \pi$ be the probabilities that a first electron of an α–β electron pair is in A ($p(A) = \pi$) or B ($p(B) = 1 - \pi$), respectively. Since both electrons on a SDW are independent and indistinguishable, we will have $p(2,0) = \pi^2$, $p(0,2) = (1 - \pi)^2$, and $p(1,1) = 2\pi(1 - \pi)$. To generalize these expressions to the correlated case, we can reason through a Bayesian analysis as follows.[106] Provided that one of the electrons is in A, the probability that the second one is in B is

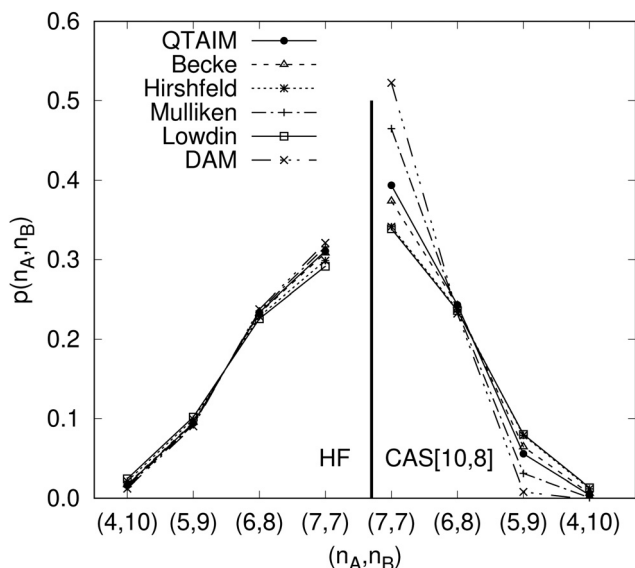$$p(B|A) = (1 + f)p(B) = (1 + f)(1 - \pi). \tag{41}$$

Similarly, we have the following expression for the conditional probability that the second electron is in A if it is for sure that the first one is in B:

$$p(A|B) = (1 + f)p(A) = (1 + f)\pi. \tag{42}$$

In eqn (41) and (42), f is a correlation factor whose value, necessarily in the range $-1 \leq f \leq +1$, measures how correlated the two electrons are. If $f = 0$, they are independent and $p(B|A) = p(B)$, $p(A|B) = p(A)$, *i.e.* the probability that one of the electrons lies in A or B does not depend on where the other electron is. Positive values of f imply that $p(A|B) > \pi$ and $p(B|A) > (1 - \pi)$. Both electrons are negatively correlated in this case and try to avoid each other: if the first one is in A(B), finding the second one in B(A) is more likely than if sites A(B) were empty. In contrast, if $f < 0$ we have $p(A|B) < \pi$ and $p(B|A) < (1 - \pi)$, and the presence of one of the electrons in A(B) increases the probability of finding the other in the same region: both electrons show a certain degree of bosonization.

The probability $p(1,1)$ is given by

$$p(1,1) = p(A|B)p(B) + p(B|A)p(A) = 2(1 + f)\pi(1 - \pi), \tag{43}$$

10242 | *Phys. Chem. Chem. Phys.*, 2023, **25**, 10231–10262

This journal is © the Owner Societies 2023

with $p(A|B)p(B) = p(B|A)p(A)$ due to electron indistinguishability. In the two limit cases $f = 1$ and $f = -1$, $p(1,1) = 4\pi(1 - \pi)$ and $p(1,1) = 0$, respectively. If, in addition, we are in the non-polar case, we have $\pi = 1 - \pi = \frac{1}{2}$, and $p(1,1) = 1$ for $f = 1$.

When an electron is in A the other is necessarily in A or B, so that $p(A|A) + p(B|A) = 1$. Similarly $p(A|B) + p(B|B) = 1$. From these two expressions and eqn (41) and (42) one obtains $p(A|A) = 1 - (1 + f)(1 - \pi)$ and $p(B|B) = 1 - (1 + f)\pi$. Finally, in addition to eqn (43) for $p(1,1)$, we have

$$p(2,0) = p(A)p(A|A) = \pi[1 - (1 + f)(1 - \pi)], \quad (44)$$

$$p(0,2) = p(B)p(B|B) = (1 - \pi)[1 - (1 + f)\pi]. \quad (45)$$

$p(2,0)$ and $p(0,2)$ can also be written as $p(2,0) = \pi^2 - \pi f(1 - \pi)$ and $p(0,2) = (1 - \pi)^2 - \pi f(1 - \pi)$, or $p(2,0) = p(2,0)^{\text{indep}} - \pi f(1 - \pi)$ and $p(0,2) = p(0,2)^{\text{indep}} - \pi f(1 - \pi)$; *i.e.* the same quantity, equal to half the increase in $p(1,1)$ due to correlation effects, must be subtracted from their corresponding independent electron values. In the end, any vector $\boldsymbol{p}_2$ is uniquely determined with two chemically relevant parameters, the net electron transfer towards site A given by $q = 2\pi - 1$, and the correlation factor f. These are easily inverted, since $f = \{p(1,1)/[2\pi(1 - \pi)]\} - 1$ and $\pi = \frac{1}{2}[1 + p(2,0) - p(0,2)]$.

If each electron has a probability $\pi \equiv S^A$ of being in A and $1 - \pi \equiv S^B = 1 - S^A$ of being in B and both electrons are independent, the three components of $\boldsymbol{p}_2$ can be obtained from the binomial distribution[106]

$$p(n_a, n_b) = \frac{2!}{n_a! n_b!}\pi^{n_a}(1 - \pi)^{n_b} \quad (46)$$

yielding $p(2,0) = p(0,2) = 1/4$ and $p(1,1) = 1/2$ in the symmetric case ($\pi = 1/2$). In a heteropolar union, one of the two fragments is more likely to retain the electrons, and the polarity parameter $\pi \neq 1/2$. In the $\pi = 0$ or $\pi = 1$ limits, $\boldsymbol{p}_2$ collapses onto $\boldsymbol{p}_2 = (0,0,1)$ and $\boldsymbol{p}_2 = (1,0,0)$, respectively. From eqn (46), $\boldsymbol{p}_2 = [\pi^2, 2\pi(1 - \pi), (1 - \pi)^2]$. This is the general expression of $\boldsymbol{p}_2$ for a (2c,2e) uncorrelated bond. A (2c,2e) bond with correlated electrons may be fully characterized from a Bayesian analysis of $\boldsymbol{p}_2$ through the π parameter (or the net electron charge transfer towards fragment A, $q = 2\pi - 1$) and a correlation factor $f = p(1,1)/[2\pi(1 - \pi)] - 1$,[106] which is the coarse-grained analogue of the standard f in density matrix theory. This is evident if the above expression is written as

$$p(1,1) = 2\pi(1 - \pi)(1 + f) = p(1,1)^{\text{indep}}[1 + f], \quad (47)$$

which is the analogue of equation $\rho^2(\boldsymbol{r}_1, \boldsymbol{r}_2) = \rho(\boldsymbol{r}_1)\rho(\boldsymbol{r}_2)[1 + f(\boldsymbol{r}_1, \boldsymbol{r}_2)]$ of density matrix theory. In this correlated case, $p(2,0) = \pi^2 - \pi(1 - \pi)f$ and $p(0,2) = (1 - \pi)^2 - \pi(1 - \pi)f$.

The correlation factor f lies in the range $-1 \leq f \leq +1$, and cleanly classifies (2c,2e) links into three categories: (1) bonds with statistically independent electrons ($f = 0$); (ii) bonds with electrons that try to avoid each other ($f > 0$ or $p(1,1) > p(1,1)^{\text{indep}}$) or normal bonds (NB); (iii) bonds with positively correlated electrons ($f < 0$ or $p(1,1) < p(1,1)^{\text{indep}}$). These are related to the charge-shifted bonds (CSBs) in valence bond

theory.[107] Note that, usually, electrons are *negatively* correlated, so that they display positive correlation factors. Up to the moment of writing, bosonized states have only been found in excited states.[105] Their electron distribution is so different from what chemists are used to that they promise to provide new insights into chemical bonding.

In the (q, f) polarity-correlation coordinates, the DI between A and B is $\delta^{AB} = 4(1 - f)\pi(1 - \pi) = (1 - f)(1 - q^2)$. Thus, non-polar ($\pi = 1/2$) NBs ($f > 0$) give $\delta^{AB} = 1 - f < 1$, and non-polar CSBs ($f < 0$) display $\delta^{AB} = 1 - f > 1$, with the limits $\delta^{AB} = 0$ and $\delta^{AB} = 2$ when $f = +1$ or $f = -1$, respectively (thus, $0 \leq \delta^{AB} \leq 2$ in non-polar bonds). The $\boldsymbol{p}_2$ vector in these two limit cases is given by $\boldsymbol{p}_2 = (0,1,0)$ and $\boldsymbol{p}_2 = (1/2,0,1/2)$. $\boldsymbol{p}_2 = (0,1,0)$ implies that, whenever one takes a picture of the system, one of the electrons lies in A and the other in B. That is, there is no electron sharing at all. In this case, interpreting δ^{AB} as a bond order is coherent. However, since $\boldsymbol{p}_2 = (1/2,0,1/2)$ means that the two electrons are either both found in A or in B, using δ^{AB} as a bond order in strongly non-binomial EDFs with $f \simeq -1$ should be undertaken with care. In this case, the electron distribution does not resemble any textbook model, and chemical intuition, which is heavily based on them, fails. Note, however, that from the point of view of the fluctuation of electron populations, δ^{AB} has the same interpretation always.

Everything we have discussed in the last paragraphs is beautifully illustrated in the triangular graphical representation of Fig. 4, where all possible two-fragment two-electron EDFs are plotted in a ternary diagram. The evolution of the delocalization index, correlation factor or net charge transferred from one
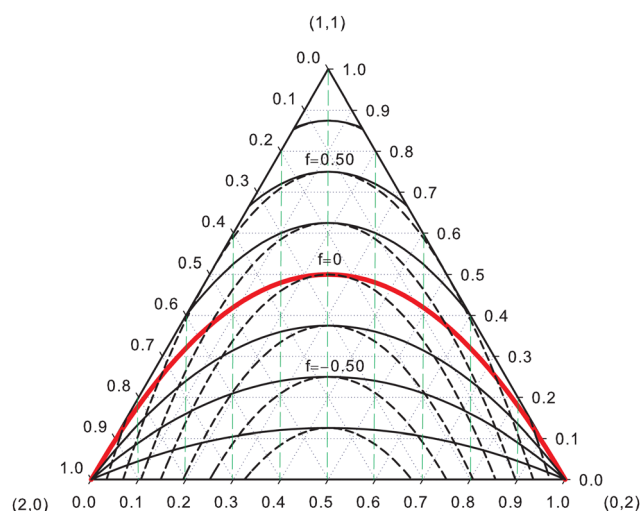

Fig. 4 Ternary representation of a two-fragment two-electron EDF. For any point inside the triangle, $p(2,0)$, $p(1,1)$, and $p(0,2)$ are given by the distances from it to the left, bottom and right sides, respectively. Isolines of f from top ($f = 1$) to bottom ($f = -1$) are represented by full solid lines at intervals of 0.25. Dashed lines, tangent to f isolines at the $p(2,0) = p(0,2)$ point, and growing from 0 (top) to 2 (bottom), in intervals of 0.25, are δ^{AB} isolines. Constants q isolines, growing from $q = -1$ (left) to $q = +1$ (right), at intervals of 0.2, are the vertical dashed green lines. The thick red solid line separates NBs (upper part) from CSBs (lower part). Reproduced from ref. 106 with permission from the Royal Society of Chemistry.

This journal is © the Owner Societies 2023

Phys. Chem. Chem. Phys., 2023, **25**, 10231–10262 | **10243**

fragment A to the other B is clearly identified. Note how the area of normal bonds with positive f values is considerably smaller (actually one third of the full area of the triangle) than that corresponding to negative correlation factors. No diatomic molecule in its ground state has been found yet to populate the negative correlation factor region.

The generalization of the above ideas to more than a single bond has already been presented.[106] The idea is to recover the full N-electron EDF, $\boldsymbol{p}_N$, in terms of the probabilities associated with a smaller number of electrons. Let us consider that the system has an even number of electrons ($N = 2n$), and assume that (a) the molecule is well described by a set of $n = N/2$ two-center, two electron (2c,2e) bonds, and (b) that all of these bonds are independent of each other. Then,

$$\boldsymbol{p}_N = \boldsymbol{p}_{2n} \simeq \otimes_{i=1}^{n} \boldsymbol{p}_2^i. \tag{48}$$

The direct product symbol ($\otimes$) in the above equation simply takes this second assumption into account. We now assume that $\boldsymbol{p}_2^i = [p^i(2,0), p^i(1,1), p^i(0,2)]$, where

$$p^i(1,1) = \pi_i(1 - \pi_i)2(1 + f_i), \tag{49}$$

$$p^i(2,0) = \pi_i^2 - \pi_i(1 - \pi_i) f_i, \tag{50}$$

$$p^i(0,2) = (1 - \pi_i)^2 - \pi_i(1 - \pi_i) f_i. \tag{51}$$

In this way, the set $\{\pi_i, f_i\}$ ($i = 1, n$) defines $\boldsymbol{p}_N$. The better the hypotheses (a) and (b), the better eqn (48) is fulfilled. The pair of atoms involved in each $\boldsymbol{p}_2^i$ can be equal or different. In the first case, one expects π_i to be close to $\frac{1}{2}$. A value of π_i exactly equal to $\frac{1}{2}$ can only occur if, in addition to both atoms being similar, they have a similar environment in the molecule. On the other hand, when the polarity of both atoms is different, π_i will deviate from its mean value, getting closer to 1 (0) when the atom A(B) is much more electronegative than B(A). The optimal set $\{\pi_i, f_i\}$ can be determined by minimizing the quantity δ, defined as

$$\delta = \sum_{S} \left[p_{\text{exact}}(S) - p_{\text{approx}}(S) \right]^2, \tag{52}$$

where $p_{\text{exact}}(S)$ are the exact probabilities and $p_{\text{approx}}(S)$ the approximated ones obtained by applying eqn (48). To exploit the above fitting strategy in those cases where one believes that hypotheses (a) and (b) are reasonably accurate, the following steps are taken: (1) A given number of types of bonds is assumed and the initial values of π_i and f_i chosen, (2) each pair of atoms of the molecule is assigned zero, one, or more of the above types, and (3) δ is minimized with respect to the $\{\pi_i, f_i\}$ parameters.

A very simple example can be used to illustrate the procedure. Let us take a hypothetical molecule $AB_2 \equiv B_1 - A - B_2$ and assume that a single (2c,2e) bond exists between the atom A and each of the two similar atoms B. Then, there exists only a type of bond and two optimizable quantities $\pi_1 = \pi_2 = \pi$ and $f_1 = f_2 = f$. The vector $\boldsymbol{p}_N$ consists of nine components $p^1(1,1)p^2(1,1)$, $p^1(1,1)p^2(2,0),\ldots$, $p^1(0,2)p^2(0,2)$. Each of these products contributes to the probability $p_{\text{approx}}(n_A, n_{B_1}, n_{B_2})$ of a specific three-center four electrons RSRS. For example,

$p^1(1,1)p^2(1,1)$ adds to $p_{\text{approx}}(2,1,1)$, $p^1(1,1)p^2(2,0)$ adds to $p_{\text{approx}}(3,1,0),\ldots$, and $p^1(0,2)p^2(0,2)$ adds to $p_{\text{approx}}(0,0,4)$.

The presence in a molecule of lone or core electron pairs on one or more of the atoms also fits into the above scheme. For instance, in the $trans$-N_2H_2 molecule, we can reasonably assume that the 1s cores of nitrogen atoms are not involved in any bond. If we set $\pi_i = 1$ and $f_i = 0$ for one of these pairs, and fix their values, its effect on $\boldsymbol{p}_N$ will be to increase the number of electrons in the corresponding atom by 2. Let us assume three types of bonds here, types 1 and 2 associated with the N–N pair, and type 3 to each N atom and the H atom closer to it. At the CAS[12,8]/6-311G(d,p) level of calculation, the results obtained after minimizing the δ quantity can be seen in Fig. 5 and Table 3. The agreement between the exact and fitted probabilities is very good. Only a few fitted $p(S)$'s deviate a little from the exact ones. As corresponds to two equivalent atoms in equivalent environments, the π value for both N–N bonds is very close to $\frac{1}{2}$ ($q \simeq 0.0$), with correlation factors being strongly positive. This results in a $p(1,1)$ probability much larger than $p(2,0) = p(0,2)$ and a $\delta_i^{N_1N_2}$ much smaller than 1.0. The π value for the N–H bond is considerably larger than 0.5, which indicates a clear polarization towards the nitrogen atom, as it is evident if we compare the $p(2,0)$ and $p(0,2)$ values: if one takes an infinite number of snapshots of the N–H bond, 48% of the time both electrons will lie within the N region. The two electrons of these N–H bonds are positively correlated ($f_i < 0$), although we suspect that the value of f_i is not very significant in this case, and that it simply absorbs other electronic delocalizations that have not been taken into account in our simple bonding model. Finally, we should notice in the final part of Table 3 that the approximate δ^{AB}'s are quite similar to the exact ones, particularly for N–H bonds. In the table, N_2–H_3 and N_1–H_4 refer to the hypothetical bonds between each N atom and the H atom farthest from it. The exact δ^{AB} for them are close to 0.0, which justifies that we have not assumed their existence in our model.
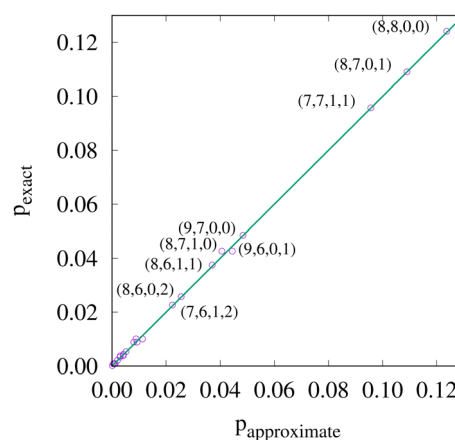

Fig. 5 Exact (y-axis) *versus* fitted (x-axis) EDF for N_2H_2 at the CAS[12,8]/6-311G(d,p) level of calculation. Only non-equivalent probabilities with $p_{\text{exact}} > 0.02$ are labeled. The four integers on each label are the number of electrons in N_1, N_2, H_1, and H_2.

Table 3 Parameters of the EDF fitting of N_2H_2 molecule at the CAS[12,8]/6-311G(d,p) level of calculation. N_1–H3 and N2–H4 are the standard polar N–H bonds, and N1–H4, N2–H3, and H3–H4 are non-bonded pairs

Pair →	N1–N2	N1–N2	N1–H3	N2–H4
q	0.000375	−0.000216	0.379834	0.379834
π	0.500187	0.499892	0.689917	0.689917
f	0.594557	0.260804	−0.015801	−0.015801
δ_i^{AB}	0.405443	0.739196	0.869247	0.869247
$p(2,0)$	0.101548	0.184691	0.479365	0.479365
$p(0,2)$	0.101173	0.184907	0.099532	0.099532
$p(1,1)$	0.797279	0.630402	0.421103	0.421103

Atom →	N1	N2	H3	H4
$\langle n_A \rangle_{\text{exact}}$	7.375559	7.375307	0.624567	0.624567
$\langle n_A \rangle_{\text{approx}}$	7.379993	7.379675	0.620166	0.620166

Pair →	N1–N2	N1–H3	N2–H3	N1–H4	N2–H4	H3–H4
δ^{AB} (exact)	1.077506	0.860953	0.032239	0.032262	0.860930	0.003975
δ^{AB} (approx)	1.144639	0.869247	0.000000	0.000000	0.869247	0.000000

The same happens with the hypothetical bond between the two H atoms.

The δ error in the above example is quite small (0.000028). When this does not occur, it is very likely due to an inappropriate choice of the proposed bonding pattern. When it is almost certain that there are no (nc,2e) multicenter bonds ($n > 2$), a decrease of δ may be achieved by including other $\boldsymbol{p}_2$ vectors in eqn (48). If, even so, the value of δ does not decrease, the initial assumption that EDF can be represented as a direct product of (2c,2e) bonds is simply wrong, and alternative models that explicitly account for these forgotten (nc,2c) bonds should be developed. Although we will not pursue this objective in this work, some didactic examples are explained in some detail in ref. 98.

5 Energy decompositions

As stated in Section 3, the second *face* of chemical bonding is energetic. After all, no bonding exists without an energetic stabilization. This statement can be assessed with respect to some appropriately defined set of fragments that interact or, in the case of metastable bonds (like that in the O_2^{2+} cation, for instance[108]), with respect to some finite geometrical perturbation. When chemical insight is to be pursued it is clearly not sufficient to report the overall dissociation energy; chemists would like to know which fragments, bonds, or moieties are responsible for it and to what extent. This background leads necessarily to consider an energy decomposition scheme. Not unexpectedly, there are dozens, if not hundreds of them out in the literature. Very grossly speaking, three families of energy decomposition analyses (EDAs) have survived through the present time. In the case of weakly interacting systems, the traditional theory of intermolecular interactions that computes the interaction between two (or more) unperturbed fragments by means of perturbation theory has evolved into very accurate and complex methods, among which we highlight the well-known symmetry adapted perturbation theory (SAPT).[109] SAPT and related perturbative approaches suffer from two very clear problems. On the one hand, they fail to converge easily in the short-range regime, so that a user never knows when the perturbation

series stops being reliable. On the other hand, the use of unperturbed monomers fails to reflect the changes that their densities, orbitals, etc. experiment after the interaction has taken place. When a supermolecule is computed and compared to the interacting fragments, the original Morokuma decomposition,[110,111] generalized by Ziegler and Rauk,[112] has turned into a set of very useful recipes, frequently used in density functional calculations.[113,114] This energy decomposition analysis depends heavily on how the fragments that interact are chosen, being thus reference dependent. Finally, if atoms are singled out from a molecule, another set of EDAs emerge which compute their energies and mutual interactions. This procedure can be done in orbital space, as for instance, in the methods proposed by Head-Gordon and coworkers,[115] which also use some artificial states borrowing ideas from Morokuma-like partitions, and depend obviously on how atoms are extracted in orbital space. If done in real space, like in the interacting quantum atom (IQA) decomposition,[70,116–119] no reference is needed at all, although the procedure now becomes dependent on how the real space atoms are defined. From a wavefunction, a consistent decomposition of the expectation value of the Hamiltonian into atomic and pairwise additive contributions is obtained. These ideas will be further discussed in the next subsection.

5.1 The IQA energy partition

Let us consider either a fuzzy or an exhaustive partition of space, as provided by a set of ω_A weights (see Section 2). Once this has been chosen, the expectation value of the Hamiltonian can be written as:

$$E = \sum_A \int_{\boldsymbol{r}_1' = \boldsymbol{r}_1} \omega_A(\boldsymbol{r}_1) \hat{h}(\boldsymbol{r}_1) \rho_1(\boldsymbol{r}_1; \boldsymbol{r}_1') d\boldsymbol{r}_1$$
$$+ \frac{1}{2} \sum_{A,B} \iint \omega_A(\boldsymbol{r}_1) \omega_B(\boldsymbol{r}_2) \frac{\rho_2(\boldsymbol{r}_1, \boldsymbol{r}_2)}{r_{12}} d\boldsymbol{r}_1 d\boldsymbol{r}_2 + V_{nn} \quad (53)$$
$$= \sum_A E_{\text{self}}^A + \frac{1}{2} \sum_{A \neq B} E_{\text{int}}^{AB},$$

This journal is © the Owner Societies 2023

Phys. Chem. Chem. Phys., 2023, **25**, 10231–10262 | **10245**

wherein $\rho_1\left(r_1; r_1'\right)$ and $\rho_2(r_1, r_2)$ are 1RDM and the 2RD, respectively, $\hat{h}(r_1)$ is the monoelectronic part of the electronic Hamiltonian as a function of the coordinates of electron 1, while r_{12} represents the distance between electrons 1 and 2 and V_{nn} is the internuclear repulsion. Finally, E_{self}^A and E_{int}^{AB} represent the energy terms which contain particles (i) in only one basin A or (ii) in two different basins A and B, respectively, and are known as the atomic self-energy of atom A and the interaction energy between atoms A and B, respectively. Eqn (53) represents the basis of the Interacting Quantum Atom (IQA) energy partition.[14,70]

The atomic self-energy contains all those energy terms that would survive after full dissociation of the system into its atoms: the kinetic energy of the electrons, the electron-own nucleus attraction and their mutual repulsion:

$$E_{self}^A = T^A + V_{en}^{AA} + V_{en}^{AA}. \quad (54)$$

As we progressively dissociate a molecule into its atomic components, all the atomic self-energies evolve to the *in vacuo* atomic energies. An atom's self-energy is the local expectation value of the atomic Hamiltonian in-the-molecule. It is rather obvious that the magnitude of a given E_{self}^A will be on the same scale as that of the *in vacuo* energy of A. Namely, about $-0.5E_h$ for a hydrogen atom, around $-100E_h$ for a F moiety. This means that, although no reference is needed to perform an IQA decomposition, if a suitable atomic reference is chosen (*e.g.* the evolved atomic states at dissociation) the energetic difference between the self-energy and this reference energy will be small, in the chemical scale, measuring the energy associated with the chemical deformation experienced by the atom on going from its reference to its in-the-molecule state. We call these differences deformation energies:

$$E_{def}^A = E_{self}^A - E_0^A, \quad (55)$$

E_0^A being the chosen reference energy for atom A. Deformation energies are typically positive, since it takes some energy to deform a free atom to get it bonded. Their values are chemically intuitive, in line with the traditional idea of valence excitation. For instance, since Li in LiF has almost lost one electron which has been taken by the very electronegative F atom, the in-the-molecule state of Li is largely cationic, so its self-energy will have been destabilised with respect to the neutral reference by about its ionization potential. Similarly, we expect that the deformation energy of fluorine in LiF to be small or even negative, since although the moiety needs to be deformed to get bonded, the atom will have also gained energy close to the electron affinity of F in the process. These intuitions are supported by actual calculations.[120]

In a similar manner, the interatomic interaction energy between two atoms, E_{int}^{AB}, contains all energetic components affecting mutual interaction of their electrons and nuclei: the attraction between the electrons on A and the nucleus of B and *vice versa*, the repulsion between the electrons lying in A and those lying in B, and the internuclear repulsion:

$$E_{int}^{AB} = V_{en}^{AB} + V_{en}^{BA} + V_{ee}^{AB} + V_{nn}^{AB}. \quad (56)$$

In the large interatomic distance limit, E_{int}^{AB} provides exactly the interaction energy that is obtained from perturbation approaches. Nevertheless, an important difference is that E_{int}^{AB}, unlike perturbational methods, has a well-defined limit at any distance. The interaction energy can be chemically exploited by dividing the pair density $\rho_2(r_1, r_2)$, into Coulombic and exchange–correlation terms, as in Eq. 10. If this is done, E_{int}^{AB} becomes a sum of a Coulombic term, which depends only on the 1RD, *i.e.* on classical electrostatics from the quantum-mechanically obtained densities, and an exchange–correlation term, purely quantum-mechanical in origin:

$$E_{int}^{AB} = V_{cl}^{AB} + V_{xc}^{AB}. \quad (57)$$

The first is clearly related to ionicity, while the second, which comes from integrating an interelectron distance-scaled, measures the energetic effect of electron fluctuation (or delocalization) and thus provides a direct connection with covalency. The interaction energy between two atoms is thus divided into a term that tends to the standard multipolar series at large interatomic distances, dominated by the fist non-zero atomic multipolar moments, and a contribution which does only exist due to quantum fluctuations. These ideas are chemically appealing and they have been documented in detail.[13]

The IQA partition can be exploited at different levels of granularity, *viz.*, it can be equally applied to groups of atoms $\mathcal{G}, \mathcal{H} \dots$ so that

$$E = \sum_{\mathcal{G}} E_{self}^{\mathcal{G}} + \frac{1}{2} \sum_{\mathcal{G} \neq \mathcal{H}} E_{int}^{\mathcal{G}\mathcal{H}}, \quad (58)$$

wherein

$$E_{self}^{\mathcal{G}} = \sum_{A \in \mathcal{G}} E_{self}^A + \frac{1}{2} \sum_{A,B \in \mathcal{G}} \sum_{A \neq B} E_{int}^{AB}, \quad (59)$$

and

$$E_{int}^{\mathcal{G}\mathcal{H}} = \sum_{A \in \mathcal{G}} \sum_{B \in \mathcal{H}} E_{int}^{AB}. \quad (60)$$

The interaction energy between two groups $\mathcal{G}$ and $\mathcal{H}$ can also be divided in Coulombic and exchange–correlation contributions, $V_{cl}^{\mathcal{G}\mathcal{H}}$ and $V_{xc}^{\mathcal{G}\mathcal{H}}$ in a similar fashion to E_{int}^{AB} in eqn (57). This ability of the IQA approach to provide chemically intuitive answers at different granularities allows for a relatively easy way to compare it to other energy decomposition methods. The other way around is not so obvious. We refer the reader to specific publications on the subject for further information.[121,122]

IQA can also be used in the multi-component MC-QTAIM formalism.[47] This is a very promising strategy that may help understand how chemical bonding evolves when the Born–Oppenheimer approximation breaks and the quantum nature of nuclei needs to be considered. We refer the reader to the above reference for further details.

Although $\rho_1\left(r_1; r_1'\right)$ and $\rho_2(r_1, r_2)$ are not attainable *via* Kohn–Sham Density Functional Theory (KS-DFT), it is possible to divide the KS-DFT electronic energies using scaling techniques as suggested in ref. 123 and 124. Taking into account the

10246 | *Phys. Chem. Chem. Phys.*, 2023, **25**, 10231–10262

This journal is © the Owner Societies 2023

popularity of the KS-DFT in modern computational chemistry, this pragmatic strategy has reinforced the applicability and interest of IQA. However, the relatively-high computational cost of IQA is the major inconvenience that remains for its widespread use. This situation, which occurs because the IQA terms involve the integration of scalar fields over very irregular regions, is aggravated for correlated scalar fields $\rho_1(r_1; r_1')$ and $\rho_2(r_1; r_2)$. We expect that such calculations could be accelerated by introducing carefully-controlled approximations, as found in the case of the partition of MP2 correlation energies using effective two-electron matrices,[125] which reduces in $\sim 80\%$ of the computational cost for double- and triple-ζ basis sets. More considerable reductions in computer time may result for larger basis sets.

5.2 Multifaceted applications of IQA

Chemists are often interested in the nature and the relative strength of covalent and noncovalent interactions under different circumstances. Indeed they characterize all kinds of interactions in terms of heuristic, intuitive chemical concepts such as steric hindrance, π-conjugation, aromaticity, cooperative and anticooperative effects, *etc.* Within this context, the IQA method can provide much valuable information, not only by assessing the energetic magnitude and essential features of chemical contacts in diverse scenarios, but also by providing quantitative descriptors of those concepts that are not associated with Dirac observables and thereby lack a rigorous mathematical definition. Thus, we will show that the applicability of the QTAIM and IQA methods is gradually expanding and, as recently noticed by Richter *et al.*,[126] their additional computational effort is more than compensated by the great amount of useful information they provide. Several authors have used IQA to provide unified models of chemical bonding. In this sense, Cukrowski,[127] has advocated for using fragments in his Fragment Attributed Molecular System Energy Change (FAMSEC) familiy of methods to solve a battery of chemically relevant problems.[128–130]
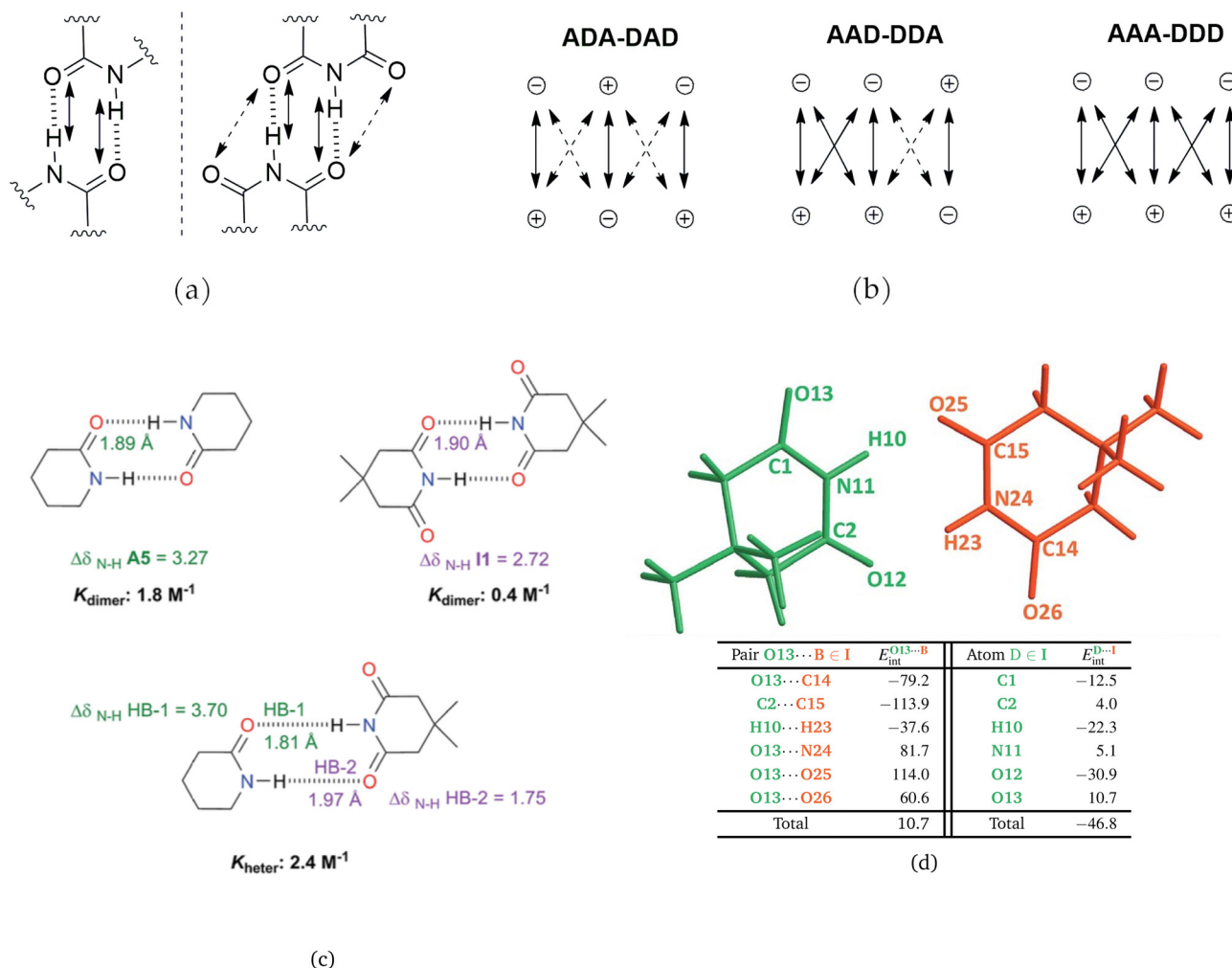
In this perspective, we will focus on the IQA analysis performed within the QTAIM framework although it can also be applied to other scalar fields such as the ELF partition.[131–133] Let us discuss first the characterization of selected noncovalent complexes, which is no doubt one of the most typical goals of EDAs. In this regard, IQA has been successfully employed to explain the experimentally observed Hydrogen Bond (HB) cooperative effects in water clusters.[134] For example, IQA has unveiled that double HB donors and acceptors of HB can also be associated with marked cooperative effects,[135] in contrast with the traditional view that associates them with anticooperative effects.[136] Likewise, the IQA partition puts forward a hierarchy of HB strength within water clusters as a function of the single/double and donor/acceptor character of the involved monomers.[137] In general, IQA has proven useful to characterize the underlying classical and quantum-mechanical effects in other prototypical noncovalent interactions, such as the crucial role played by the exchange–correlation stabilization complementing the electrostatic picture of both anion–π[138] and halogen bonding[139,140] complexes.

Perhaps one of the major appealing features of IQA is the determination of the attractive or repulsive character of A$\cdots$B or $\mathcal{G}\cdots\mathcal{H}$ interactions as well as their covalent and ionic contributions. For instance, the stabilizing role of the H$\cdots$H interaction proposed by Matta and coworkers[143] has been the subject of considerable debate.[144,145] Several IQA studies[146–148] have confirmed the attractive character of this interaction. In like manner, the IQA energy partition and other EDAs have been exploited to determine that the CH$\cdots$HC interactions in the "in–in" conformation of ortho-xylene are also attractive.[149] Therefore, the larger stability of the "out–out" conformer is due to other factors which include charge delocalization and aromaticity.

Let us consider in more detail another similar problem, the IQA assessment of the so-called Jørgensen Secondary Interaction Hypothesis (JSIH).[141,142] The JSIH states that the relative strength of similar H-bond complexes can be determined by the balance between the attractive and repulsive interactions among the frontier atoms between the interacting monomers. For example, JSIH correctly predicts that amides dimerize more strongly than imides because imide dimerization is impaired by a repulsion that involves the oxygens of the spectator carbonyls (dashed arrows in Fig. 6(a)). Additionally, the JSIH rightly foretells that AAA–DDD complexes are stronger than those of the type AAD–DDA wherein A stands for HB acceptors and D for HB donors. In turn, AAD–DDA clusters are stronger than those of the sort ADA–DAD (Fig. 6(b)). Nevertheless, the JSIH wrongly foresees that the strength of amide–imide heterodimers should be intermediate between that of the corresponding homo-dimers (Fig. 6(c)). However, the IQA descriptors indicate that all the atoms within the monomers should be considered to properly account for the intermolecular formation energy (see for example atom C1 in Fig. 6(d)). Ref. 141 concludes that the relative strengths of homo- and hetero-dimers of amides and imides can be better explained by considering the acidity and the basicity of the involved HB donors and acceptors, respectively.

As stated above, the QTAIM and IQA methods of wave function analysis contribute to the understanding of intuitive and heuristic chemical ideas. An intuitive chemical concept whose quantum mechanical foundation has been addressed by means of IQA is Sterical Hindrance (SH).[150] For a given pair of frontier atoms A$\cdots$B located in different molecules, their deformation energies E_{def}^A and E_{def}^B can be fitted to an exponential decaying function,[151] which corresponds to the repulsive part of the Buckingham potential $U_{rep} \sim \exp(-\alpha r)$.[152] This observation has led to the proposal that $E_{def}^A + E_{def}^B$ equals the short-range repulsion energy of these atoms, and that such repulsive interaction acts over distances longer than previously envisioned (other IQA studies[153] predict a different behavior of the H atom in this regard). More recently, it has been pointed out[154] that changes in the number of electrons have a very significant contribution in deformation energies. In other words, an assessment of the SH energetics would be biased by alterations in the electronic population of the atoms in a process under consideration. Hence, charge transfer energy should be subtracted from the deformation energy to yield a quantitative measure of the SH

This journal is © the Owner Societies 2023

Phys. Chem. Chem. Phys., 2023, **25**, 10231–10262 | **10247**

Fig. 6 (a) and (b) Jorgensen Secondary Interaction Hypothesis (JSIH) applications to the study of hydrogen bonded systems. Solid/dashed arrows indicate JSIH attractions/repulsions between the interacting molecules. The JSIH predicts that (a) the amide homodimers are more strongly bound than imide homodimers and (b) the order of strength for complexes with hydrogen bond acceptors (A) and donors (D) is AAA-DDD > AAD-DDA > ADA-DAD. (c) Association constants and changes in chemical shift in CDCl$_3$ at 25° of δ-valerolactam and 3,3-dimethylglutarimide. The heterodimer is more strongly bound than the two homodimers. (d) IQA energy partition for the dimerization of 3,3-dimethylglutarimide. One monomer and its atoms are indicated in green color. Ditto for the other monomer and orange color. The values are reported in kcal mol^{-1}. Note that the interactions of C1 with the interacting monomer I are also important to the interaction between the two monomers. The deformation energies of the monomers are 16.4 and 20.0 kcal mol^{-1} so that the formation energy of the dimer is − 10.4 kcal mol^{-1}. Adapted from ref. 141 and 142 with permission from the Royal Society of Chemistry.

of atom A, that is, $E_{SH}^{A} = E_{def}^{A} - E_{CT}^{A}$ where $E_{CT}^{A} = E_{ref}^{A}(N) - E_{ref}^{A}(N^0)$ estimates the charge transfer contribution when N and N^0 are the electrons of A in its final and initial (reference) states, respectively. The suitability of the E_{SH}^{A} expression has been validated in different archetypical systems such as atomic compression and S_N2 reactions in which SH is usually invoked.

Clearly, the strengthening or weakening of chemical interactions under different scenarios as provided by IQA can be very useful to understand chemical reactivity, especially when the appropriate IQA descriptors are monitored along the process to determining which interactions or atoms are mostly responsible for the occurrence (or lack of) of a chemical reaction, what might result in directives for the tuning of chemical modifications in reactants. In addition the selection of group-based IQA quantities is normally required given that, besides the atoms involved directly in the bond forming/breaking,

other contributions need to be considered in order to account for the net energy changes along the reaction profiles.[155] For instance, the changes in the steric energy associated with reacting molecules (*i.e.*, $E_{SH}^{\mathcal{G}}$) supports the kinetic role of SH that is traditionally claimed to play in the competition between S_N2 and E2 reactions.[156] On the other hand, the geometric and electronic deformation of a diene/dienophile helps to understand the origin of the endo–exo preference in prototypical Diels–Alder reactions[157] while the atomic IQA decomposition of the IRC profiles explains the synchronous or asynchronous character of the polar Diels–Alder reactions.[126] Focusing also on the proper fragment quantities, the IQA study of the bifunctional catalysis played by water clusters[158] shows how water monomers encompassing the reaction between SO$_3$ and H$_2$O to yield H$_2$SO$_4$ mitigate the changes in chemical bonding across the rate-limiting step of the process, thereby reducing the activation energy as more water

molecules are included in the system. Similar results are obtained for the hydrolysis of oxyrane and its methyl derivatives in neutral water.[159]

The utility of IQA to describe chemical reactivity can be augmented by coupling it with the reaction force, $F(\xi) = -(dE(\xi)/d\xi)$, a projection of the Hellmann–Feynman forces acting on the nuclei of a molecular system onto a reaction coordinate ξ that is usually determined by an intrinsic reaction coordinate algorithm. Thus, the IQA decomposition of $F(\xi)$ into self-atomic/group components and classical/exchange–correlation interaction terms, which can be obtained through differentiation of cubic splines, yields chemically appealing images in terms of bonds, covalency and ionicity for different types of reactions.[160,161] Similar descriptions can be obtained with the closely-related Reduced Energy Gradient (REG) technique,[162] which relates the gradient of selected IQA components to the gradient of the total energy with respect to an arbitrary reaction coordinate for binding or reactive processes.

The versatility of IQA is further illustrated by its application to the study of excited-state chemistry, including noncovalent interactions, charge transfer and photochemical reactions.[164] Indeed, the EOM-CCSD excitation energies can be divided into intra and inter-atomic energies according to the IQA formalism,[163,165] allowing thus to establish the atoms and chemical bonds wherein the excitation energy resides. This kind of analysis has been performed in the 1 $^1A''$ and 2 $^1A'$ electronic states of the water dimer in the $\mathscr{C}_s$ configuration (Fig. 7). Also of particular interest may be the relevant applications on molecular crystals, like the detailed characterization[166] of the polymorphism in succinic acid crystals or the assessment of noncovalent contacts within selected hydrogen storage materials $KN(CH_3)_2BH_3$ and $LiN(CH_3)_2BH_3$.[167] Other materials that have been examined with the IQA energy partition are the donor–acceptor charge–transfer tetrathiafulvalene–tetracyanoquinodimethane cocrystals.[168] More specifically, the IQA approach unveils the stabilizing (or destabilizing) character of $C\cdots S$, $C_{sp^3}–H\cdots S$ and $S\cdots S$ interactions within these systems. Likewise, the IQA method characterizes $Cl\cdots S$, $Cl\cdots Cl$ and $O\cdots Cl$ contacts in trimers of 2-chloro-5-methoxy-naphtho[1,2-*d*]thiazole, used as an archetype in the study of organic semiconductors.[169] Actually, a specific implementation of the IQA method for the study of crystals has been developed and

successfully tested in crystals with different types of bondings.[170] Eventually, this enhanced IQA methodology will permit to tackle interesting and challenging problems, such as the origin of different stabilities of crystalline phases (*e.g.* graphite *versus* diamond).

5.3 Understanding organometallics using IQA

Computational chemistry has been intensively (and successfully) applied to investigate the structure and properties of organometallic complexes, which are usually attractive targets for the design of catalysts and functional materials.[171] Thus, the activity of such systems can be carefully tuned through ligand design and metal selection based on the structure–property relationships predicted by modern QM methods. However, nontrivial electronic structure effects usually introduce additional complexity in the interpretation of the properties of organometallic compounds, which represent, thus, a particular challenge to the various EDA methodologies. Hence, we review here some representative studies showing the capability of IQA to yield valuable insight into organometallic chemistry.

One of the characteristic features of IQA, the assessment on an equal-footing of all metal$\cdots$ligand, ligand$\cdots$ligand and/or metal$\cdots$metal pairwise interactions can shed further light on complex bonding effects involving either direct or through-space interactions. A striking example is found in the recent analysis[172] of the $[M^{n+}\cdots CR_3]^{1-n}$ pyramidal adducts constituted by alkaline and alkaline-earth cations ($M^{n+} = Li^+, Na^+, Ca^{2+}, \ldots$) and various anionic fragments (*e.g.*, $C(CN)_3^-, CF_3^-, C(Ph)_3^-$). For these species, the IQA shows unambiguously that the M^{n+} cation gives only slightly-favorable or repulsive interactions with the central C atom, but establishes significant exchange–correlation interactions with the rest of the atoms that account for the overall stabilization of the adduct. Interestingly, this energetic pattern is markedly different from those of the typical covalent or ionic bonds dominated by direct (*i.e.*, 1,2) contributions, suggesting thus that the collective interactions resulting from through-space (1,*n* with $n > 2$) interactions constitute a genuine type of chemical bonding characteristic of organometallic complexes.[172]

Other non-evident or surprising electronic properties have been observed in metal$\cdots$metal bonds like the Rh$\cdots$Cr bond in rhodium(I) complexes stabilized by hemichelation (*i.e.*, hetero-bisligation where one of the two sites binds the metal noncovalently),[173] which turns out to be mainly governed by electrostatics according to the QTAIM and IQA analysis. The same methods have been applied to the Ag$\cdots$Ag[174,175] and Au$\cdots$Au[176] interactions, revealing significant cooperative effects in the Au$\cdots$Au bonds. Similarly, the nature of the metal–carbene bonds has been examined in the cyclopropenylidene$\cdots MX_2$ and imidazol-2-ylidene$\cdots MBr_2$ complexes in which M = Be, Mg, Zn and X = Br, H.[177] Curiously, the results show that Be forms the strongest M–C bonds followed by Mg and Zn while the H atoms bound to the metal centers hinder the M–C bond in comparison with the electron-withdrawing Br atoms. This observation is consistent with the fact that the

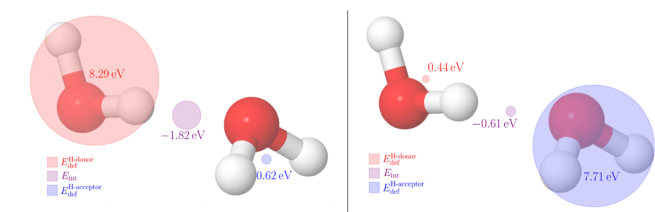**Fig. 7** Deformation energies of the hydrogen bond donor and acceptor in $(H_2O)_2$ in its electronic systems 1 $^1A''$ (left) and 1 $^1A'$ due to electronic photoexcitation. The IQA interaction energy between the monomers is reported as well. Reproduced from ref. 163. Copyright 2020 John Wiley and Sons, Inc.

main contribution to the M–C bond energetics is again electrostatics. Some metal–carbonyl compounds, which are usually recognized as archetypes for the study of metal–metal bonding and the ligand-bridges between metallic centers, have been also subject to IQA analysis, as in the case of the $[Ni_2(CO)_n]^-$ complexes in which the Ni–CO bond is dominated by the covalent contribution even to the extent that the electrostatic component of the energetics of the Ni–C chemical bond is slightly repulsive.[178] In contrast, the metal–CO bonds in the recently synthesized $[M(CO)_8]$ complexes with M = Ca, Sr, Ba turn out to be dominated by electrostatics without any significant π-back donation according to the corresponding IQA pairwise contributions complemented with several QTAIM descriptors.[179] Regarding the role of noncovalent interactions within organometallic complexes, we find a representative example in ref. 180, which addresses the intramolecular contacts within the six-coordinated Zn complexes, $[Zn(bpy)(H_2O)_4]^{2+}$, $[Zn(bpy)_2(H_2O)_2]^{2+}$ and $[Zn(bpy)_3]^{2+}$ in which bpy = 2,2′-bipyridyl. The IQA results reveal the magnitude of cooperative effects exerted by the bpy ligands, *i.e.*, the Zn–O and Zn–N bond strengths decrease with the number of bpy ligands bonded to Zn while the CH···N and CH···O interactions within the coordination complexes are reinforced.

Concerning organometallic catalysis, it is clear that the computation and analysis of the IQA descriptors along the reaction profiles may offer a wealth of information useful to elucidate the relative importance of the metal and substituent effects. This is shown, for example, in a mechanistic study of ammonia fixation by Ir-based complexes,[181] showing how the ionic contribution of the Ir–X bonds with different ligands modulates the activation energies. In another recent study,[182] the breaking of a Ru–O chemical bond during the initiation step of Hoveyda–Grubbs Catalysts (HGCs),[183] which are extensively used in olefine methathesis reactions, has been rationalized thanks to the IQA picture of the reactive Ru–O bond as mainly dominated by electrostatics (roughly 90% of E_{int}^{Ru-O} comes from the classical contribution in eqn (57)). In this way, the impact on the initiation kinetics due to substitution at different positions of HGCs is well understood in terms of their electron donor and withdrawing influence. Moreover, the most labile HGC precatalysts have the smallest values of $|E_{int}^{Ru-O}|$,[182] which may be considered as a reliable reactivity index.

Finally, we briefly comment on the growing interest in understanding the role of noncovalent contacts in organometallic reactivity.[184] In this respect, the agostic interactions, whose nature is still unclear,[185,186] are frequently crucial in the understanding and tuning of reactivity, *e.g.*, in C–H bond activation *via* Concerted Metallation Deprotonations (CDM).[187] For instance, Fig. 8 displays the different interactions within the agostic species involved in the CMD mechanism of cyclopalladation and cyclonickelation of *N,N*-dimethylbenzylamine determined with QTAIM, IQA and Local Energy Decompositions (LED). One can see that several contributions govern the interactions between the metal and its surrounding environment such as electrostatics, charge transfer and covalency. The first two-mentioned components of the interaction energy are consistent
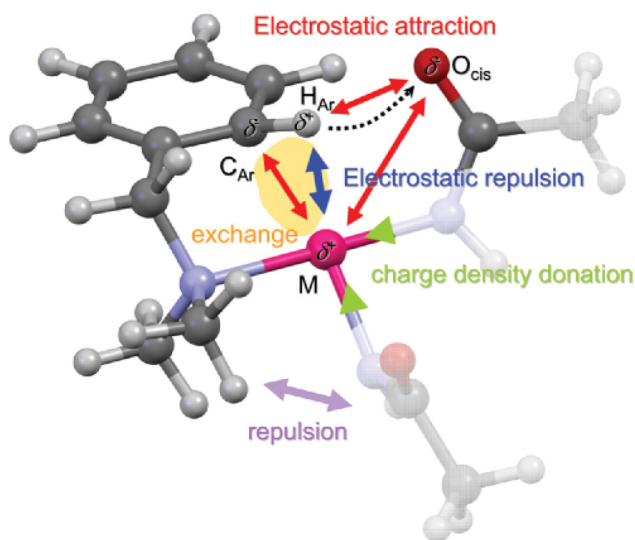
Agostic intermediate

Fig. 8 Agostic species in the concerted metalation deprotonation mechanism in the cyclopalladation and cyclonickelation of *N,N*-dimethylbenzylamine. The IQA, QTAIM and LED analyses reveal the different kinds of interactions between the metallic center and other atoms within the molecule, namely, electrostatic attractions and repulsions, and exchange and charge-transfer interactions. Figure taken from ref. 187.

with the observation that the overall process is very sensitive to the charge of the metallic center. Another metalation process that has been investigated using the QTAIM and IQA methods is the cyclometalation of CpCo(III) species *via* base-promoted CDM.[188] By tracking the changes in the pairwise ionic and covalent contributions throughout the whole reaction path, it has been possible to ascertain the key role played by Co···O contacts as the driving force for the reaction to take place. The IQA analyses also reveal that bulky ligands of HGCs participate in CH···Cl contacts and CH···Ru agostic interactions,[182] and may contribute to the weakening of the reactive Ru–O bonds. Overall, these and other examples suggest that the IQA and QTAIM approaches might be critical in building a paradigm of chemical reactivity based on noncovalent interactions as suggested by Cornaton and Djukic.[184]

5.4 IQA as a computational tool for biomolecular modelling

Some of the early studies in QCT made clear that the real-space theories provide useful descriptors that correlate with biological/pharmacological properties and identify all kinds of noncovalent interactions.[189–191] In this respect, IQA could represent a significant leap forward in pharmalocoly by discerning the actual energetic impact of specific interactions on the stability and conformational properties of large biomolecules. The prospects of achieving such long-term goals are continuously increasing, not merely because of the higher performance of computers, but, more importantly, because of the methodological advances. Thus, the *ad hoc* adoption of additive exchange–correlation Khon–Sham energies into the IQA framework,[123,124] which can be complemented with pairwise dispersion energies as calculated with the Grimme's D3 potential,[192] is especially remarkable

10250 | *Phys. Chem. Chem. Phys.*, 2023, **25**, 10231–10262

This journal is © the Owner Societies 2023

given that modern DFT methods are the default choice for large systems. The computational hurdles are also being reduced by the efficient IQA functionality in the popular AIMAll suite[193] or by the nearly linear-scaling version of our PROMOLDEN code, which relies on atomic subsets of localized MOs and employs fast multipolar algorithms for the calculation of distant exchange–correlation interactions.[75] As a result, the IQA partitioning of the total energies derived from DFT densities is currently feasible for medium-sized molecules (50–200 atoms). We also note that, according to recent results,[194] the IQA-style partitioning of the electronic energy calculated with fast semi-empirical QM methods could give atomic and interatomic energy descriptors for large molecules close to those derived from conventional IQA/DFT.

In recent years, several computational studies have validated different IQA protocols and applied them to obtain new chemical insight into biomolecular properties. Thus, it has been shown that the DFT-D3 (or HF-D3) IQA categorizes the S66 set of noncovalent complexes similarly as perturbation methods do and, interestingly, unveils the atomic hot spots involved in the interactions.[195] The same approach has been extended to the analysis of conformational energies of organic and peptide molecules[196] in such a way that, once that a convenient fragmentation is chosen, IQA provides a balanced description of various intramolecular effects associated with classical electrostatics, exchange–correlation, *etc.* Other works have also exploited the IQA ability to assess both intramolecular and intermolecular contacts in systems relevant in biology. For instance, the IQA analysis of the conformers of vitamin C[197] or proline[198] points out that the intramolecular HBs are the main factors determining their relative stability in the gas-phase. Considering molecular association, the IQA descriptors reveal the relative strength and the nature of the key interactions. Selected examples include the alkaline/alkaline-earth cations in complex with bioorganic ligands (dominated by electrostatics, but modulated by exchange–correlation), the H-bonded aspartate dimer (mainly electrostatic, but encompassing a certain

covalency),[199] and the arrangements of neutral/charged DNA nucleobases (the exchange–correlation energy between the H-bonded atoms is the determinant for the neutral forms whereas both the H-bonded and the adjacent atoms contribute to the electrostatic stabilization of the charged bases; see Fig. 9).[200] Other representative IQA studies on molecular clusters have focused on the characterization of cooperative effects (a guanine quartet in complex with metal cations or porphyrin molecules),[201,202] the identification of preferred binding sites (the adeninate anion interacting with Na^+/K^+ counterions),[203] and the strength of charged-assisted H-bonds.[204]

The IQA scoring of key interactions between a ligand and its biological target could be particularly useful for fragment-based drug design by assessing the suitability of chemical modifications, as suggested by the recent studies on zimlovisertib, an interleukin-1 receptor-associated kinase 4 inhibitor, currently in trials for its use in patients of COVID-19 pneumonia,[205] and on two drug candidates targeting the hepatitis C virus NS5B protein.[206] Similarly, an insightful view of enzymatic catalysis can be gained by tracking the strengthening/forming or weakening/breaking of chemical bonds through the evolution of selected IQA terms along the energy profiles derived from cluster models. This idea is nicely demonstrated in the complex energetic mechanisms that have been drawn using the REG method for the peptide hydrolysis in the aspartic active site of the HIV-1 protease[207] and the phosphoryl-transfer process in β-phosphoglucomutase.[208]

Molecules of biological relevance range from those formed by a few atoms (*e.g.*, water, ions, small drugs, *etc.*) to flexible and large macromolecules like proteins and nucleic acids. The properties of these molecules are generally simulated using classical force field (FF) methods that comprise bonded energy terms (bond-angle-dihedral) and pairwise terms accounting for the long-range non-bonded interactions. For some specific interactions, whose inclusion in FFs may be problematic, IQA can provide rigorous quantitative descriptions like that of the charge penetration energy.[209] This contribution to the interaction energy is characterized by IQA as an intramolecular electrostatic effect closely related to other deformation components induced by intermolecular overlap (*e.g.*, the repulsive SH). Furthermore, to overcome some of the limitations of the classical FFs, there is growing interest in the use of the EDAs for the design, parametrisation, and validation of the next-generation (*ab initio*) FF methods.[210] Among the ongoing projects in this field, we point out here the development of the FFLUX method[191] by Popelier and co-workers that is based on a rigorous QTAIM formalism. This development exploits the machine-learning method kriging to construct accurate models that represent the fluctuating atomic IQA energies or the (polarized) atomic multipole moments as a function of positions of all atoms in the system. FFLUX combines the (kriging) intraatomic energy with the electrostatic energy among the (kriging) atomic multipole moments, including also an empirical dispersion potential. The latest FFLUX implementation, which has been efficiently parallelized, reproduces minimum-energy conformations of small molecules and peptides,[211,212]
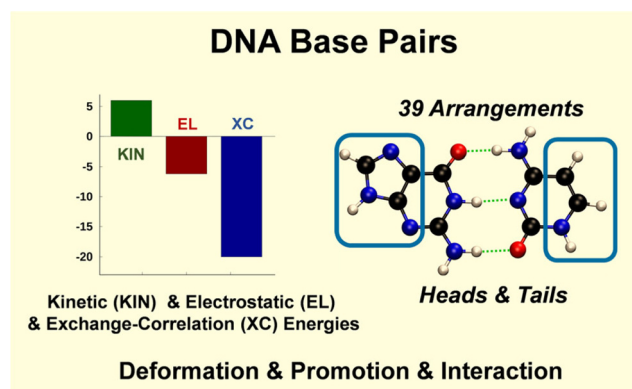

Fig. 9 IQA contributions to the bond energy for the G···C base-pairing interaction. Geometries and electron densities were computed for 39 different base pairs and their corresponding individual bases at the M06-2X/TZVP computational level. Reprinted with permission from ref. 200. Copyright 2021 American Chemical Society.

and simulates both water clusters and liquid water.[213–215] Work is still on progress to optimize the method for developing chemically accurate and transferable kriging models of atomic properties,[216,217] as well as to include the non-electrostatic intermolecular energy in a fully integrated and unified way.[215]
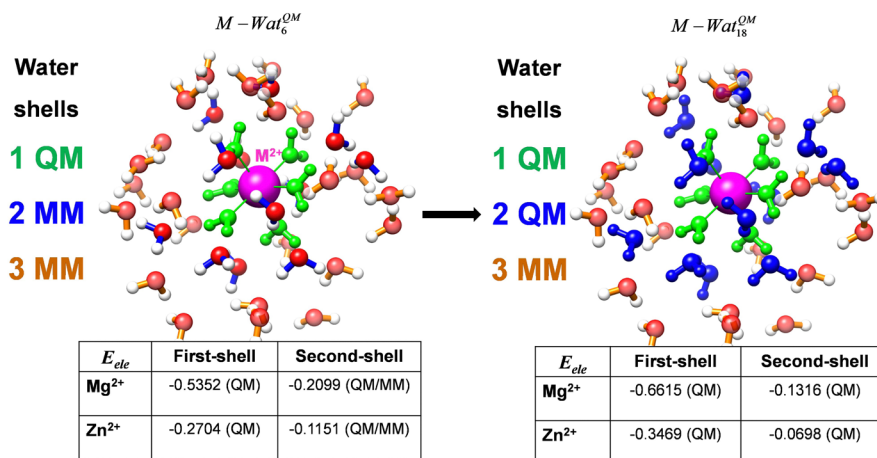
The pursuit to quantify atomic and group energy contributions in biomolecular systems requires the treatment of solvent and environmental effects within the IQA framework. Although the EDA decompositions of QM energies including environmental effects have been scarce, it turns out that the IQA net atomic energies can easily absorb the electrostatic continuum-solvent effects,[219] allowing thus the partition of hydration energies into effective atomic and group contributions. Similarly, in the case of hybrid QM/MM (molecular mechanics) methodologies, which combine the QM description of a region of interest with the classical FF representation of the surroundings, the electrostatic interaction between QM and MM atoms can be readily included as one more pairwise IQA term.[218] The pairwise QM–MM dispersion energy as well as the effective atomic solvation energies extracted from classical Poisson-Boltzmann (PB) calculations are analogously incorporated, so that a consistent IQA partitioning of the QM/MM-PB interaction energies in protein-ligand systems is now feasible. In addition, the IQA descriptors of the QM/MM model systems can detect and monitor the underlying unbalance between QM–QM and QM–MM interactions, quantifying thus the overpolarisation of the QM region (see Fig. 10).[218] Hence, IQA and other EDAs[220] could help in the diagnosis of QM/MM methodological problems and in the evaluation of possible solutions.

Certainly, the significant number and scope of the computational studies that are reviewed in this subsection support the potential of the IQA-based descriptors to gain valuable data and information from the QM and QM/MM calculations on biomolecules, ranging from the energetic assessment of all kinds of interactions (covalent and noncovalent, short and long-range) to the determination of reference data useful for the development and validation of modern FF and hybrid methods.

However, various obstacles lie ahead for the development and consolidation of more user-friendly IQA tools that may become the favorite EDA method in this field. Obviously, despite the latest advances, it is still required to simplify and speed up the challenging biomolecular applications of IQA as well as to control and ameliorate the impact of the numerical errors that affect especially the decomposition of relative energy differences. Hopefully, the IQA applicability may be enhanced by introducing controlled approximations, for example, by constructing machine-learning models for selected IQA components as a function of molecular geometry. But in addition to faster implementations, it will be necessary to optimize and standardise the selection and/or averaging of the myriad of atomic and fragment-based IQA terms that arise in large systems in order to design meaningful and robust descriptors that may help guide the design and optimization of biomolecules.

6 The electron counting-bond energy link

One of the most interesting features that emerges from using a single framework to derive both electron counting descriptors as well as energetic ones is the possible algebraic relationship between both. This notion lies deep in traditional chemical intuition, which takes for granted that bond energies are proportional to bond orders. For instance, a double C–C bond displays close to double the bond energy of a C–C single link. One of the main problems to formalize this relationship is the absence of an universally accepted definition of bond energy (BE).[221,222] As soon as we move from a diatomic to a general polyatomic system, a large set of phenomena, including relaxation of fragments, non-additivity effects, *etc.*, sets on, precluding a consensus on how to define such an important chemical concept as bond strength from an energetic viewpoint. For many, all these effects can only be separated apropriately if we

E_{ele}	First-shell	Second-shell
Mg^{2+}	-0.5352 (QM)	-0.2099 (QM/MM)
Zn^{2+}	-0.2704 (QM)	-0.1151 (QM/MM)

E_{ele}	First-shell	Second-shell
Mg^{2+}	-0.6615 (QM)	-0.1316 (QM)
Zn^{2+}	-0.3469 (QM)	-0.0698 (QM)

Fig. 10 Schematic representation of the formal MM → QM conversion of the water molecules in the second shell around one M(II) cation. Note that the electrostatic interaction energies (in au) between the metal and the first and second water shells depend on the QM-MM boundary. The structures were built from molecular dynamics snapshots and each cation is solvated by a spherical cap of 5400 MM waters. The IQA calculations were performed at the HF-D3/cc-pVTZ(-g)/MM level. Reprinted with permission of the authors from ref. 218.

are able to quantify the energetic cost of transforming an isolated atom into an atom-in-the-molecule. This leads to the so-called intrinsic bond energies.[223,224] It has been shown[225] that a real space partition like IQA provides a conceptually clean way out. $E_{\mathrm{int}}^{\mathrm{AB}}$ can be safely read as an *in situ* bond energy (IBE) that behaves exactly as other intrinsic bond energies proposed in the literature do. The IBE is the interaction (bond) energy between two fragments that have already been deformed to their in-the-molecule state. The total energy is fully recovered as a pairwise additive sum of all these IBEs plus the fragments' deformation energy costs (the IQA E_{def}s). Interestingly, the BE non-additivity problem is solved by allowing for the existence of interactions between all pair of fragments, not only between those who are directly bonded in a chemical sense (drawing a dash in between).

IQA thus provides a consistent definition of the (*in situ*) bond energy which can now be compared to bond orders (BOs). To do so, we notice that both the electrostatic (or classical or ionic) and the exchange–correlation (or covalent) contributions to the interatomic interaction energies can be written in a formally equivalent way:

$$E_{\mathrm{cl\ or\ xc}}^{\mathrm{AB}} = \int_A d\boldsymbol{r}_1 \int_B d\boldsymbol{r}_2 \frac{\tau_{\mathrm{cl\ or\ xc}}(\boldsymbol{r}_1, \boldsymbol{r}_2)}{r_{12}},$$
$$\tau_{\mathrm{cl}}(\boldsymbol{r}_1, \boldsymbol{r}_2) = \rho_t(\boldsymbol{r}_1)\rho_t(\boldsymbol{r}_2), \qquad (61)$$
$$\tau_{\mathrm{xc}}(\boldsymbol{r}_1, \boldsymbol{r}_2) = -\rho_{\mathrm{xc}}(\boldsymbol{r}_1, \boldsymbol{r}_2).$$

In this expression, a classical nuclear density, $\rho_n(\boldsymbol{r}) = \sum_\alpha Z_\alpha \delta(\boldsymbol{r} - \boldsymbol{R}_\alpha)$, where α runs over the nuclei and Z denotes the nuclear charge, has been added to the electron density ρ to define a total (electronic plus nuclear) charge density, $\rho_t(\boldsymbol{r}) = \rho_n(\boldsymbol{r}) - \rho(\boldsymbol{r})$. We now recall that the covalent bond order, as measured by the delocalization index δ^{AB}, given by eqn (39) which, apart from the r_{12} interelectron distance, is just a scaled $E_{\mathrm{xc}}^{\mathrm{AB}}$. Using a bipolar expansion, which is always convergent unlike the more commonly found multipolar expansion,[226] it has been shown[71] that both the covalent and ionic terms can be written as Taylor series in which the leading terms are

$$E_{\mathrm{xc}}^{\mathrm{AB}} \approx -\frac{\delta^{\mathrm{AB}}}{2R_{\mathrm{AB}}}, \qquad (62)$$

$$E_{\mathrm{cl}}^{\mathrm{AB}} \approx \frac{Q^A Q^B}{R_{\mathrm{AB}}}, \qquad (63)$$

where Q_A, and Q_B are the total (nuclear plus electronic) charges of A and B. In this sense, $\iota^{\mathrm{AB}} = -Q_A Q_B$ can be taken as an ionic bond order. Doing so, a total bond order $\varepsilon^{\mathrm{AB}} = \iota^{\mathrm{AB}} + \delta^{\mathrm{AB}}$ can be defined such that the total interaction energy $E_{\mathrm{int}}^{\mathrm{AB}} \approx -\varepsilon^{\mathrm{AB}}/R_{\mathrm{AB}}$.

An algebraic relationship is thus uncovered between electron counting descriptors (bond orders) and (*in situ*) bond energies. Surprisingly, the leading term in the covalent energy contribution follows an inverse power law much as the ionic one. It is very satisfying that a clear model of this behavior is straightforward from the analysis of EDFs. In a purely covalent bond, as examined, the total probability of finding two electrons in one
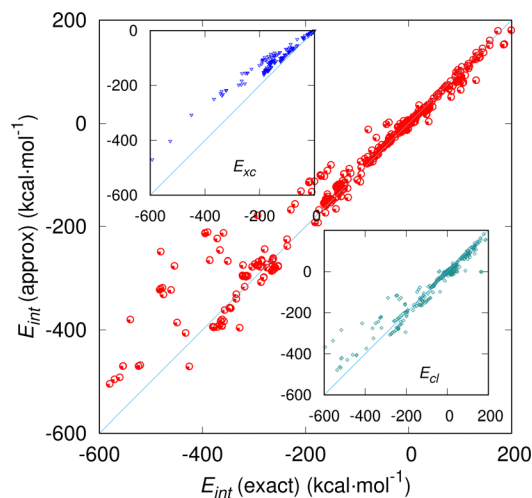

Fig. 11 Comparison of the leading order covalent (E_{xc}), ionic (E_{cl}), and total interaction energies (E_{int}) with their exactly computed values for a set of over 800 different compounds covering several types of bonding regimes. Taken from ref. 228, where more details can be found, with permission granted by the retained rights of the authors. Data are provided in kcal mol^{-1}.

center is 1/4 + 1/4 = 1/2. In these situations a $-1/R_{\mathrm{AB}}$ attraction exists between them, leading to an overall $-1/(2R_{\mathrm{AB}})$ interaction. No interaction, to first order, occurs when one electron lies in each neutral center. We believe that this model shows neatly that the origin of all interactions in a Coulombic Hamiltonian is electrostatic in nature.

The first order approximation reproduces reasonably well the exactly computed IQA/QTAIM covalent, ionic, and total interaction energies. Fig. 11 shows this comparison. In most cases, the leading order term of the expansion leads to semi-quantitative agreement with the exactly computed values. We have also shown that the agreement improves considerably if further order in the series expansion of both the covalent and ionic energies is taken into account.[227]

7 Recovering one-electron pictures

Regardless of the intrinsic power that real space methods have shown in chemical bonding issues, it cannot be denied that most chemists still use and pursue orbital pictures to rationalize their findings. Since delocalized canonical orbitals do not conform to the standard Lewis image, localized functions have become important in one-particle images of the chemical bond. Being Slater determinants invariant under unitary transformations of their orbitals, many different localization techniques have been devised over the years, like the now standard Edmiston–Ruedenberg[229] or Pipek–Mezey[230] procedures. Simultaneously, a quest for a simplified description of a complex wavefunction in terms of a set of atomic-like orbitals as close as possible to a minimal basis set has led to well-known procedures, like Weinhold and coworkers' natural bond orbital (NBO) formalism,[231] that has been severely criticized (see for instance ref. 232). Newer ideas have not ceased to be proposed,

This journal is © the Owner Societies 2023

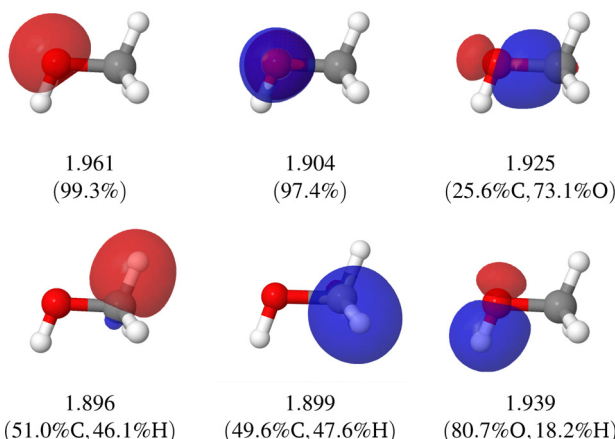*Phys. Chem. Chem. Phys.*, 2023, **25**, 10231–10262 | **10253**

Fig. 12 $|\phi| = 0.08$ a.u. isosurface of the non-core valence 1c and 2c DAFH functions found in methanol at the CCSD(T)//cc-pVDZ level. 1c and 2c occupations and percentage of population localized are also shown. Reproduced from ref. 255 with permission from the Royal Society of Chemistry.

like in the case of the so-called intrinsic atomic orbitals proposed by Knizia,[233] or in the adaptive natural density partitioning (AdNDP) method of Zubarev and Boldyrev,[234] that allows to tell easily two- from multi-center bonds, and that has been also generalized to solids.[235] Clearly, chemists are used to manipulate orbitals in very many clever ways, and it is relevant to examine the possibility of recovering effective one-particle functions from real space methods.

The combined use of a real space partition into fuzzy or nonfuzzy atoms together with an Open Quantum Systems (OQS) perspective of QCT[236–238] is a relatively straightforward, yet powerful way to access one-electron images of different flavors.

These one-electron functions can be visualized and compared between different systems, as well as with orbitals obtained by other methods as those described in the previous paragraph. Their analyses allow drawing significant conclusions, which are difficult or impossible to obtain in other ways. Among the different existing possibilities, in this work we will only comment on three of them: the domain averaged Fermi hole (DAFH) orbitals, the natural adaptive molecular orbitals (NAdOs), and the fragment natural orbitals (FNO). Interestingly, all of them converge onto the domain natural orbitals (DNO) developed by Ponec in the case of one region and SDWs. When describing how these one-electron functions are obtained, we will only present an illustrative example, without further discussion (see Fig. 12–14), for which we refer the reader to the original references.

7.1 Domain-averaged Fermi hole orbitals (DAFH)

The DAFH molecular orbitals of atom or fragment A are obtained by diagonalizing the exchange–correlation density ρ_2^{xc} after one of the electron coordinates has already been integrated over A. In a basis of canonical orbitals ϕ_i, assuming for simplicity a closed-shell ($N = 2n$) molecule, real spin–orbitals, and after integrating out the spin variables, we arrive at

$$\rho_2^{\mathrm{xc}}(\boldsymbol{r}_1, \boldsymbol{r}_2) = \sum_{ijkl}^{M} \eta_{ijkl} \phi_i(\boldsymbol{r}_1)\phi_j(\boldsymbol{r}_1)\phi_k(\boldsymbol{r}_2)\phi_l(\boldsymbol{r}_2) \qquad (64)$$

Threrein, M is the size of the MO basis, and η_{ijkl} are coefficients coming from the expansion of the wavefunction in terms of Slater determinants, with $\eta_{ijkl} = 2\delta_{ik}\delta_{jl}$ for SDWs. If electron 2 is integrated over fragment A, the spinless DAFH $G^A(\boldsymbol{r})$ function is

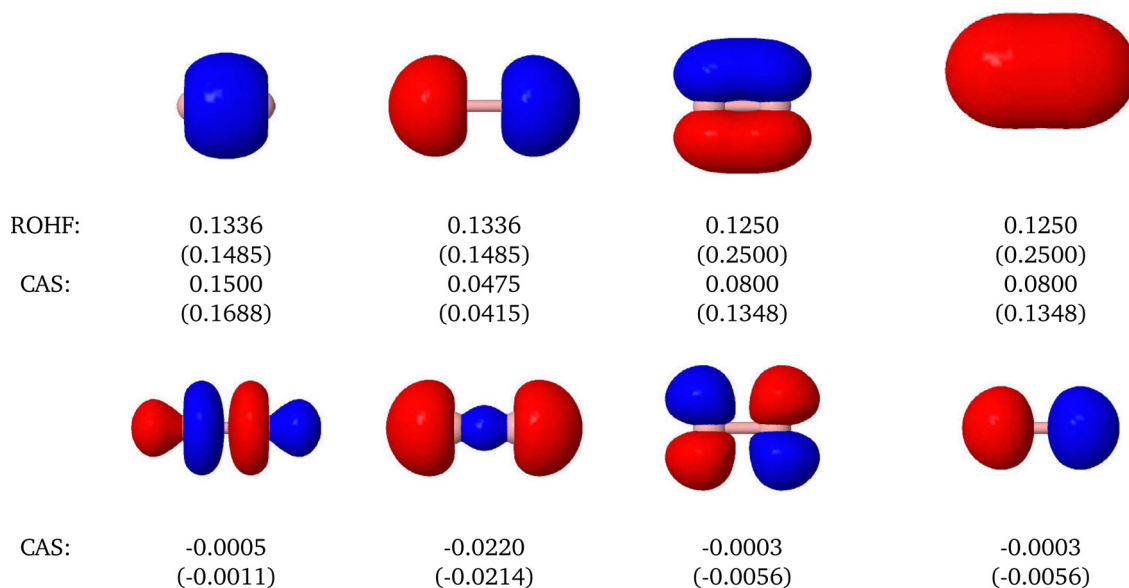**Fig. 13** $|\psi| = 0.05$ a.u. isosurfaces for the non-core NAdOs in the B2 and C2 molecules. The numbers below correspond to their respective occupations n_i^{ab} at the ROHF and CAS levels, with a 6-311G(d,p)++ basis set. C$_2$ data in parenthesis. Reproduced from ref. 256. Copyright 2015 John Wiley and Sons, Inc.
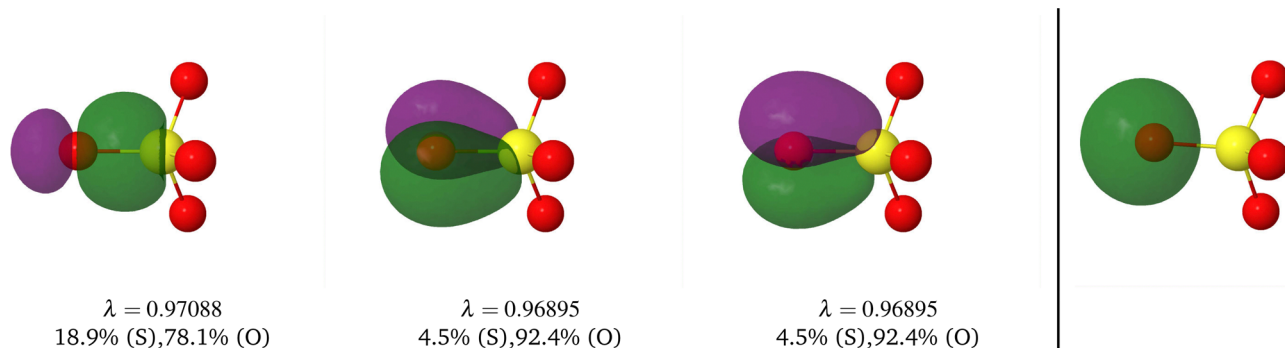
10254 | *Phys. Chem. Chem. Phys.*, 2023, **25**, 10231–10262

This journal is © the Owner Societies 2023

$$\lambda = 0.97088$$
18.9% (S),78.1% (O)

$$\lambda = 0.96895$$
4.5% (S),92.4% (O)

$$\lambda = 0.96895$$
4.5% (S),92.4% (O)

Fig. 14 $|\varphi| = 0.05$ a.u. isosurface of the σ (left) and π (center and right) S–O FNOs of the SO_4^{2-} anion at the B3LYP//def2-QZVPPD level of calculation. The rightmost graph corresponds to the lone pair of oxygen atom. Reprinted with permission of the authors from ref. 257.

obtained:

$$G^A(\boldsymbol{r}_1) = \int_A d\boldsymbol{r}_2 \rho_2^{\mathrm{xc}}(\boldsymbol{r}_1,\boldsymbol{r}_2) = \sum_{ij} \phi_i(\boldsymbol{r}_1) G_{ij}^A \phi_j(\boldsymbol{r}_2), \quad (65)$$

where $G_{ij}^A = \sum_{kl} \eta_{ijkl} S_{kl}^A$. The diagonalization of $G^A/2 = G_\alpha^A = G_\beta^A$ leads to a set of M DAFH MOs $\phi_i^A(\boldsymbol{r})$ and their corresponding occupation numbers n_i^A. The DAFH MOs of highest occupancy for the methanol molecule and their occupation numbers at the CCSD(T)//cc-pVDZ level are provided in Fig. 12. These are well-defined functions obtained at any level of theory that preserve conventional chemical wisdom and that are invariant under orbital tranformations of the underlying wavefunction. Notice how close to two the propulations are, much as in NBO analyses, without the need of the involved and some times *ad hoc* transformations that lead to natural bond orbitals.

We can use the DAFH to write

$$G^A(\boldsymbol{r}) = \sum_i^M 2n_i^A \left[\phi_i^A(\boldsymbol{r})\right]^2, \quad (66)$$

where the factor 2 accounts for both the α and β components of G^A, which turn out to be equal in a closed-shell molecule. The above expression was originally derived by Ponec,[239,240] and the analysis of the ϕ_i^A and n_i^A functions was carried out later by Ponec and other authors.[241–250] The formalism has been applied to a very large number of systems, both for fuzzy- and non-fuzzy partitions of space, and at equilibrium and non-equilibrium geometries. DAFHs are also intimately related to the effective atomic orbitals of Mayer,[251] which have been very successfully used by Salvador and coworkers to obtain oxidation states in agreement with the IUPAC's recommendations.[252,253] From now on, we will call the ϕ_i^A s obtained for SDWs domain natural orbitals (DNOs). In the SDW case, G^A acquires a very simple form, since it is given by $G^A = 2S^A$, where S^A is the AOM defined in eqn (26).

The occupation numbers n_i^A satisfy $2\sum_i^M n_i^A = \langle n_A \rangle$, the average number of electrons in A. Given that $\int_{R^3} \rho_{\mathrm{xc}}(\boldsymbol{r},\boldsymbol{r}_2) d\boldsymbol{r}_2 = \rho(\boldsymbol{r})$, we also have $\sum_A G^A(\boldsymbol{r}) = \rho(\boldsymbol{r})$. From eqn (39), (65) and (66), the

delocalization index between A and B, δ^{AB}, is given by[248]

$$\delta^{AB} = 4\sum_i n_i^A \int_B \left[\phi_i^A(\boldsymbol{r})\right]^2 d\boldsymbol{r} = 4\sum_i n_i^B \int_A \left[\phi_i^B(\boldsymbol{r})\right]^2 d\boldsymbol{r}, \quad (67)$$

$$= 2\sum_i n_i^A \int_B \left[\phi_i^A(\boldsymbol{r})\right]^2 d\boldsymbol{r} + 2\sum_i n_i^B \int_A \left[\phi_i^B(\boldsymbol{r})\right]^2 d\boldsymbol{r}. \quad (68)$$

eqn (68) arises due to the symmetry $\int_B G^A(\boldsymbol{r})d\boldsymbol{r} = \int_A G^B(\boldsymbol{r})d\boldsymbol{r}$. δ^{AB} takes a simpler form when the sum of fragments A and B exhaust the system ($A \cup B = R^3$). Then, the first integral in eqn (68) is equal to $1 - s_i^A$, where $s_i^A = \int_A \left[\phi_i^A(\boldsymbol{r})\right]^2 d\boldsymbol{r}$., and the second becomes $1 - s_i^B$, where $s_i^B = \int_B \left[\phi_i^B(\boldsymbol{r})\right]^2 d\boldsymbol{r}$, so δ^{AB} can be written as

$$\delta^{AB} = 2\sum_i n_i^A (1 - s_i^A) + 2\sum_i n_i^B (1 - s_i^B). \quad (69)$$

As already stated, both contributions to δ^{AB} are equal. However, $\phi_i^A \neq \phi_i^B$ and $n_i^A(1 - s_i^A) \neq n_i^B(1 - s_i^B)$ in general wavefunctions. Nonetheless, further simplifications in the formalism, very illuminating as regards the relevance of DNOs in chemical bonding theory, take place for SDWs when $A \cup B = R^3$.[254] In this case, using the property $S^B = I - S^A$, it can be shown that $\phi_i^A = \phi_i^B$, and not only that: DNOs, in addition to being orthonormal in R^3, are also orthogonal in A and B, with $\langle \phi_i^A | \phi_j^A \rangle_A = \delta_{ij}s_i^A = \delta_{ij}(1 - \langle \phi_i^B | \phi_j^B \rangle_B) = \delta_{ij}(1 - s_i^B)$. Moreover, the occupations of both fragments are related by $n_i^A = 1 - n_i^B$, and are equal to the respective overlaps in the fragments, $n_i^A = s_i^A$ and $n_i^B = s_i^B$. In the end, all these transformations allow us to write eqn (69) as

$$\delta^{AB} = 4\sum_i s_i^A (1 - s_i^A) = 4\sum_i s_i^B (1 - s_i^B). \quad (70)$$

The relevance of the above equation is that it connects the bond order between A and B, measured through δ^{AB}, with the localized or delocalized character of the DNOs. A DNO highly localized in A ($s_i^A = 1 - s_i^B \simeq 1$) or in B ($s_i^B = 1 - s_i^A \simeq 1$) hardly contributes to δ^{AB} and only those orbitals significantly delocalized in both fragments give rise to significant contributions to the bond order. In an indirect way, the exchange–correlation interaction energy between two fragments A and B (V_{xc}^{AB}), as long as $A \cup B = R^3$ and the wavefunction is a SDW expressed in terms of the DNOs, is completely dominated by those DNOs with appreciable delocalization in A and B simultaneously. The contribution of

This journal is © the Owner Societies 2023

Phys. Chem. Chem. Phys., 2023, **25**, 10231–10262 | **10255**

those DNOs that are strongly localized in one of the two fragments is very small. This picture offers an extraordinarily coherent image of our electron counting formalism plus IQA energy partitioning method. Expressed in a language quite familiar to chemists: the core electrons of a system (represented in this case by highly localized DNOs in one of the fragments) have little relevance, both from the point of view of the bond order (*i.e.* the δ^{AB} value), as well as from the energetic viewpoint (*i.e.* the V_{xc}^{AB} value).

7.2 Natural adaptive molecular orbitals (NAdOs)

The use of cumulant densities allow for a rather simple generalization of DNOs to the multicenter case. As we have seen, if one electron coordinate of the nth-order cumulant density (nCD), ρ_n^c, is integrated out we recover the $(n-1)$th CD (eqn (13)). Taking, for instance, $n = 3$,

$$\rho_2^c(\mathbf{r}_1, \mathbf{r}_2) = \rho_{xc}(\mathbf{r}_1, \mathbf{r}_2) = \int_{R^3} d\mathbf{r}_3 \rho_3^c(\mathbf{r}_1, \mathbf{r}_2, \mathbf{r}_3), \qquad (71)$$

Alternatively, if we integrate $\mathbf{r}_1$ in a region Ω_A and $\mathbf{r}_2$ in another region Ω_B, what it is obtained is the one-electron function $\rho_{ab}(\mathbf{r})$.

$$\rho_{ab}(\mathbf{r}) = \int_{\Omega_A} d\mathbf{r}_1 \int_{\Omega_B} d\mathbf{r}_2 \rho_3^c(\mathbf{r}_1, \mathbf{r}_2, \mathbf{r}). \qquad (72)$$

Expressed in the basis $\{\phi_i\}$ of canonical orbitals,

$$\rho_{ab}(\mathbf{r}) = (\phi_1 \phi_2 \cdots) \mathbf{D}^{ab} (\phi_1 \phi_2 \cdots)^\dagger, \qquad (73)$$

where $\mathbf{D}^{ab}$ is a symmetric matrix that can be diagonalized. In terms of its eigenvalues $\{n_i^{ab}\}$ and eigenvectors $\{\psi_i^{ab}\}$

$$\rho_{ab}(\mathbf{r}) = \sum_i n_i^{ab} |\psi_i^{ab}(\mathbf{r})|^2. \qquad (74)$$

Since $\int_{R^3} d\mathbf{r} \rho_{ab}(\mathbf{r}) = \delta^{AB}/2$, and each $\psi_i^{ab}(\mathbf{r})$ is normalized, the n_i^{ab}s obey the sum rule $2\sum_i n_i^{ab} = \delta^{AB}$. Thus, $2 \times n_i^{ab}$ is the contribution of $\psi_i^{ab}(\mathbf{r})$ to the bond order between A and B, and each ψ_i^{ab} itself defines a two-center natural adaptive orbital (NAdO). This means that two-center NAdOs induce a one-electron decomposition of any two-center delocalization index.

The generalization to an arbitrary n is straightforward:[256]

$$\rho_{ab\cdots n}(\mathbf{r}) = \int_{\Omega_A} d\mathbf{r}_1 \int_{\Omega_B} d\mathbf{r}_2 \cdots \int_{\Omega_n} d\mathbf{r}_n \rho_{n+1}^c(\mathbf{r}_1, \ldots, \mathbf{r}_n, \mathbf{r}), \qquad (75)$$

$$= (\phi_1 \phi_2 \cdots) \mathbf{D}^{ab\cdots n} (\phi_1 \phi_2 \cdots)^\dagger, \qquad (76)$$

and

$$= \sum_i n_i^{ab\cdots n} |\psi_i^{ab\cdots n}(\mathbf{r})|^2, \qquad (77)$$

where $\{\psi_i^{ab\cdots n}\}$ and $\{n_i^{ab\cdots n}\}$ are the n-center NAdOs and their eigenvalues, respectively. Since $\int_{R^3} d\mathbf{r} \rho_{ab\cdots n}(\mathbf{r}) = \delta^{AB\cdots n}/n!$ and the $\psi_i^{ab\cdots n}(\mathbf{r})$'s are again normalized, the sum rule is now $n! \sum_i n_i^{ab\cdots n} = \delta^{AB\cdots n}$, than can be taken as an n-center delocalization index. When $n = 1$, the generalized density $\rho_a(\mathbf{r})$ coincides with the DAFH function $G^A(\mathbf{r})$ defined in the previous subsection, and the 1-center NAdOs $\psi_i^a(\mathbf{r})$ and their eigenvalues

n_i^a's are equal to twice the DAFH occupancies ($2n_i^A$) and DAFH MOs $\phi_i^A(\mathbf{r})$.

The n-center NAdOs provide clear images of n-center bonds, and are adaptively localized or delocalized over the n centers used to compute them. If one NAdO is fully localized over one center, it represents a core or lone-pair orbital of that center and does not contribute to any n-center bond ($n > 1$). If one of the NAdOs is completely localized over n centers, it describes a pure n-center bond. In contrast, a NAdO which is only partly localized on n centers signals the existence of higher order multicenter bonding. For instance, NAdOs obtained for $n = 1$ can be fully localized on one center (*i.e.* they describe core or lone pair orbitals) or delocalized over two or more centers, describing in this second case the existence of at least two-center bonding. This means that the NAdOS obtained by diagonalizing $\rho_a(\mathbf{r})$ can be used to analyze chemical bonds in real space if we focus our attention on their delocalized components. This procedure is, in fact, the usual way in which Ponec's DAFHs have generally been used since they were proposed. Nonetheless, we note that the formalism just introduced is more suitable for this purpose. Moreover, n-center NAdOs obtained as described here transform according to the irreducible representations of the group of the n centers involved in obtaining them. No *a posteriori* matrix transformation as, for instance, an isopycnic rotation, is necessary to achieve this.

As an example, the valence NAdOs obtained for the B_2 and C_2 molecules, described at the restricted open shell HF (ROHF) as well as the CAS levels are shown in Fig. 13. It can be clearly seen that their shape is easily interpreted with standard chemical wisdom, and that we clearly isolate σ or π contributions as in standard molecular orbital theory. NAdOs, however, contain extra information, since their occupation numbers measure their contribution to the total bond order. Thus we see that both in dicarbon and diboron the σ_g and σ_u functions contribute considerably to bonding at the mean-field level, leading to a close to quadruple bond image in C_2, but that the σ_u function becomes considerably less important upon inclusion of correlation.

7.3 Fragment natural orbitals (FNOs)

Much as in the NBO paradigm it is the atomic blocks of the 1RDM written in an atom-centered basis which is diagonalized to provide natural atomic orbitals,[231] the consideration of an atom or fragment in real space as an open quantum system (OQS) can be used to define real space analogues of an atomic RDMs. We call fragment natural orbitals (FNOs) the orbitals obtained for a fragment A of a molecule after diagonalizing its OQS 1RDM. It can be shown[238] that the 1RDM of an atom or fragment A can be written as $\rho_A(\mathbf{r};\mathbf{r}') = \omega_A(\mathbf{r})\omega_A(\mathbf{r}')\rho(\mathbf{r};\mathbf{r}')$, where ω_A is a weight factor as defined above (when A is a single atom) or the sum of the weight factors of all the atoms that make up the fragment otherwise, and $\rho(\mathbf{r};\mathbf{r}')$ is the standard 1RDM of the whole molecule. When the latter is expressed in a basis of orthonormal orbitals $|u_i\rangle$,

$$\rho(\mathbf{r};\mathbf{r}') = \sum_{i,j} u_i^*(\mathbf{r}')\rho_{ij} u_j(\mathbf{r}) = |u\rangle \rho \langle u|, \qquad (78)$$

$\rho_A(\mathbf{r};\mathbf{r}')$ results

10256 | *Phys. Chem. Chem. Phys.*, 2023, **25**, 10231–10262

This journal is © the Owner Societies 2023

$$\rho_{A}(\boldsymbol{r};\boldsymbol{r}') = \omega_{A}(\boldsymbol{r})|u\rangle\rho\langle u|\omega_{A}(\boldsymbol{r}'). \tag{79}$$

The matrix representation of $\rho_A(\boldsymbol{r};\boldsymbol{r}')$ in the $|u_i\rangle$ basis is simply $S^A\rho S^A$, where S^A is the standard AOM matrix (eqn (26)) when A is an atom, or the sum of the AOMs of all the atoms that make up the fragment A. The FNOs of this fragment are obtained by diagonalizing $S^A\rho S^A$, taking care that the basis $|u_i\rangle$ is not orthonormal in A. This is equivalent to diagonalize $\rho_A = (S^A)^{1/2}\rho(S^A)^{1/2}$, i.e. $\rho_A U = U\mathrm{diag}(\lambda^A)$. An alternative possibility is to first express the standard 1RDM in the Löwdin orthogonalized basis $|u^p\rangle$, defined as $|u^p\rangle = |u\rangle(S^A)^{-1/2}$. In this basis, the matrix representation of $\rho_A(\boldsymbol{r};\boldsymbol{r}')$ is directly ρ_A. Be that as it may, FNOs of fragment A are given by $|\varphi\rangle = |u^p\rangle U = |u\rangle (S^A)^{-1/2}U \equiv |u\rangle C$. The φ_i functions are orthonormal in A but not in R^3, since $\langle\varphi|\varphi\rangle_{R3} = U^\dagger(S^A)^{-1}U = C^\dagger C \neq I$.

In SDWs, $\rho = 2I$ (where I is the identity matrix) and, therefore, $\rho_A = (S^A)^{1/2}\rho(S^A)^{1/2} = 2S^A$, so that the matrix representation of $\rho_A(\boldsymbol{r};\boldsymbol{r}')$ coincides with twice the AOM in fragment A. In other words, ρ_A it is equal to the G^A matrix that is diagonalized in the derivation of Ponec's DNOs. This means that DNOs and FNOs are the same in this case, as well as their respective occupations, $\lambda_i^A = 2n_i^A$. Furthermore, since S^A is positive definite, all λ_i^As are greater than zero, so there are no DNOs or FNOs with negative occupations in case of SDWs. This equivalence between DNOs and FNOs in SDWs extends also to 1- and 2-center NAdOs provided that $A\cup B = R^3$, since $D^a = S^A$, $D^b = S^B$, and $D^{ab} = (S^AS^B + S^BS^A)/2$ in SDWs. The diagonalization of these three matrices lead to the same eigenvectors, $\psi_i^a = \psi_i^b = \psi_i^{ab}$, for $S^B = I - S^A$. Moreover, occupations derived from D^a and D^b are related by $n_i^a = 1 - n_i^b$ and each n_i^a is the self-overlap integral of ψ_i^a in A, $n_i^a = \int_{\Omega_A}\psi_i^{*a}(\boldsymbol{r})\psi_i^a(\boldsymbol{r})d\boldsymbol{r}$.

We took the SO_4^{2-} anion as an example to illustrate FNOs. In Fig. 14 we present the bonding FNOs for one of the four equivalent S–O pairs, as well as the oxygen lone pair FNO. As we clearly see, there is a triple S–O bond (one σ and two equivalent π bonds).

8 Summary and conclusions

We have reviewed in this perspective some recent advances in the concept of an atom-in-a-molecule from a real space viewpoint. We have shown that both fuzzy and non-fuzzy decompositions can be dealt with, on the same footing, when atomic weight functions are used and have examined a few of the best-known weights in both categories. Once an atom (or fragment) is so defined, a wealth of chemically relevant information becomes accessible by using reduced densities or density matrices and their irreducible parts, the so-called cumulant densities or density matrices. We have stressed how the expectation value of any operator can be written as a sum of atomic contributions. This is not the case in many other methodologies. When the expectation values of the densities themselves are partitioned, we obtain atomic, interatomic, or, in general, polyatomic populations that provide, in the limit, the full statistical electron distribution function. The relationship between the fluctuation of the atomic or fragment populations and the real space multicenter bond orders has been highlighted. This link is particularly important, and not so well known. When

the total Hamiltonian operator is partitioned instead, an energy decomposition arises, the interacting quantum atoms (IQA) method, which writes the total energy of a system as a sum of atomic or fragment self-energies and pairwise additive interatomic (interfragment) interactions. We have focused on recent expansions of IQA to intermolecular interactions and biologically important compounds. A straightforward link between electron counting and IQA has also been reviewed. Finally, a means to recover one-electron functions, i.e. orbitals, from real space partitions, has also been provided.

The definition of an atom-in-a-molecule as a real space object provides a unique way to examine the spatial distribution of the electrons in a molecule. By adopting this viewpoint, fully compatible with the underlying quantum mechanical reality, the chemist's language shifts from orbitals (which if endowed with an energetic signature must be delocalized) to interactions. Instead of isolating electrons from nuclei and considering more or less delocalized objects that exactly host one or two electrons, the real space perspective considers spatial regions associated with interacting atoms or fragments. These regions do not possess an immutable but a fluctuating number of particles. The fluctuations can be followed if the probabilities of finding a given partition of the electrons in the set of atomic regions, i.e. the electron distribution function, are computed. The number of atoms involved in these population fluctuations decides whether we have two-center or multi-center bonds, which can be visualized by building appropriate one-electron functions that further decompose bond orders using an orbital-like narrative.

Author contributions

Conflicts of interest

There are no conflicts to declare.

Acknowledgements

References

1 C. A. Coulson, Rev. Mod. Phys., 1960, 32, 170–177.
2 F. Neese, M. Atanasov, G. Bistoni, D. Maganas and S. Ye, J. Am. Chem. Soc., 2019, 141, 2814–2824.
3 K. T. Butler, D. W. Davies, H. Cartwright, O. Isayev and A. Walsh, Nature, 2018, 559, 547–555.

This journal is © the Owner Societies 2023

Phys. Chem. Chem. Phys., 2023, 25, 10231–10262 | 10257

4   A. Aspuru-Guzik, M.-H. Baik, S. Balasubramanian, R. Banerjee, S. Bart, N. Borduas-Dedekind, S. Chang, P. Chen, C. Corminboeuf, F.-X. Coudert, L. Cronin, C. Crudden, T. Cuk, A. G. Doyle, C. Fan, X. Feng, D. Freedman, S. Furukawa, S. Ghosh, F. Glorius, M. Jeffries-EL, N. Katsonis, A. Li, S. S. Linse, S. Marchesan, N. Maulide, A. Milo, A. R. H. Narayan, P. Naumov, C. Nevado, T. Nyokong, R. Palacin, M. Reid, C. Robinson, G. Robinson, R. Sarpong, C. Schindler, G. S. Schlau-Cohen, T. W. Schmidt, R. Sessoli, Y. Shao-Horn, H. Sleiman, J. Sutherland, A. Taylor, A. Tezcan, M. Tortosa, A. Walsh, A. J. B. Watson, B. M. Weckhuysen, E. Weiss, D. Wilson, V. W.-W. Yam, X. Yang, J. Y. Ying, T. Yoon, S.-L. You, A. J. G. Zarbin and H. Zhang, *Nat. Chem.*, 2019, **11**, 286–294.

5   J. M. Galbraith, S. Shaik, D. Danovich, B. Braïda, W. Wu, P. Hiberty, D. L. Cooper, P. B. Karadakov and T. H. Dunning, *J. Chem. Educ.*, 2021, **98**, 3617–3620.

6   M. Kohout, K. Pernal, F. R. Wagner and Y. Grin, *Theor. Chem. Acc.*, 2004, **112**, 453–459.

7   M. Kohout, K. Pernal, F. R. Wagner and Y. Grin, *Theor. Chem. Acc.*, 2005, **113**, 287–293.

8   M. Kohout, F. R. Wagner and Y. Grin, *Theor. Chem. Acc.*, 2007, **119**, 413–420.

9   K. Ruedenberg and M. W. Schmidt, *J. Phys. Chem. A*, 2009, **113**, 1954–1968.

10 W. A. Kato, *Commun. Pure Appl. Math.*, 1957, **10**, 151.

11 P. Hohenberg and W. Kohn, *Phys. Rev.*, 1964, **136**, B864–B871.

12 R. F. W. Bader, *Atoms in Molecules*, Oxford University Press, Oxford, 1990.

13 J. M. Guevara-Vela, E. Francisco, T. Rocha-Rinza and Á. Martín Pendás, *Molecules*, 2020, **25**, 4028.

14 E. Francisco, Á. Martín Pendás and M. A. Blanco, *J. Chem. Theory Comput.*, 2006, **2**, 90–102.

15 Á. Martín Pendás, M. Kohout, M. A. Blanco and E. Francisco, in *Modern Charge-density analysis*, ed. C. Gatti and P. Macchi, Springer, Dordrecht., 2012, p. 165.

16 C. Kittel, *Introduction to solid state physics*, John Wiley & Sons, Nashville, TN, 8th edn, 2004.

17 J. C. Slater, *J. Chem. Phys.*, 1964, **41**, 3199–3204.

18 R. F. W. Bader, T. T. Nguyen-Dang and Y. Tal, *Rep. Prog. Phys.*, 1981, **44**, 893–948.

19 J. S. M. Anderson, P. W. Ayers and J. I. R. Hernandez, *J. Phys. Chem. A*, 2010, **114**, 8884–8895.

20 A. D. Becke and K. E. Edgecombe, *J. Chem. Phys.*, 1990, **92**, 5397–5403.

21 B. Silvi and A. Savin, *Nature*, 1994, **371**, 683–686.

22 V. Polo, J. Andres, S. Berski, L. R. Domingo and B. Silvi, *J. Phys. Chem. A*, 2008, **112**, 7128–7136.

23 J. Andrés, S. Berski and B. Silvi, *Chem. Commun.*, 2016, **52**, 8183–8195.

24 M. Kohout, *Int. J. Quantum Chem.*, 2003, **97**, 651–658.

25 In *Chemical applications of atomic and molecular electrostatic potentials*, ed. P. Politzer and D. G. Truhlar, Springer, New York, NY, 1981st edn, 1981.

26 S. R. Gadre and R. D. Bendale, *Chem. Phys. Lett.*, 1986, **130**, 515–521.

27 S. R. Gadre, S. A. Kulkarni and I. H. Shrivastava, *J. Chem. Phys.*, 1992, **96**, 5253–5260.

28 I. Mata, E. Molins and E. Espinosa, *J. Phys. Chem. A*, 2007, **111**, 9859–9870.

29 S. R. Gadre, C. H. Suresh and N. Mohan, *Molecules*, 2021, **26**, 3289.

30 Á. Martín Pendás and J. Hernández-Trujillo, *J. Chem. Phys.*, 2012, **137**, 134101.

31 J. Dillen, *J. Comput. Chem.*, 2015, **36**, 883–890.

32 V. Tsirelson and A. Stash, *Acta Crystallogr., Sect. B: Struct. Sci., Cryst. Eng. Mater.*, 2020, **76**, 769–778.

33 N. O. J. Malcolm and P. L. A. Popelier, *Faraday Discuss.*, 2003, **124**, 353.

34 P. Popelier, *Coord. Chem. Rev.*, 2000, **197**, 169–189.

35 B. Landeros-Rivera, M. Gallegos, J. Munárriz, R. Laplaza and J. Contreras-García, *Phys. Chem. Chem. Phys.*, 2022, **24**, 21538–21548.

36 Á. Martín Pendás, M. A. Blanco, A. Costales, P. M. Sánchez and V. Luaña, *Phys. Rev. Lett.*, 1999, **83**, 1930–1933.

37 R. Saha, P. Das and P. K. Chattaraj, *ChemPhysChem*, 2022, e202200329-1-17.

38 M. Marqués, M. I. McMahon, E. Gregoryanz, M. Hanfland, C. L. Guillaune, C. J. Pickard, G. J. Ackland and R. J. Nelmes, *Phys. Rev. Lett.*, 2011, **106**, 095502.

39 V. Postils, M. Garcia-Borràs, M. Solà, J. M. Luis and E. Matito, *Chem. Commun.*, 2015, **51**, 4865–4868.

40 S. Noorizadeh, *Chem. Phys. Lett.*, 2016, **652**, 40–45.

41 Á. Martín Pendás, E. Francisco, M. Blanco and C. Gatti, *Chem. – Eur. J.*, 2007, **13**, 9362–9371.

42 S. Shahbazian, *Chem. – Eur. J.*, 2018, **24**, 5401–5405.

43 M. Yu and D. R. Trinkle, *J. Chem. Phys.*, 2011, **134**, 064111.

44 M. Goli and S. Shahbazian, *Theor. Chem. Acc.*, 2013, **132**, 1365.

45 M. Goli and S. Shahbazian, *Phys. Chem. Chem. Phys.*, 2014, **16**, 6602.

46 M. Goli and S. Shahbazian, *ChemPhysChem*, 2019, **20**, 831–837.

47 S. Shahbazian, *Advances in Quantum Chemical Topology Beyond QTAIM*, Elsevier, 2023, pp. 73–109.

48 A. D. Becke, *J. Chem. Phys.*, 1988, **88**, 2547–2553.

49 P. Salvador and E. Ramos-Cordoba, *J. Chem. Phys.*, 2013, **139**, 071103.

50 C. Fonseca Guerra, J.-W. Handgraaf, E. J. Baerends and F. M. Bickelhaupt, *J. Comput. Chem.*, 2003, **25**, 189–210.

51 A. N. Petelski and C. Fonseca Guerra, *Chem. – Asian J.*, 2022, **17**, e202201010.

52 D. Svatunek, T. Hansen, K. N. Houk and T. A. Hamlin, *J. Org. Chem.*, 2021, **86**, 4320–4325.

53 A. M. Köster, R. Flores-Moreno and J. U. Reveles, *J. Chem. Phys.*, 2004, **121**, 681–690.

54 R. Stratmann, G. E. Scuseria and M. J. Frisch, *Chem. Phys. Lett.*, 1996, **257**, 213–223.

55 F. L. Hirshfeld, *Theor. Chem. Acc.*, 1977, **44**, 129–138.

56 K. Kullback and R. A. Leibler, *Ann. Math. Statistics*, 1951, **22**, 79.

10258 | *Phys. Chem. Chem. Phys.*, 2023, **25**, 10231–10262

This journal is © the Owner Societies 2023

57 R. F. Nalewajski, *Information origins of the chemical bond*, Nova Science, Hauppauge, NY, 2010.

58 P. Bultinck, C. V. Alsenoy, P. W. Ayers and R. Carbó-Dorca, *J. Chem. Phys.*, 2007, **126**, 144111.

59 K. Finzel, Á. Martín Pendás and E. Francisco, *J. Chem. Phys.*, 2015, **143**, 084115.

60 F. Heidar-Zadeh, P. W. Ayers, T. Verstraelen, I. Vinogradov, E. Vöhringer-Martinez and P. Bultinck, *J. Phys. Chem. A*, 2017, **122**, 4219–4245.

61 T. C. Lillestolen and R. J. Wheatley, *J. Chem. Phys.*, 2009, **131**, 144101.

62 J. F. Rico, R. López and G. Ramírez, *J. Chem. Phys.*, 1999, **110**, 4213–4220.

63 R. McWeeny, *Rev. Mod. Phys.*, 1960, **32**, 335–369.

64 E. Francisco, Á. Martín Pendás and M. A. Blanco, *J. Chem. Phys.*, 2007, **126**, 094102-1–094102-13.

65 C. Outeiral, M. A. Vincent, A. Martín Pendás and P. L. A. Popelier, *Chem. Sci.*, 2018, **9**, 5517–5529.

66 I. Mayer, *Chem. Phys. Lett.*, 1983, **97**, 270–274.

67 M. S. Giambiagi, M. Giambiagi and F. E. Jorge, *Theor. Chim. Acta*, 1985, **68**, 337–341.

68 J. G. Ángyán, E. Rosta and P. R. Surján, *Chem. Phys. Lett.*, 1999, **299**, 1–8.

69 A. Julg and P. Julg, *Int. J. Quantum Chem.*, 1978, **13**, 483–497.

70 M. A. Blanco, Á. Martín Pendás and E. Francisco, *J. Chem. Theory Comput.*, 2005, **1**, 1096–1109.

71 E. Francisco, D. Menéndez-Crespo, A. Costales and Á. Martín Pendás, *J. Comput. Chem.*, 2017, **38**, 816–829.

72 W. Kutzelnigg and D. Mukherjee, *J. Chem. Phys.*, 1999, **110**, 2800–2809.

73 P. Ziesche, *Int. J. Quantum Chem.*, 1996, **60**, 1361–1374.

74 C. Aslangul, R. Constanciel and R. Daudel, *Adv. Quantum Chem.*, 1972, **6**, 93–141.

75 E. Francisco, Á. Martín Pendás and M. A. Blanco, *Comput. Phys. Commun.*, 2008, **178**, 621–634.

76 E. Francisco, Á. Martín Pendás, M. García-Revilla and R. Álvarez Boto, *Comput. Theor. Chem.*, 2013, **1003**, 71–78.

77 M. Giambiagi, M. S. de Giambiagi and K. C. Mundim, *Struct. Chem.*, 1990, **1**, 423–427.

78 K. C. Mundim, M. Giambiagi and M. S. de Giambiagi, *J. Phys. Chem.*, 1994, **98**, 6118–6119.

79 R. Ponec, P. Bultinck and A. G. Saliner, *J. Phys. Chem. A*, 2005, **109**, 6606–6609.

80 R. Bochicchio, R. Ponec, A. Torre and L. Lain, *Theor. Chem. Acc.*, 2001, **105**, 292–298.

81 L. Lain, A. Torre, R. Bochicchio and R. Ponec, *Chem. Phys. Lett.*, 2001, **346**, 283–287.

82 A. Torre, L. Lain and R. Bochicchio, *J. Phys. Chem. A*, 2002, **107**, 127–130.

83 R. Bochicchio, L. Lain and A. Torre, *J. Comput. Chem.*, 2003, **24**, 1902–1909.

84 R. C. Bochicchio, A. Torre and L. Lain, *J. Chem. Phys.*, 2005, **122**, 084117.

85 A. Torre, D. R. Alcoba, L. Lain and R. C. Bochicchio, *J. Phys. Chem. A*, 2010, **114**, 2344–2349.

86 D. R. Alcoba, A. Torre, L. Lain and R. C. Bochicchio, *J. Chem. Theory Comput.*, 2011, **7**, 3560–3566.

87 E. Cancès, R. Keriven, F. Lodier and A. Savin, *Theor. Chem. Acc.*, 2004, **111**, 373–380.

88 Á. Martín Pendás, E. Francisco and M. A. Blanco, *J. Chem. Phys.*, 2007, **127**, 144103-1–144103-9.

89 E. Francisco, Á. Martín Pendás and M. A. Blanco, *Theor. Chem. Acc.*, 2010, **128**, 433–444.

90 E. Chamorro, P. Fuentealba and A. Savin, *J. Comput. Chem.*, 2003, **24**, 496–504.

91 A. Gallegos, R. Carbó-Dorca, F. Lodier, E. Cancès and A. Savin, *J. Comput. Chem.*, 2005, **26**, 455–460.

92 O. M. Lopes, B. Braïda, M. Causà and A. Savin, *Advances in the Theory of Quantum Systems in Chemistry and Physics*, Springer, Netherlands, 2011, pp. 173–184.

93 M. Menéndez and A. M. Pendás, *Theor. Chem. Acc.*, 2014, **133**, 1539.

94 M. Causà and A. Savin, *J. Phys. Chem. A*, 2011, **115**, 13139–13148.

95 A. Scemama, M. Caffarel and A. Savin, *J. Comput. Chem.*, 2006, **28**, 442–454.

96 G. Acke, S. D. Baerdemacker, P. W. Claeys, M. V. Raemdonck, W. Poelmans, D. V. Neck and P. Bultinck, *Mol. Phys.*, 2016, **114**, 1392–1405.

97 D. V. Hende, L. Lemmens, S. D. Baerdemacker, D. V. Neck, P. Bultinck and G. Acke, *J. Comput. Chem.*, 2022, **43**, 457–464.

98 Á. Martín Pendás and E. Francisco, *ChemPhysChem*, 2019, **20**, 2722–2741.

99 R. F. W. Bader and M. E. Stephens, *J. Am. Chem. Soc.*, 1975, **97**, 7391.

100 R. F. W. Bader and M. E. Stephens, *Chem. Phys. Lett.*, 1974, **26**, 445–449.

101 Y. Grin, A. Savin and B. Silvi, *The Chemical Bond*, Wiley-VCH Verlag GmbH & Co. KGaA, 2014, pp. 345–382.

102 B. Silvi and E. Alikhani, *J. Chem. Phys.*, 2022, **156**, 244305.

103 K. Wiberg, *Tetrahedron*, 1968, **24**, 1083–1096.

104 I. Mayer, *J. Comput. Chem.*, 2006, **28**, 204–221.

105 J. L. Casals-Sainz, J. Jara-Cortés, J. Hernández-Trujillo, J. M. Guevara-Vela, E. Francisco and Á. Martín Pendás, *Chem. – Eur. J.*, 2019, **25**, 12169–12179.

106 Á. Martn Pendás, E. Francisco and M. A. Blanco, *Phys. Chem. Chem. Phys.*, 2007, **9**, 1087–1092.

107 J. L. Casals-Sainz, F. Jiménez-Grávalos, E. Francisco and Á. Martín Pendás, *Chem. Commun.*, 2019, **55**, 5071–5074.

108 L. Zhao, M. Hermann, W. H. E. Schwarz and G. Frenking, *Nat. Rev. Chem.*, 2019, **3**, 48–63.

109 B. Jeziorski, R. Moszynski and K. Szalewicz, *Chem. Rev.*, 1994, **94**, 1887–1930.

110 K. Kitaura and K. Morokuma, *Int. J. Quantum Chem.*, 1976, **10**, 325–340.

111 K. Morokuma, *Acc. Chem. Res.*, 1977, **10**, 294–300.

112 T. Ziegler and A. Rauk, *Inorg. Chem.*, 1979, **18**, 1558–1565.

113 L. Zhao, M. von Hopffgarten, D. M. Andrada and G. Frenking, *Wiley Interdiscip. Rev.: Comput. Mol. Sci.*, 2017, **8**, e1345-1-37.

This journal is © the Owner Societies 2023

Phys. Chem. Chem. Phys., 2023, **25**, 10231–10262 | **10259**

114 F. M. Bickelhaupt and E. J. Baerends, *Rev. Comp. Chem.*, John Wiley & Sons, Inc., 2007, pp. 1–86.

115 D. S. Levine and M. Head-Gordon, *Proc. Natl. Acad. Sci. U. S. A.*, 2017, **114**, 12649–12656.

116 Á. Martín Pendás, M. A. Blanco and E. Francisco, *J. Comput. Chem.*, 2007, **28**, 161–184.

117 Á. Martín Pendás, M. A. Blanco and E. Francisco, *J. Chem. Phys.*, 2006, **125**, 184112-1–184112-20.

118 D. Tiana, E. Francisco, M. A. Blanco, P. Macchi, A. Sironi and Á. Martín Pendás, *J. Chem. Theory Comput.*, 2010, **6**, 1064–1074.

119 Á. Martín Pendás, M. A. Blanco and E. Francisco, *J. Comput. Chem.*, 2009, **30**, 98–109.

120 Á. Martín Pendás and E. Francisco, *Nat. Commun.*, 2022, **13**, 3327-1-10.

121 E. Francisco and A. Martín Pendás, in *Non-covalent Interactions in Quantum Chemistry and Physics*, ed. A. Otero-de-la Roza and G. DiLabio, Elsevier, Amsterdam, 2017, ch. Energy Partition Analyses: Symmetry-Adapted Perturbation Theory and Other Techniques, pp. 27–64.

122 S. Racioppi, A. Sironi and P. Macchi, *Phys. Chem. Chem. Phys.*, 2020, **22**, 24291–24298.

123 E. Francisco, J. L. Casals-Sainz, T. Rocha-Rinza and A. Martín Pendás, *Theor. Chem. Acc.*, 2016, **135**, 1–8.

124 P. Maxwell, Á. Martín Pendás and P. L. A. Popelier, *Phys. Chem. Chem. Phys.*, 2016, **18**, 20986–21000.

125 J. L. Casals-Sainz, J. M. Guevara-Vela, E. Francisco, T. Rocha-Rinza and Á. Martín Pendás, *J. Comput. Chem.*, 2020, **41**, 1234–1241.

126 L. F. Feitosa, R. B. Campos and W. E. Richter, *J. Mol. Graphics*, 2023, **118**, 108326.

127 I. Cukrowski, *Wiley Interdiscip. Rev.: Comput. Mol. Sci.*, 2021, **12**, e1579.

128 I. Cukrowski, D. M. E. van Niekerk and J. H. de Lange, *Struct. Chem.*, 2017, **28**, 1429–1444.

129 J. H. de Lange, D. M. E. van Niekerk and I. Cukrowski, *Phys. Chem. Chem. Phys.*, 2019, **21**, 20988–20998.

130 I. Cukrowski and P. Mangondo, *J. Comput. Chem.*, 2016, **37**, 1373–1387.

131 Á. Martín-Pendas, E. Francisco and M. A. Blanco, *Chem. Phys. Lett.*, 2008, **454**, 396–403.

132 J. Munárriz, R. Laplaza, Á. Martín Pendás and J. Contreras-García, *Phys. Chem. Chem. Phys.*, 2019, **21**, 4215–4223.

133 J. Munárriz, M. Gallegos, J. Contreras-García and Á. Martín Pendás, *Molecules*, 2021, **26**, 513.

134 J. M. Guevara-Vela, R. Chávez-Calvillo, M. García-Revilla, J. Hernández-Trujillo, O. Christiansen, E. Francisco, Á. MartínPendás and T. Rocha-Rinza, *Chem. – Eur. J.*, 2013, **19**, 14304–14315.

135 J. M. Guevara-Vela, E. Romero-Montalvo, A. Costales, Á. Martín Pendás and T. Rocha-Rinza, *Phys. Chem. Chem. Phys.*, 2016, **18**, 26383–26390.

136 T. Steiner, *Angew. Chem., Int. Ed.*, 2002, **41**, 48–76.

137 V. M. Castor-Villegas, J. M. Guevara-Vela, W. E. V. Narváez, Á. Martín Pendás, T. Rocha-Rinza and A. Fernández-Alarcón, *J. Comput. Chem.*, 2020, **41**, 2266–2277.

138 C. Foroutan-Nejad, Z. Badri and R. Marek, *Phys. Chem. Chem. Phys.*, 2015, **17**, 30670–30679.

139 M. A. Niyas, R. Ramakrishnan, V. Vijay, E. Sebastian and M. Hariharan, *J. Am. Chem. Soc.*, 2019, **141**, 4536–4540.

140 F. Jimeńez-Grávalos, M. Gallegos, Á. Martín-Pendás and A. S. Novikov, *J. Comput. Chem.*, 2021, **42**, 676–687.

141 W. E. V. Narváez, E. I. Jiménez, E. Romero-Montalvo, A. S. de la Vega, B. Quiroz-García, M. Hernández-Rodríguez and T. Rocha-Rinza, *Chem. Sci.*, 2018, **9**, 4402–4413.

142 W. E. V. Narváez, E. I. Jiménez, M. Cantú-Reyes, A. K. Yatsimirsky, M. Hernández-Rodríguez and T. Rocha-Rinza, *Chem. Commun.*, 2019, **55**, 1556–1559.

143 C. F. Matta, J. Hernández-Trujillo, T.-H. Tang and R. F. W. Bader, *Chem. – Eur. J.*, 2003, **9**, 1940–1951.

144 J. Poater, M. Solà and F. M. Bickelhaupt, *Chem. – Eur. J.*, 2006, **12**, 2889–2895.

145 J. Poater, M. Solà and F. M. Bickelhaupt, *Chem. – Eur. J.*, 2006, **12**, 2902–2905.

146 K. Eskandari and C. V. Alsenoy, *J. Comput. Chem.*, 2014, **35**, 1883–1889.

147 P. Matczak, *Bull. Chem. Soc. Jpn.*, 2016, **89**, 92–102.

148 P. L. A. Popelier, P. I. Maxwell, J. C. R. Thacker and I. Alkorta, *Theor. Chem. Acc.*, 2018, **138**, 12-1-16.

149 M. P. Mitoraj, F. Sagan, D. W. Szczepanik, J. H. Lange, A. L. Ptaszek, D. M. E. Niekerk and I. Cukrowski, *ChemPhysChem*, 2020, **21**, 494–502.

150 J. Clayden, N. Greeves and S. Warren, *Organic Chemistry*, Oxford University Press, London, England, 2nd edn, 2012.

151 A. L. Wilson and P. L. A. Popelier, *J. Phys. Chem. A*, 2016, **120**, 9647–9659.

152 R. A. Buckingham, *Proc. R. Soc. London, Ser. A*, 1938, **168**, 264–283.

153 B. C. B. Symons, D. J. Williamson, C. M. Brooks, A. L. Wilson and P. L. A. Popelier, *ChemistryOpen*, 2019, **8**, 560–570.

154 M. Gallegos, A. Costales and Á. Martín Pendás, *ChemPhysChem*, 2021, **22**, 775–787.

155 J. Jara-Cortes, B. Landeros-Rivera and J. Hernandez-Trujillo, *Phys. Chem. Chem. Phys.*, 2018, **20**, 27558–27570.

156 M. Gallegos, A. Costales and Á. Martín Pendás, *J. Phys. Chem. A*, 2022, **126**, 1871–1880.

157 J. L. Casals-Sainz, E. Francisco and Á. Martin Pendas, *Z. Anorg. Allg. Chem.*, 2020, **646**, 1062–1072.

158 E. Romero-Montalvo, J. M. Guevara-Vela, W. E. V. Narváez, A. Costales, Á. Martín Pendás, M. Hernández-Rodríguez and T. Rocha-Rinza, *Chem. Commun.*, 2017, **53**, 3516–3519.

159 A. Sauza-de la Vega, H. Salazar-Lozas, W. E. V. Narváez, M. Hernández-Rodríguez and T. Rocha-Rinza, *Org. Biomol. Chem.*, 2021, **19**, 6776–6780.

160 C. Barrales-Martínez, S. Gutierrez-Oliva, A. Toro-Labbe and A. Martin-Pendas, *ChemPhysChem*, 2021, **22**, 1976–1988.

161 J. Jara-Cortes, E. Leal-Sanchez and J. Hernandez-Trujillo, *J. Phys. Chem. A*, 2020, **124**, 6370–6379.

162 J. C. R. Thacker and P. L. A. Popelier, *Theor. Chem. Acc.*, 2017, **136**, 86-1-13.

10260 | *Phys. Chem. Chem. Phys.*, 2023, **25**, 10231–10262

This journal is © the Owner Societies 2023

163 A. Fernández-Alarcón, J. M. Guevara-Vela, J. L. Casals-Sainz, A. Costales, E. Francisco, Á. Martín Pendás and T. R. Rinza, *Chem. – Eur. J.*, 2020, **26**, 17035–17045.

164 J. Jara-Cortés, J. M. Guevara-Vela, Á. Martín Pendás and J. Hernández-Trujillo, *J. Comput. Chem.*, 2017, **38**, 957–970.

165 A. Fernández-Alarcón, J. L. Casals-Sainz, J. M. Guevara-Vela, A. Costales, E. Francisco, Á. Martín Pendás and T. Rocha-Rinza, *Phys. Chem. Chem. Phys.*, 2019, **21**, 13428–13439.

166 A. Sauza-de la Vega, L. J. Duarte, A. F. Silva, J. M. Skelton, T. Rocha-Rinza and P. L. A. Popelier, *Phys. Chem. Chem. Phys.*, 2022, **24**, 11278–11294.

167 F. Sagan, R. Filas and M. Mitoraj, *Crystals*, 2016, **6**, 28.

168 M. A. Niyas, R. Ramakrishnan, V. Vijay and M. Hariharan, *Chem. – Eur. J.*, 2018, **24**, 12318–12329.

169 A. T. John, A. Narayanasamy, D. George and M. Hariharan, *Cryst. Growth Des.*, 2022, **22**, 1237–1243.

170 D. M. Crespo, F. R. Wagner, E. Francisco, Á. Martín Pendás, Y. Grin and M. Kohout, *J. Phys. Chem. A*, 2021, **125**, 9011–9025.

171 K. D. Vogiatzis, M. V. Polynski, J. K. Kirkland, J. Townsend, A. Hashemi, C. Liu and E. A. Pidko, *Chem. Rev.*, 2019, **119**, 2453–2523.

172 S. Sowlati-Hashjin, V. Sadek, S. Sadjaji, M. Karttunen, Á. Martín Pendás and C. Foroutan-Nejad, *Nat. Commun.*, 2022, **13**, 2069-1-9.

173 C. Werlé, C. Bailly, L. Karmazin-Brelot, X.-F. LeGoff, M. Pfeffer and J.-P. Djukic, *Angew. Chem., Int. Ed.*, 2014, **53**, 9827–9831.

174 A. Caballero-Muñoz, J. M. Guevara-Vela, A. Fernández-Alarcón, M. A. Valentín-Rodríguez, M. Flores-Álamo, T. Rocha-Rinza, H. Torrens and G. Moreno-Alcántar, *Eur. J. Inorg. Chem.*, 2021, 2702–2711.

175 C. Lacaze-Dufaure, Y. Bulteau, N. Tarrat, D. Loffreda, P. Fau, K. Fajerwerg, M. L. Kahn, F. Rabilloud and C. Lepetit, *Inorg. Chem.*, 2022, **61**, 7274–7285.

176 J. M. Guevara-Vela, K. Hess, T. Rocha-Rinza, Á. Martín Pendás, M. Flores-Álamo and G. Moreno-Alcántar, *Chem. Commun.*, 2022, **58**, 1398–1401.

177 F. Sagan, M. Mitoraj and M. Jabłoński, *Int. J. Mol. Sci.*, 2022, **23**, 14668.

178 Z. Liu, Y. Bai, Y. Li, J. He, Q. Lin, H. Xie and Z. Tang, *Phys. Chem. Chem. Phys.*, 2020, **22**, 23773–23784.

179 J. F. Van der Maelen, *Organometallics*, 2020, **39**, 132–141.

180 I. Cukrowski, J. H. de Lange and M. Mitoraj, *J. Phys. Chem. A*, 2014, **118**, 623–637.

181 J. Munárriz, E. Velez, M. A. Casado and V. Polo, *Phys. Chem. Chem. Phys.*, 2018, **20**, 1105–1113.

182 P. Śliwa, M. P. Mitoraj, F. Sagan and J. Handzlik, *J. Mol. Model.*, 2019, **25**, 331.

183 V. Thiel, M. Hendann, K.-J. Wannowius and H. Plenio, *J. Am. Chem. Soc.*, 2011, **134**, 1104–1114.

184 Y. Cornaton and J.-P. Djukic, *Acc. Chem. Res.*, 2021, **54**, 3828–3840.

185 M. A. Sajjad, J. A. Harrison, A. J. Nielson and P. Schwerdtfeger, *Organometallics*, 2018, **37**, 3659–3669.

186 J. A. Harrison, A. J. Nielson, M. A. Sajjad and P. Schwerdtfeger, *Organometallics*, 2019, **38**, 1903–1916.

187 Y. Cornaton and J.-P. Djukic, *Phys. Chem. Chem. Phys.*, 2019, **21**, 20486–20498.

188 F. Wu, C. Deraedt, Y. Cornaton, J. Contreras-Garcia, M. Boucher, L. Karmazin, C. Bailly and J.-P. Djukic, *Organometallics*, 2020, **39**, 2609–2629.

189 C. F. Matta, *J. Comput. Chem.*, 2014, **35**, 1165–1198.

190 P. Popelier, *Curr. Top. Med. Chem.*, 2012, **12**, 1924–1934.

191 P. L. A. Popelier, *J. Mol. Model.*, 2022, **28**, 276-1-41.

192 S. Grimme, *Wiley Interdiscip. Rev.: Comput. Mol. Sci.*, 2011, **1**, 211–228.

193 T. A. Keith, *AIMAll 19.10.12*, 2019, **http://aim.tkgritsmill.com**.

194 H. Salazar-Lozas, J. M. Guevara-Vela, Á. Martín Pendás, E. Francisco and T. Rocha-Rinza, *Phys. Chem. Chem. Phys.*, 2022, **24**, 19521–19530.

195 D. Suárez, N. Díaz, E. Francisco and Á. Martín Pendás, *ChemPhysChem*, 2018, **19**, 973–987.

196 N. Díaz, F. Jímenez-Grávalos, D. Suárez, E. Francisco and Á. Martín Pendás, *Phys. Chem. Chem. Phys.*, 2019, **21**, 25258–25275.

197 S. Ebrahimi, H. A. Dabbagh and K. Eskandari, *Phys. Chem. Chem. Phys.*, 2016, **18**, 18278–18288.

198 A. V. Belyakov, M. A. Gureev, A. V. Garabadzhiu, V. A. Losev and A. N. Rykov, *Struct. Chem.*, 2015, **26**, 1489–1500.

199 M. O. Miranda, D. J. R. Duarte and I. Alkorta, *ChemPhysChem*, 2020, **21**, 1052–1059.

200 B. J. R. Cuyacot, I. Durnik, C. Foroutan-Nejad and R. Marek, *J. Chem. Inf. Model.*, 2021, **61**, 211–222.

201 B. Milovanović, A. Stanojević, M. Etinski and M. Petković, *J. Phys. Chem. B*, 2020, **124**, 3002–3014.

202 A. Stanojević, B. Milovanović, I. Stanković, M. Etinski and M. Petković, *Phys. Chem. Chem. Phys.*, 2021, **23**, 574–584.

203 D. M. Buyens, L. A. Pilcher and I. Cukrowski, *Coordination Sites for Sodium and Potassium Ions in Nucleophilic Adeninate Contact ion-Pairs: A Molecular-Wide and Electron Density-Based (MOWED) Perspective*, 2022.

204 V. Sudarvizhi, T. Balakrishnan, M. J. Percino, H. Stoeckli-Evans and S. Thamotharan, *J. Mol. Struct.*, 2020, **1220**, 128701.

205 C. A. Zapata-Acevedo, J. M. Guevara-Vela, P. L. A. Popelier and T. Rocha-Rinza, *ChemPhysChem*, 2022, e20220045-1-4.

206 C. A. Zapata-Acevedo and P. L. A. Popelier, *Pharmaceuticals*, 2022, **15**, 1237.

207 J. C. R. Thacker, M. A. Vincent and P. L. A. Popelier, *Chem. – Eur. J.*, 2018, **24**, 11200–11210.

208 A. J. Robertson, A. L. Wilson, M. J. Burn, M. J. Cliff, P. L. A. Popelier and J. P. Waltho, *ACS Catal.*, 2021, **11**, 12840–12849.

209 F. Jiménez-Grávalos and D. Suárez, *J. Chem. Theory Comput.*, 2021, **17**, 4981–4995.

210 C. Liu, J.-P. Piquemal and P. Ren, *J. Chem. Theory Comput.*, 2019, **15**, 4122–4139.

211 Z. E. Hughes, J. C. R. Thacker, A. L. Wilson and P. L. A. Popelier, *J. Chem. Theory Comput.*, 2019, **15**, 116–126.

This journal is © the Owner Societies 2023

Phys. Chem. Chem. Phys., 2023, **25**, 10231–10262 | **10261**

212 J. C. R. Thacker, A. L. Wilson, Z. E. Hughes, M. J. Burn, P. I. Maxwell and P. L. A. Popelier, *Mol. Simul.*, 2018, **44**, 881–890.

213 Z. E. Hughes, E. Ren, J. C. R. Thacker, B. C. B. Symons, A. F. Silva and P. L. A. Popelier, *J. Comput. Chem.*, 2020, **41**, 619–628.

214 B. C. B. Symons, M. K. Bane and P. L. A. Popelier, *J. Chem. Theory Comput.*, 2021, **17**, 7043–7055.

215 B. C. B. Symons and P. L. A. Popelier, *J. Chem. Theory Comput.*, 2022, **18**, 5577–5588.

216 M. J. Burn and P. L. A. Popelier, *J. Comput. Chem.*, 2022, **43**, 2084–2098.

217 T. L. Fletcher and P. L. A. Popelier, *J. Comput. Chem.*, 2017, **38**, 1005–1014.

218 R. López, N. Díaz, E. Francisco, Á. Martín Pendás and D. Suárez, *J. Chem. Inf. Model.*, 2022, **62**, 1510–1524.

219 F. Jiménez-Grávalos, N. Díaz, E. Francisco, Á. Martín Pendás and D. Suárez, *ChemPhysChem*, 2018, **19**, 3425–3435.

220 A. Pérez-Barcia, G. Cárdenas, J. J. Nogueira and M. Mandado, *J. Chem. Inf. Model.*, 2023, **63**, 882–897.

221 M. Kaupp, D. Danovich and S. Shaik, *Coord. Chem. Rev.*, 2017, **344**, 355–362.

222 H. S. Johnston and C. Parr, *J. Am. Chem. Soc.*, 1963, **85**, 2544–2551.

223 D. Cremer, A. Wu, A. Larsson and E. Kraka, *J. Mol. Model.*, 2000, **6**, 396–412.

224 J. Grunenberg, *Int. J. Quantum Chem.*, 2017, **117**, e25359.

225 D. Menéndez-Crespo, A. Costales, E. Francisco and Á. Martín Pendás, *Chem. – Eur. J.*, 2018, **24**, 9101–9112.

226 Á. Martín Pendás, M. A. Blanco and E. Francisco, *J. Chem. Phys.*, 2004, **120**, 4581.

227 Á. Martín Pendás, J. L. Casals-Sainz and E. Francisco, *Chem. – Eur. J.*, 2018, **25**, 309–314.

228 Á. Martín Pendás and E. Francisco, *Phys. Chem. Chem. Phys.*, 2018, **20**, 16231–16237.

229 C. Edmiston and K. Ruedenberg, *Rev. Mod. Phys.*, 1963, **35**, 457–464.

230 J. Pipek and P. G. Mezey, *J. Chem. Phys.*, 1989, **90**, 4916–4926.

231 F. Weinhold and C. R. Landis, *Valency and bonding*, Cambridge University Press, Cambridge, England, 2005.

232 A. J. Stone, *J. Phys. Chem. A*, 2017, **121**, 1531–1534.

233 G. Knizia, *J. Chem. Theory Comput.*, 2013, **9**, 4834–4843.

234 D. Y. Zubarev and A. I. Boldyrev, *Phys. Chem. Chem. Phys.*, 2008, **10**, 5207.

235 T. R. Galeev, B. D. Dunnington, J. R. Schmidt and A. I. Boldyrev, *Phys. Chem. Chem. Phys.*, 2013, **15**, 5022.

236 H.-P. Breuer and F. Petruccione, *The theory of open quantum systems*, Oxford University Press, Oxford New York, 2002.

237 M. Nielsen and I. L. Chuang, *Quantum computation and quantum information*, Cambridge University Press, Cambridge New York, 2010.

238 Á. Martín Pendás and E. Francisco, *J. Chem. Theory Comput.*, 2018, **15**, 1079–1088.

239 R. Ponec, *J. Math. Chem.*, 1997, **21**, 323–333.

240 R. Ponec, *J. Math. Chem.*, 1998, **23**, 85–103.

241 R. Ponec and F. Feixas, *J. Phys. Chem. A*, 2009, **113**, 8394–8400.

242 R. Ponec and F. Feixas, *J. Phys. Chem. A*, 2009, **113**, 5773–5779.

243 R. Ponec, D. Cooper and A. Savin, *Chem. – Eur. J.*, 2008, **14**, 3338–3345.

244 D. L. Cooper, R. Ponec and M. Kohout, *Mol. Phys.*, 2015, **114**, 1270–1284.

245 P. Bultinck, D. L. Cooper and R. Ponec, *J. Phys. Chem. A*, 2010, **114**, 8754–8763.

246 D. L. Cooper and R. Ponec, *Phys. Chem. Chem. Phys.*, 2008, **10**, 1319.

247 R. Ponec and D. L. Cooper, *J. Mol. Struct.: THEOCHEM*, 2005, **727**, 133–138.

248 A. I. Baranov, R. Ponec and M. Kohout, *J. Chem. Phys.*, 2012, **137**, 214109.

249 E. Francisco, Á. Martín Pendás and A. Costales, *Phys. Chem. Chem. Phys.*, 2014, **16**, 4586–4597.

250 R. Ponec and D. L. Cooper, *Struct. Chem.*, 2017, **28**, 1033–1043.

251 I. Mayer and P. Salvador, *J. Chem. Phys.*, 2009, **130**, 234106.

252 E. Ramos-Cordoba, V. Postils and P. Salvador, *J. Chem. Theory Comput.*, 2015, **11**, 1501–1508.

253 V. Postils, C. Delgado-Alonso, J. M. Luis and P. Salvador, *Angew. Chem., Int. Ed.*, 2018, **57**, 10525–10529.

254 E. Francisco, Á. Martín Pendás and M. A. Blanco, *J. Chem. Phys.*, 2009, **131**, 124125.

255 Á. Martín Pendás and E. Francisco, *Phys. Chem. Chem. Phys.*, 2018, **20**, 21368–21380.

256 M. Menéndez, R. Álvarez Boto, E. Francisco and Á. Martín Pendás, *J. Comput. Chem.*, 2015, **36**, 833–843.

257 E. Francisco, A. Costales, M. Menéndez-Herrero, Á. Martín Pendás and E. Francisco, *J. Phys. Chem. A*, 2021, **125**, 4013–4025.

10262 | *Phys. Chem. Chem. Phys.*, 2023, **25**, 10231–10262

This journal is © the Owner Societies 2023